UNIVERSITÁ DEGLI STUDI DI PADOVA

SCUOLA DI INGEGNERIA

DIPARTIMENTO DI INGEGNERIA INDUSTRIALE

CORSO DI LAUREA MAGISTRALE IN INGEGNERIA DEI MATERIALI

TESI DI LAUREA

3D-PRINTING OF A PRECERAMIC POLYMER FOR BIOMEDICAL APPLICATIONS

Relatore: Ch.mo Prof. Paolo Colombo

Correlatore: Ch.mo Prof. Enrico Bernardo

Laureanda: Giorgia Franchin

Matr. n. 1035035

Anno Accademico 2012-2013

ABSTRACT

This research investigates the possibility of using a preceramic material based on a silicone resin in order to print simple structures through low cost fused deposition techniques. These structures are intended to be used as scaffolds for applications in bone tissue engineering; for this reason, they have to withstand a heating treatment in order to be converted to a ceramic material compatible with human tissues.

A first specific objective of this work is the selection and characterization of an optimal mixture of preceramic, filler and plasticizer in order to obtain a formability window suitable for the 3D printing technique; viscosity tests and XRD measurements have been performed and the proper combination of reagents has been chosen. Pyrolysis process has also been optimized in order to convert the preceramic material to the desired ceramic without losing the component shape.

Once the mixture has been chosen, the printer has been reconfigured and set up in order to use it instead of PLA or ABS. This step required both selection of different process parameters and rearrangement of the printer hardware; the most significant adaptions regarded the extrusion system and the printing bed material.

Finally, some samples have been realized and pyrolyzed; then biological tests in SBF have been performed at the Friedrich-Alexander Universität Erlangen-Nürnberg with the help of Professor Aldo Boccaccini and his staff. Treated samples have been characterized through SEM-EDX analysis in terms of chemical structure, morphology and biological behavior.

ACKNOWLEDGMENTS

I would like to thank: Professor Paolo Colombo and Professor Enrico Bernardi for their interest and help provided during this whole work; Professor Aldo Boccaccini from the Friedrich-Alexander Universität Erlangen-Nürnberg, for his helpfulness and his interesting advices and for letting me perform bioactivity tests in his laboratory with the supervision of Valentina Miguez Pachego; all the colleagues in the laboratory, especially Tommaso and Alberto, for their suggestions and support; Micaela for her patience and contribution; my parents, my family, Alessandro and all my friends for having always trusted me.

TABLE OF CONTENTS

INTRODUCTION

In the last years cooperation among research in materials, process technology and medicine has led to the realization of innovative structures and components, which can solve problems linked to human illnesses with a higher efficiency.
Bone scaffolds represent one of these products: their complex geometry requires advanced studies and techniques in order to be reproduced.
In the present study the focus is on the possibility of using a preceramic material based on a silicone resin in order to print simple scaffolds through low cost fused deposition techniques; scaffolds will withstand a heat treatment in order to be converted to a ceramic material compatible with human tissues.

Specific objectives of this work are:

- selection and characterization of an optimal mixture of preceramic, filler and plasticizer in order to obtain a formability window suitable for the 3D printing technique;
- reconfiguration and setup of the printer in order to print with preceramic material instead of PLA or ABS;
- realization and pyrolysis of samples and their characterization in terms of chemical structure, morphology and biological behavior.

In the first chapter the state of the art in terms of Polymer Derived Ceramics (PDCs) will be analyzed, with a particular interest in polysiloxanes as preceramic material; the role of passive and active fillers will also be investigated.
The second chapter will focus on the rapid prototyping technique: the state of the art, together with its advantages and disadvantages, will be discussed in detail.
The concepts of biomaterial and tissue engineering will be the topic of the third chapter; characteristics and geometry that the chosen material should have, together with the interaction between an ideal scaffold and the human environment, will be explained with a particular attention to scaffolds for bone restoration.

The experimental section will start with the presentation of all the techniques and instruments used in this work in order to characterize the materials and to produce the samples; chapter five will show the characterization of pure silicone and of different mixtures of silicone, calcium carbonate and wax in terms of thermal behavior, rheology and resistance to the thermal treatment.

In the sixth chapter, some tests with the 3D printer will be shown; the problems in terms of reconfiguration and setup of the printer will be highlighted in order to demonstrate the limitations in strength, precision and accuracy. Samples resulting from these attempts, which have been pyrolyzed, will be shown and characterized to highlight the resulting chemical structure and the biological behavior in a simulated human environment.

CHAPTER 1: POLYMER DERIVED CERAMICS (PDCs)

The technique chosen in order to obtain ceramic materials for biomedical application during this activity is the polymer derived ceramics (PDCs) technology. It is based on the production of silicate ceramics through the pyrolysis of preceramic polymers. The composition and morphology of the resulting so called polymer derived ceramics depend on the molecular structure of the polymeric precursor.

The advantages of this technique are unique, especially in terms of formability. In fact, it is possible to apply the classical plastic forming technologies like injection molding, extrusion, resin transfer molding, melt spinning etc. to ceramics. This means lower production costs for ceramic objects, thanks also to the lower processing temperatures (below 1200°C)[1,2].

The table below shows some of the most common precursors in use and their ceramic product.

Preceramic polymer	**Polymeric unit**	**Ceramic**	**Ceramic yield (%)**
Polycarbosilane	$(-R_2SiCH_2-)_n$	SiC	65
Polysiloxane	$(-R_2SiO-)_n$	Si-O-C	30-60
Polysilazane	$(-R_2SiNR-)_n$	Si_3N_4	20-90
Aluminum amide	$(-AlNR-)_n$	AlN	20-50
Polyborazine	$(-B_3N_3H_x-)_n$	BN	85
Polytitanium imide	$(-Ti(NR)_2-)_n$	TiN	50-70

Table 1. Preceramic polymers

Preceramic polymers are organic-inorganic polymers whose structure usually contains Si atoms; they transform into ceramics through a thermal treatment which eliminates the organic fraction. In fact, between 600°C and 800°C their C-H bond breaks and H_2, CH_4 and other compounds are released.

Production steps from polymers to ceramics, with focus on porous ceramics, are summed up in the figure below.

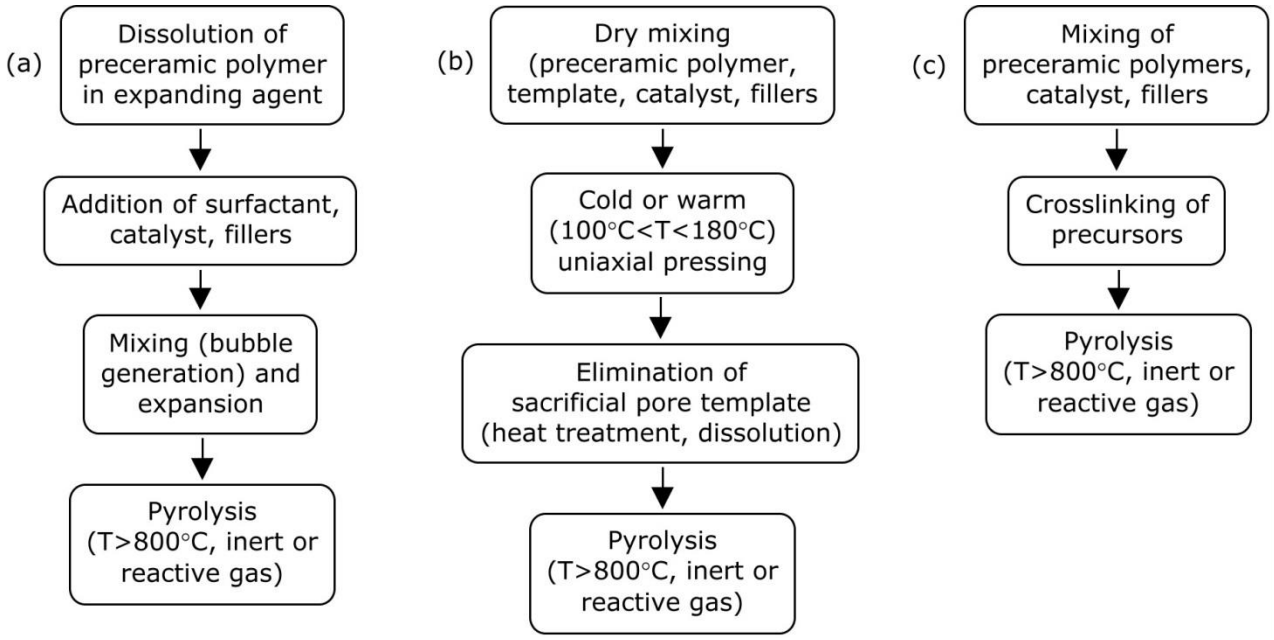

Figure 1. Production steps for porous ceramics fabrication from preceramic polymers[3]

The last step is the conversion from polymer to ceramic, which can be induced thermally (pyrolysis in a traditional oven, through microwaves or laser heating) or not thermally (ion-irradiation), usually in an inert or oxidizing atmosphere. The introduction of fillers leads to engineered ceramics production.

Preceramic polymers have been successfully used for 40 years to fabricate advanced components with some advantages compared to conventional powder synthesis, like production of materials with different compositions[1].

The main applications of these ceramics are:

- fibers: the first and most successful application field (SiC and SiBCN);
- ceramic matrix composites: advantages in terms of simplicity, costs, processing temperatures, time needed and component geometry;
- high porous components: porosity variable from some nm to some mm, interesting for biomedical applications;
- coatings: preceramic polymers can be deposited on various substrates
- micro components smaller than 1 μm with applications in MEMS (Micro-Electro Mechanical Systems);
- resistors: components with high temperature and thermal shock resistance.

Process characteristics:

One of the main advantages of the PDCs technique is the possibility to combine chemical synthesis and forming process together. In fact, ceramic components can be easily shaped by applying the conventional plastic forming techniques to the precursors and converting then them to ceramics through a thermal treatment.

Preceramic polymers show polymeric behavior in the forming process temperature range. They can be liquid or solid depending on their structure and molecular weight; in the second case, they can be dissolved in solvents or fused at low temperatures (below 150°C).

Looking at the process in detail, different steps can be recognized. Generally, after an initial weight of the reagents, precursor polymer is dissolved into an adequate solvent (like acetone or isopropanol); filler powders are added to this solution in order to obtain a diluted suspension. The use of a solvent can be necessary in order to dissolve the polymer and/or to disperse the filler.

Mixtures are then mixed (magnetically, through ultrasounds etc.) to obtain a stable suspension; then they are dried in air to produce powders of preceramic polymer and filler.

A solution is not necessary to obtain a homogeneous mixture when an efficient mixing method is used in the temperature range in which the polymer is fluid.

Powders are then shaped through different methods like cold or warm pressing, extrusion, injection molding etc..

After forming, preceramic materials are submitted to different thermal treatments in terms of atmosphere, temperature (between 800°C and 1550°C), heating rate and time in order to obtain the desired ceramic composition.

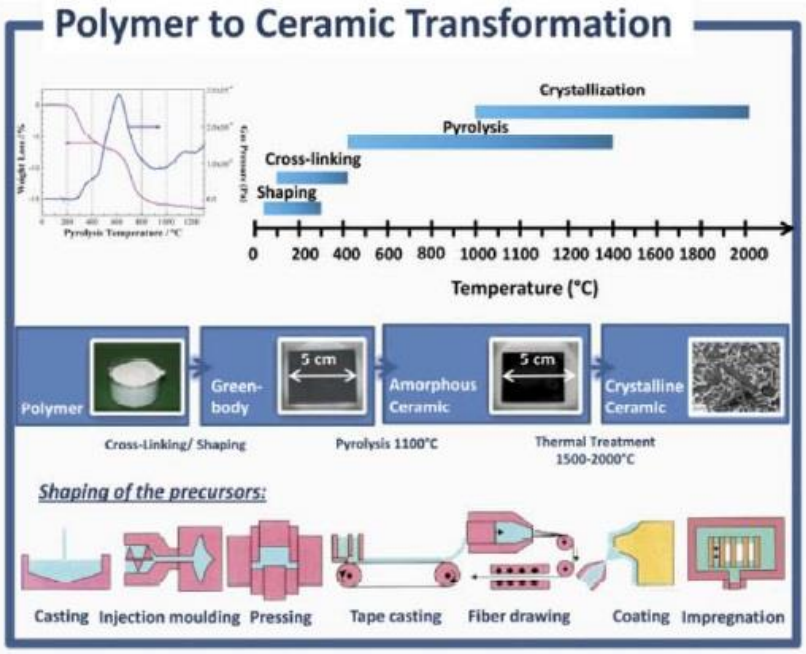

Figure 2. PDCs process steps[3]

A necessary step in the PDCs technique is the conversion in a thermosetting structure able to maintain its shape after forming during ceramisation; this kind of structure is achieved by the condensation of functional groups like Si-H, Si-OH etc., which is usually spontaneous below 200°C (thermal cross-linking). Cross-linked fraction slightly influences the rheological properties of the polymer, so it has to get through accurate controls during forming.

The presence of filler also influences the conservation of a shape: high amounts of fillers can be enough to support the polymeric matrix even without cross-linking, keeping the shape of the component.

After forming and cross-linking, preceramic phase has to be converted into ceramic material. Conversion leads to decomposition or elimination of organic fractions and Si-H, Si-OH or Si-NH; the most adopted method is pyrolysis.

Temperature and other related process parameters like heating rate and maintenance time influence composition and microstructure, together with crystallization, carbothermal and active fillers reactions. Pyrolysis leads to an amorphous compound; if a crystallized structure is desired, a subsequent thermal treatment is needed. Heating rate influences also the ceramic yield; if there is not enough time for cross-linking during heating, some oligomers can be released with a yield decrease.

Fillers:

Main disadvantages of the ceramisation process are poor shrinkage control and a high gas release which lead to pores and leaks; these defects affect the component mechanical properties and allow just thin wall structures to be produced. Greil has been the first who has been able to overcome these limits through the use of passive or active fillers[4]. Adding active fillers such as metallic or intermetallic particles leads to shrinkage control and so to relatively dense and leak-free monoliths. During polymeric decomposition and pyrolysis fillers can react with gaseous products forming carbides- or nitrides-based ceramics; expansion due to metallic to ceramic conversion limits both shrinkage and defects formation. Passive fillers do not react; they just limit shrinkage by diluting the reactive mass.

Filler dimensions can vary from microns to nanometers; in the second case, they form stable suspensions with higher homogeneity and their high aspect ratio increases their reactivity. There is also a higher tendency to form crystalline equilibrium phases with nano fillers.

Pyrolysis in air at temperatures above 400°C causes oxidation of organic fractions forming highly reactive silica that can easily form silicates with the filler powders.

Researchers have recently tried to produce advanced ceramic materials containing oxygen from polymeric precursors and nanometric oxides as fillers; they react with decomposition products (pure silica etc.) giving new kinds of desired pure ceramic phases with really high kinetics (thanks to their dimensions) at low temperatures too. Fillers react giving single ceramic phases and they avoid leaks maintaining polymer formability at the same time.

Comparing to sol-gel methods, there is no need of a strict synthesis control and of inflammable solvents or precursors, and plastic forming techniques can be used.

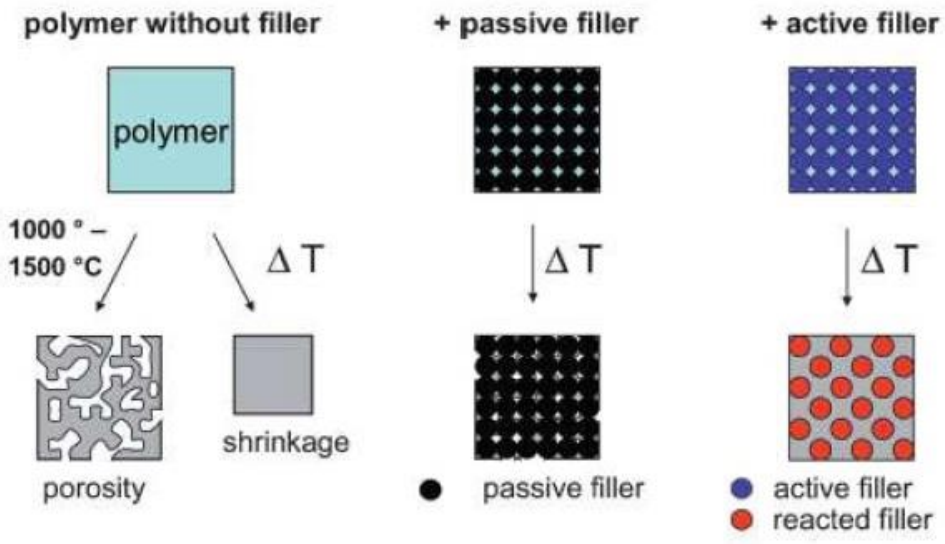

Figure 3. Comparison of ceramics derived from polymers and polymers added with passive and active fillers[3]

The nature and amount of fillers influence some ceramic properties like:

- porosity and pore distribution;
- Young modulus;
- Electric conductivity;
- Thermal conductivity;
- Creep and corrosion resistance.

This leads to production of near net-shape components.

Pores are not always to be avoided: PDCs method can be the key to produce ceramics with high porosity varying in micro-, meso- and macro-pores ranges.
One strategy is to introduce some additives which decompose between 80°C and 250°C releasing high amounts of gases; polymers can also be mixed with expandable or sacrificial polymeric microspheres, then formed by cold pressing and heated to eliminate spheres and reach the desired porosity.
Of course the simplest way to control porosity is to design it; thus, the focus of this work is on realization of preceramic structures with specific geometry of both material and pores through 3D printing (see Chapter 6). Developing a 3D image of the desired ceramic component assures the highest precision of pores dimension, morphology and position with lower costs and without using any sacrificial material.
Another solution can be the impregnation of polymeric foam (generally PU) with a preceramic polymer. The foam is compressed to eliminate exceeding material and then heated to dissolve the sacrificial skeleton and convert the polymer into ceramic through pyrolysis reaction. The resulting material presents an interconnected open porosity given by the foam morphology.

Materials involved in PDCs process:

Preceramic polymer selection among the various available choices considers composition, rheology and ceramic yield. Typical examples are conventional silicones used to produce fibers, coatings, porous and near net-shape components. They can be used as a basis to form silicates; their partially covalent bond leads to a slow interdiffusion among components and thus to a high thermal and chemical stability but also to a difficult production through solid state sintering.

Silicones with fillers are the answer in order to synthesize and form monolithic ceramic oxides; they are easily soluble in common solvents such as acetone, toluene or isopropylic acid leading to homogeneous nanofiller suspensions and thus homogeneous powders.

Silicones are classified depending on their physical status, and thus on their reticulation degree:

- Silicone fluids: composed by linear chains terminating with a trimethylic group, their viscosity depends on chains reticulation degree and they are not water soluble.
- Silicone gels: lightly reticulated thanks to the introduction of trifunctional molecules (like CH_3SiCl_3) which link with vinyl groups;
- Elastomeric silicones: fluids with higher cross-linking;
- Silicone resins: tetrahedral monomers are dominant and determine a strong reticulation.

Silicones are thus classified with focus on their main properties, chain length and functional groups ramification (reticulation degree). Pre-mixtures of polymer and reticulating agent are called one-component systems, whereas bi-component systems need an in situ mixing of the two components; reticulation in one-component systems is generally slower. The most common way to reticulate silicones is peroxide method (for example using dibenzoilperoxide); reticulation reaction can be schematized like below.

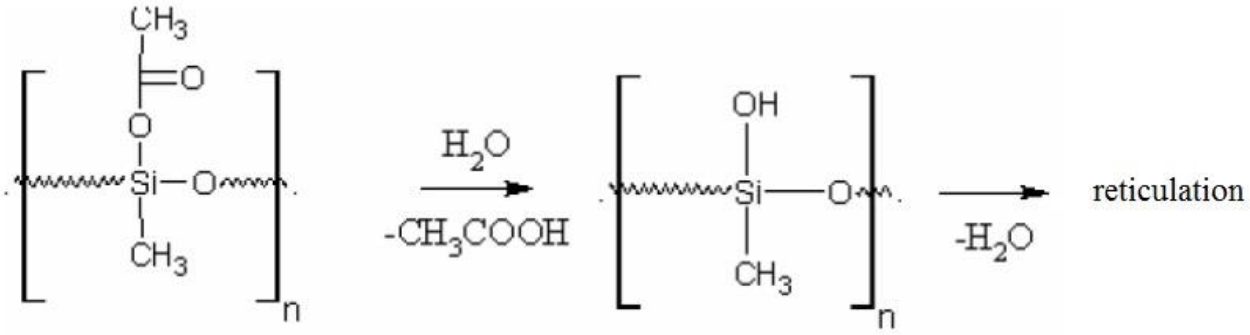

Figure 4. Silicone reticulation reaction[3]

From 1960 ceramics from preceramic polymers have been synthesized directly from organosilicones pyrolysis. Ainger and Herbert, Chantrell and Popper produced non-oxide ceramics from molecular precursors; after some years, Verbeek and his colleagues presented for the first time transformations from polymers to ceramics of polysilazanes, polysiloxanes and polycarbosilanes[1].

The relatively low temperatures necessary in order to synthesize PDCs made this technology economically interesting compared to conventional ceramic synthesis. Second, binary systems

like Si_3N_4 and SiC cannot dissolve C or N in order to form the ternary composition of SiCN; at the same way, SiO_2 and SiC cannot dissolve C or O to form ceramics with composition SiCO. The possibility to synthesize PDCs like SiCN and SiCO can be attributed to the strong bond between Si and C in the polymeric chain which impedes the C volatilization during pyrolysis.

Molecular structure and preceramic polymer type influence not only composition but also phase number and distribution and ceramic microstructure; this means that physical and chemical properties of PDCs can be tailored in a wide range by accurately designing the molecular precursor. For this reason, preceramic polymer synthesis is of great importance in PDCs technique.

Figure below shows a general simplified formula of an organosilicone which can be used to synthesize ceramic materials.

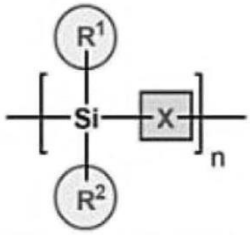

Figure 5. Structural unit of a silicon base polymer[3]

Both R substituents and X group in the chain can be tailored in order to modify the preceramic polymer at a molecular level. The table below shows the different silicon based polymers obtained by varying the X group.

Polymer	**X group**
Polysilane	Si
Polycarbosilane	CH_2
Polysiloxane	O
Polysilazane	NH
Polycarboxylediimmide	N=C=N

Table 2. Silicon based polymers

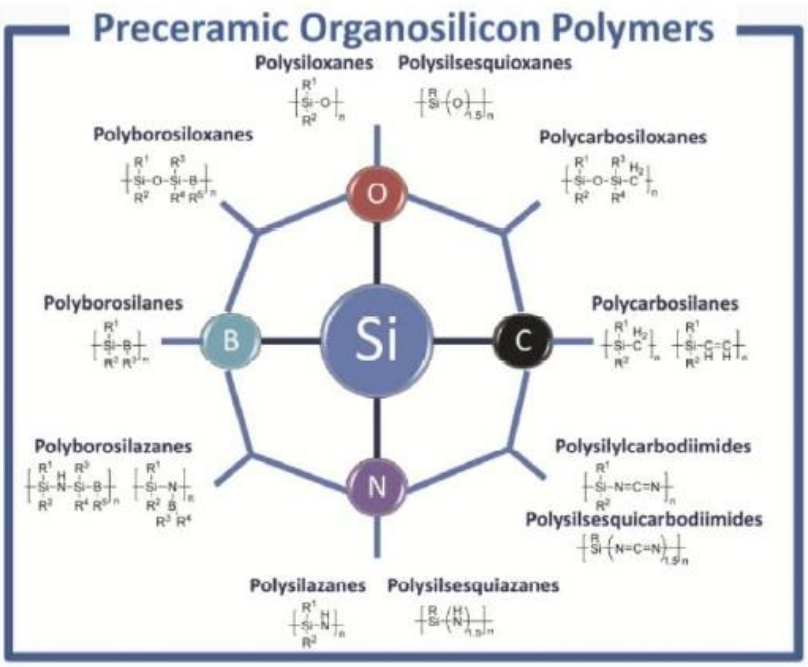

Figure 6. Silicon based polymers[3]

Changing the functional groups R^1 and R^2 leads to variation in thermal and chemical stability, solubility, electrical, optical and rheological properties; most common R groups are H, aromatic or aliphatic groups.

In order to be competitive with traditional ceramics, preceramic polymers have to be either cheap or able to produce components with new compositions or special properties.

Silicon based polymers synthesis starting from clorosilanes is represented below.

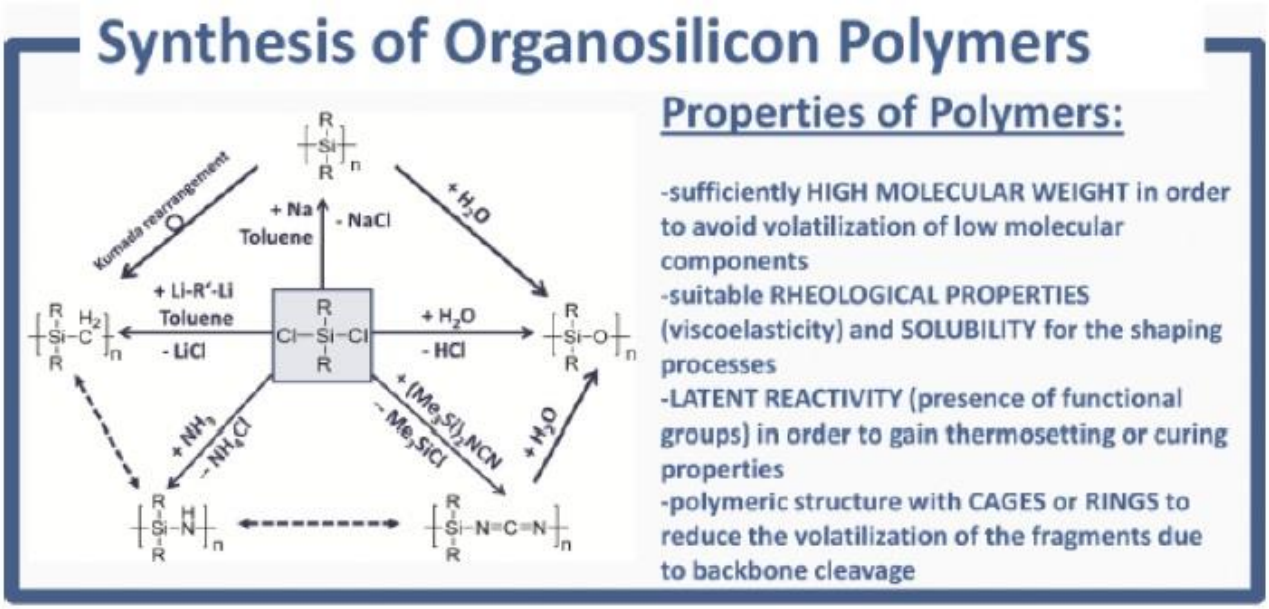

Figure 7. Silicon based polymer synthesis[3]

Clorosilanes (R_xSiCl_{4-x}) are the most used precursors because of their high availability and low price. In order to be efficient during the thermal decomposition process, polymers should have an enough high molecular weight in order to avoid volatilization of lower molecular weight; secondly, they should have rheological properties and solubility suitable for the forming processes. Finally, latent reactivity is required for cross-linking reactions.

Wollastonite synthesis through PDCs process:

PDCs technique is used in order to produce 3D-printed samples and scaffolds made of wollastonite.

A polysiloxane added with calcium carbonate fillers (micro- and nanometric) is chosen for both experiments. Detailed descriptions and exact amounts are reported in the experimental section in order to distinguish peculiarities and specific procedures in each case (see Chapter 5).

Polysiloxanes:

Polysiloxanes or silicones are mostly used as sealers; the many derivatives available on commerce are cheap and have excellent chemical, physical and electrical properties.

Generally, polysiloxanes synthesis starts with a reaction between water and clorosilanes. Recently, new polysiloxanes rich in Si (the so called polysilil-ethers) have been synthesized through polycondensation of ω-functionalized α linear silanes and through ROP (ring opening polymerization) of cyclic silil-ethers. These hybrid materials combine polysilanes and polysiloxanes properties.

Polysiloxanes synthesis is based on a hydrolysis reaction controlled by dichlormethylsilane and on the subsequent condensation reaction:

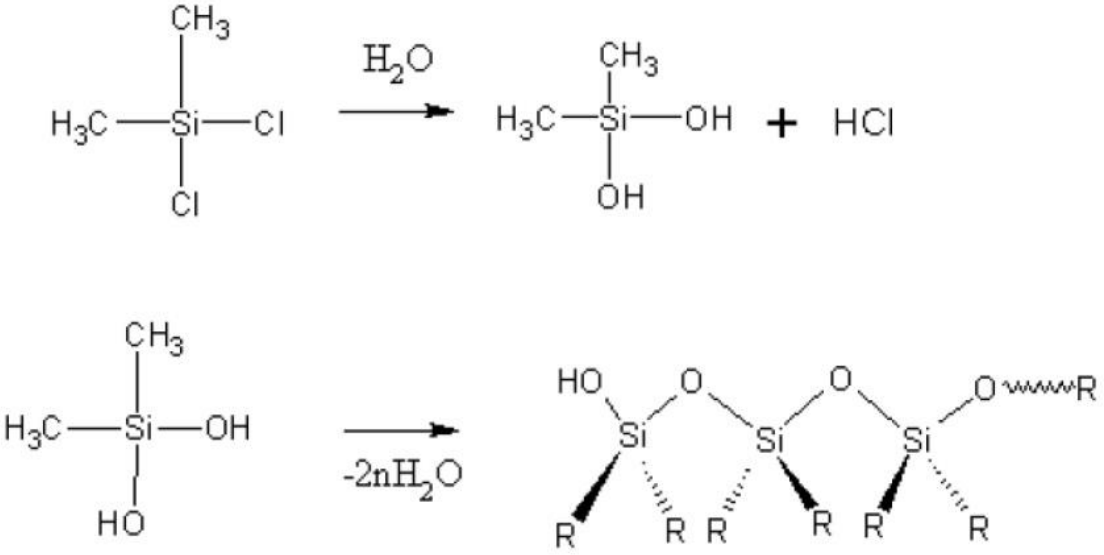

Figure 8. Polysiloxanes synthesis[3]

Condensation reaction defines silicone reticulation degree and thus final properties of the printed component; the more the polymer is already reticulated, the lower will be its reticulation degree during heating treatment.

For this reason branched nanoblock polysilsesquioxanes $–[RSi\text{-}O_{1.5}]_n$- are of some interest; their different configurations are shown in the figure below.

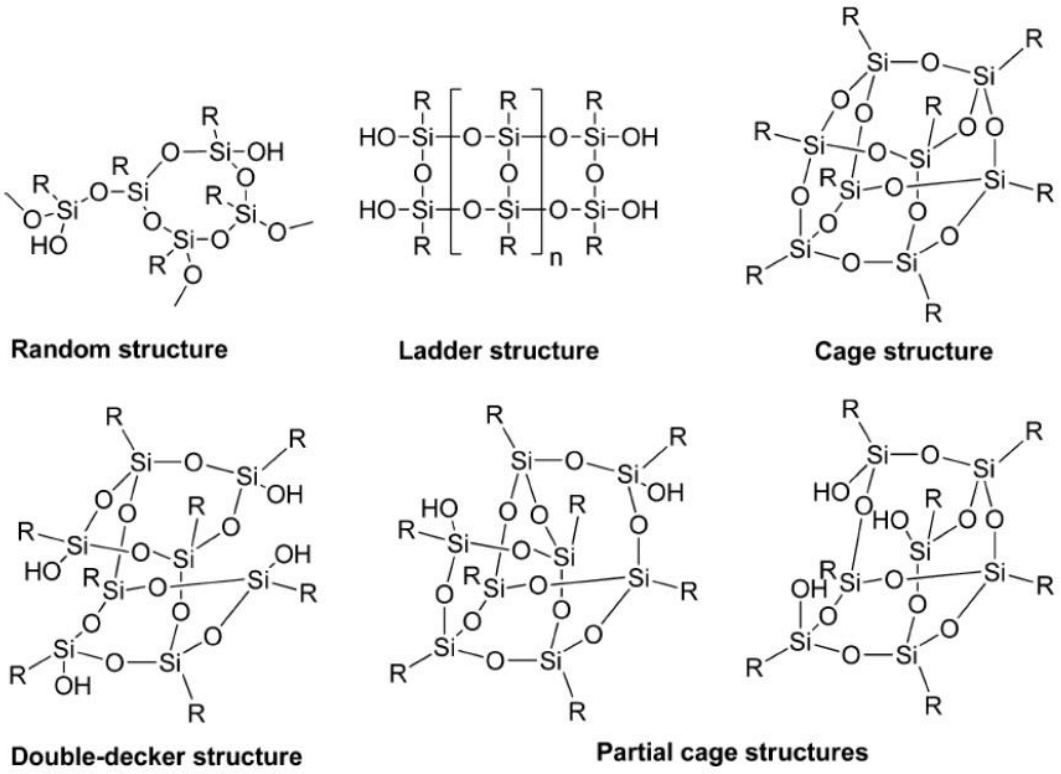

Figure 9. Polysilsesquioxanes[3]

Recent studies on SiCO ceramics derived from polysiloxanes rich in C have shown that these materials have a higher stability in avoiding crystallization and high temperature resistance.

CHAPTER 2: RAPID PROTOTYPING

In this study a rapid prototyping technique has been employed to produce ceramic scaffolds: 3D printing; a structure like a 3D scaffold is important for many applications, but it is very complicated if not impossible to be produced with the conventional ceramic techniques.

The new rapid prototyping methods introduced in the 90's have allowed new possibilities for producing complex geometries as the 3D scaffolds are; these have soon attracted the interest of researchers. The focus of this work is on the possible biomedical applications: future research might succeed in regenerating or replacing damaged tissues with laboratory grown parts such as bones and cartilage; for these objectives, ceramic scaffolds based on calcium silicates and phosphates (with particular attention on hydroxyapatite) have gained increasing attentions over the past years[5-8].

Ceramic scaffolds are also interesting as support for active material depositions in filters and sensors; a transparent glass scaffold can be an optimal support for a gas-sensing thin layer deposition.

In this section a general introduction on Rapid Prototyping will be given, with a focus on techniques for ceramics; the 3D printing technology chosen for this work will be explained in depth.

Rapid Prototyping:

A prototype is an approximation of an object or of its components produced for a definite purpose in its implementation; it permits to visualize, analyze and test an idea or project before its production. For this reasons, it would be really helpful to find a way to shorten the time needed for the development of a prototype: with this intent many manufacturing technologies were developed in the 80's and 90's with the name of Rapid Prototyping (RP). The rise of these techniques was possible thanks to the Computer-Aided Design or CAD.

RP techniques are various and very different, but have at least two features in common:

- RP techniques are almost always performed with an Additive Manufacturing: material is not removed nor shaped, but added step by step (layer by layer).
- They can be classified as Solid Freeform Manufacturing; Solid is used because while the initial state may be liquid, powder, pellets or laminates, the end result will be solid, 3D object, while freeform stresses on the ability of RP to build complex shapes with little constraints on its form.

The basic approach adopted by all these techniques can be synthesized as follows:

1. A model or component is modeled as closed surfaces on a CAD-CAM (Computer-aided manufacturing) system;
2. The solid model is converted into a .stl file, which approximates the surface of the model by polygons; the file format takes its name from Stereolithography, which is the first RP technology developed;
3. A computer program analyzes the STL file and "slices" the model into cross sections, which are systematically reproduced through the solidification of liquids or powders and then combined to form a 3D objects; sections can be already thin, solid foils that are glued together to form the object.

The first RP systems were developed to work with resins because of the low temperature required; then they have been adapted to metals and ceramics and other systems have been developed. The paragraphs below present the RP techniques developed for ceramics.

Rapid prototyping techniques for ceramics:

The use of technical ceramics has been traditionally limited by technological problems: for the use as piezoelectric devices, magnetic ceramics, gas and humidity sensors, varistors etc., complex shapes are required; nevertheless, their manufacturing is complicated and high costs for machining and dies make inconvenient the production of small quantities.

These factors delay the prototyping, so industrial applications of ceramic materials are restricted by the lack of net-shaping capability for components with complex structures.

Ceramic Rapid Prototyping solutions came out in the middle '90s: some of them are stereolithography, extrusion of ceramic paste, fused deposition of ceramic-loaded polymer filament, laminated object manufacturing, selective laser sintering of ceramic powder and 3D printing. In the next paragraphs the most important processes will be presented following a review by Tian, Li and Heinrich[9].

Stereolithography of ceramic slurry:

Stereolithography (SL) was the first RP technology to be developed; the first system available in commerce was released by 3D Systems company in 1988.

Commercial SL machines produce plastic prototypes from epoxy resins by photo-polymerization of a liquid monomer with a UV laser; compared to other RP techniques, it presents the best surface finish and one of the highest accuracies.

In order to produce ceramic prototypes, liquid monomer is replaced by a suspension of ceramic powder dispersed in a UV-curable resin. Process steps can be synthesized as follows:

1. Laser scanning of the cross section on the surface of the ceramic resin in order to cure a thin layer (150-200μm); the part is attached by supports to an elevator platform which is situated beneath the surface of the ceramic resin;
2. The elevator platform dips into the suspension allowing the liquid resin to flow over the cured portion of the part;
3. A doctor blade sweeps over the surface to leave a fresh ceramic suspension layer;
4. Laser scanning on the new layer cures the next portion; repeating this process builds up the 3D green body of the component;
5. The green body is post sintered in furnace to obtain dense ceramic objects.

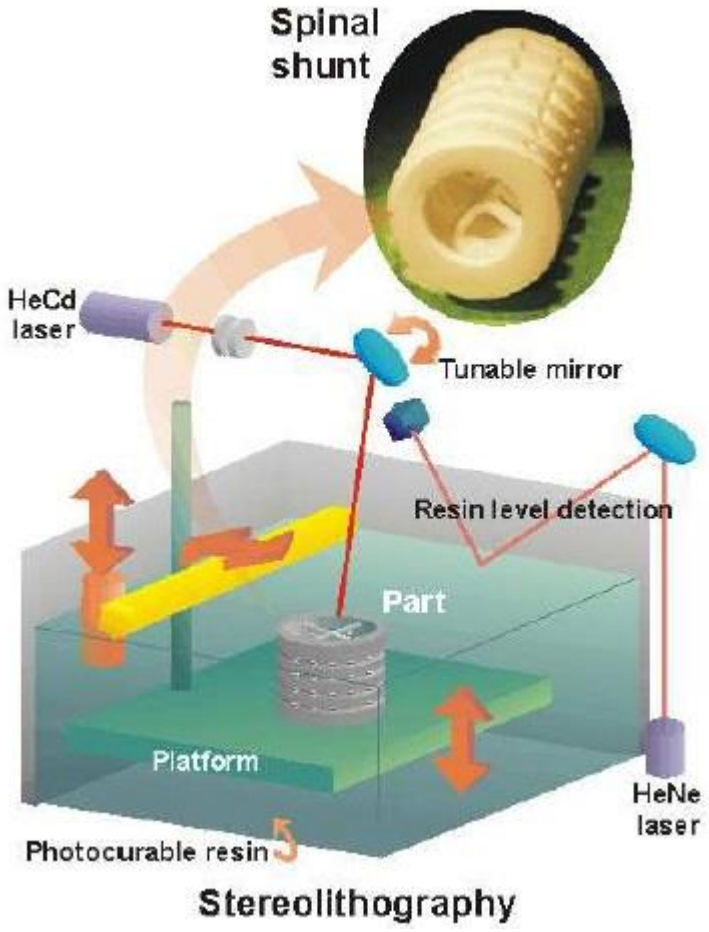

Figure 10. Schematic representation of a stereolithography process[10]

Common lasers are He Cd gas, Ar ion gas and solid state Nd-YVO_4 lasers. Note that the solidified sample is surrounded by liquid material, so a support has to be designed and produced.

Laminated object manufacturing:

Laminated object manufacturing (LOM) was developed by Helisys in 1985 and then taken over by Cubic Technologies.

LOM generates 3D ceramic objects by sequential stacking, laminating and shaping of pre-ceramic paper or ceramic green tape; it is a hybrid between additive and subtractive processes. Each layer is cut by a knife or laser beam according to the cross section given by the model; bond between layers is provided by a thermoplastic adhesive coating on the bottom side of the sheets, activated by heat and pressure during the LOM.

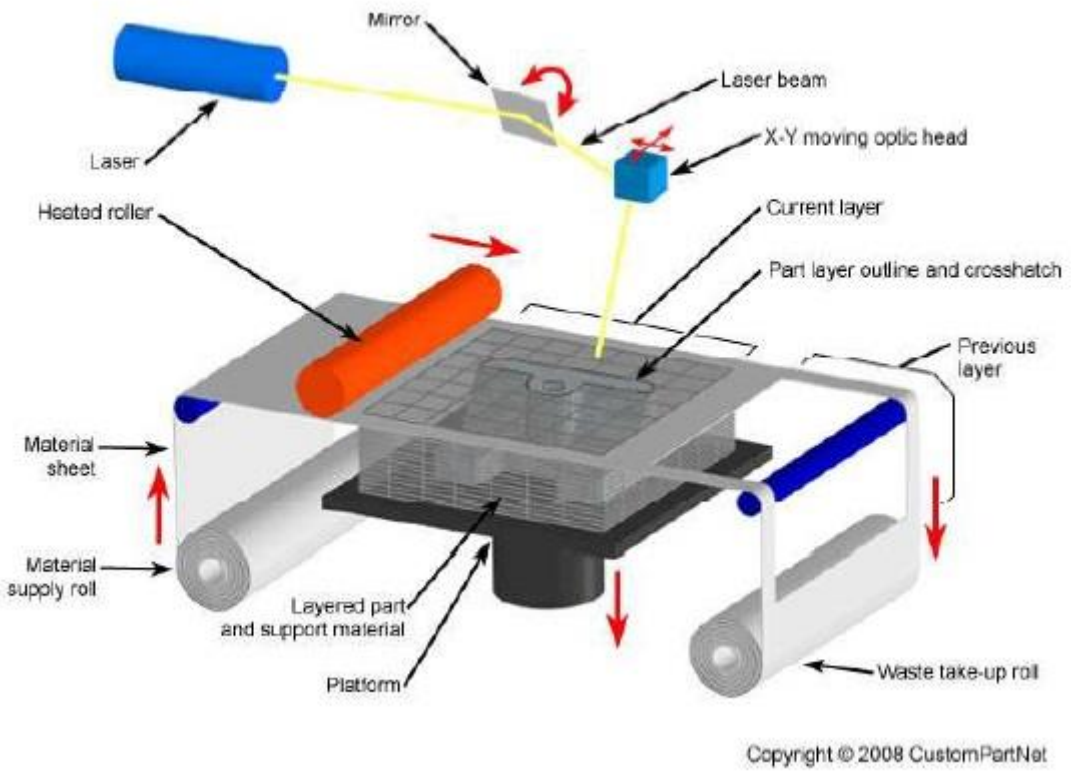

Figure 11. Schematic representation of Laminated Object Manufacturing[10]

Main advantages are wide variety of materials, fast build time and high precision; on the other sides, parts are difficult to remove at the end and thin walls are difficult to fabricate.

Selective laser sintering:

Selective laser sintering (SLS) was developed at the University of Texas and the first commercial machine was shipped in 1992 by DTM Corporation.

The basic principles are the following:

1. A thin powder layer is spread by a roller from the container to the platform;
2. The new powder layer is selectively sintered by a laser via a computer controlled scanner according to the cross section of the CAD model; non-sintered powder is left intentionally: it will be the support for the following layers;
3. The laser sintered part is obtained at the end by removing the non-sintered powder.

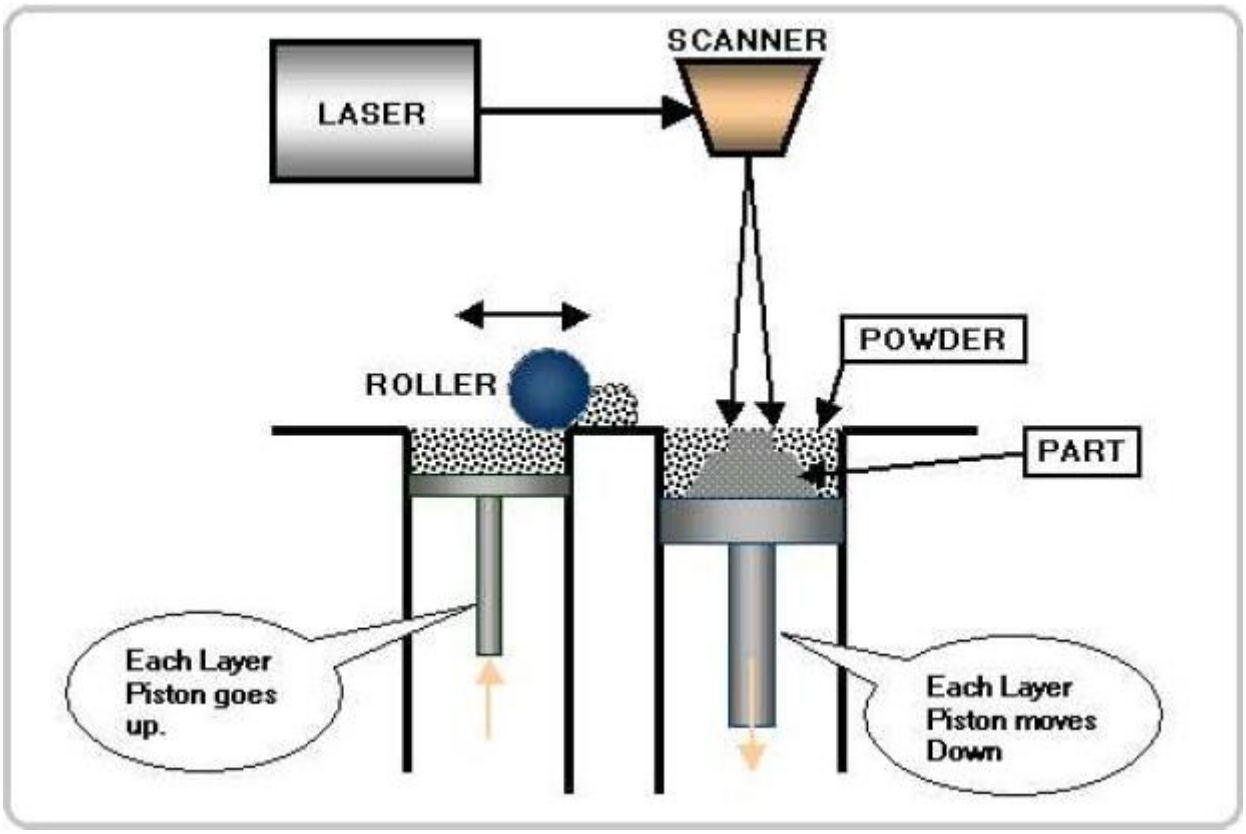

Figure 12. Schematic representation of Selective Laser Sintering[10]

The main advantages of this technology are the wide variety of thermoplastic, metallic, ceramic materials and also thermoplastic composites printable, together with the fact that no support is needed and that just little post processing is required: when a high mechanical strength is not necessary, the sintered part is already solid enough to be handled. For ceramic powders post treatment is often required to densify the microstructure and achieve higher mechanical strength[11].

Alumina, silica and yttria-zirconia powders have been sintered with Nd:YAG laser, but density and mechanical properties of the samples were not enough for a medical application as dental bridges.

PDC parts with complex shapes have been produced by selective laser curing (SLC), thanks to a selective sintering of SiC loaded polysiloxane powder with a CO_2 laser beam which locally induces curing reaction of the polymer phase at about 400°C. Laser-cured bodies were converted to Si-O-C/SiC ceramics with a pyrolysis treatment at 1200°C in inert atmosphere; liquid silicon infiltration was carried out in order to produce dense parts with higher strength.

Particle bonding can follow three different mechanisms:

- Solid state sintering: thermal process driven by diffusion and neck formation between particles;
- Liquid phase sintering: bond due to a molten binder or a molten fraction in the material;
- Full melting: fully dense structure with higher mechanical properties can be produced.

Liquid phases promote higher rates leading to shorter sintering times; for this reason solid phase sintering is not feasible in selective laser sintering, where short laser irradiation requires rapid particle bonding and sintering.

Other methods instead of classic roll spreading of the powder bed provide an increase of the green layer density; one of them is spraying of a ceramic slurry. The main advantage of this method is that a density up to 70% can be reached; but for each material a different slurry has to be prepared and optimized and this limits the process versatility.

Direct ceramic ink-jet printing:

Direct ceramic ink-jet printing makes use of ink-jet printers to create components by multilayer printing of a colloidal suspension dispersed with ceramic powder.

The main advantages of this technique are the potential to produce a wide range of fine ceramic contours with high resolution enabling miniature components to be manufactured. According to the multiple nozzles functional gradients and multi-material components can be fabricated. By adjusting the aperture of the printing head and by controlling the spreading phenomenon of the droplet, a standard definition of 50μm can be reached.

Powder head 3D printing (indirect printing):

Powder based 3D printing was developed at the Massachusetts Institute of Technology in 1992 as method to create prototypes from powdered metals and ceramics.

It is based on the following steps:

1. An individual 2D layer is created by adding a layer of powder to the top of a powder bed;
2. Ink-jet printing of a binder material builds the new component layer following the cross section of the CAD model;
3. The powder bed (with the already printed part) is lowered down through a piston and a new powder layer is spread out and selectively welded until the part is completely printed;
4. The unbound powder is removed through an air flow and the fabricated part is submitted to heat treatment to increase its density.

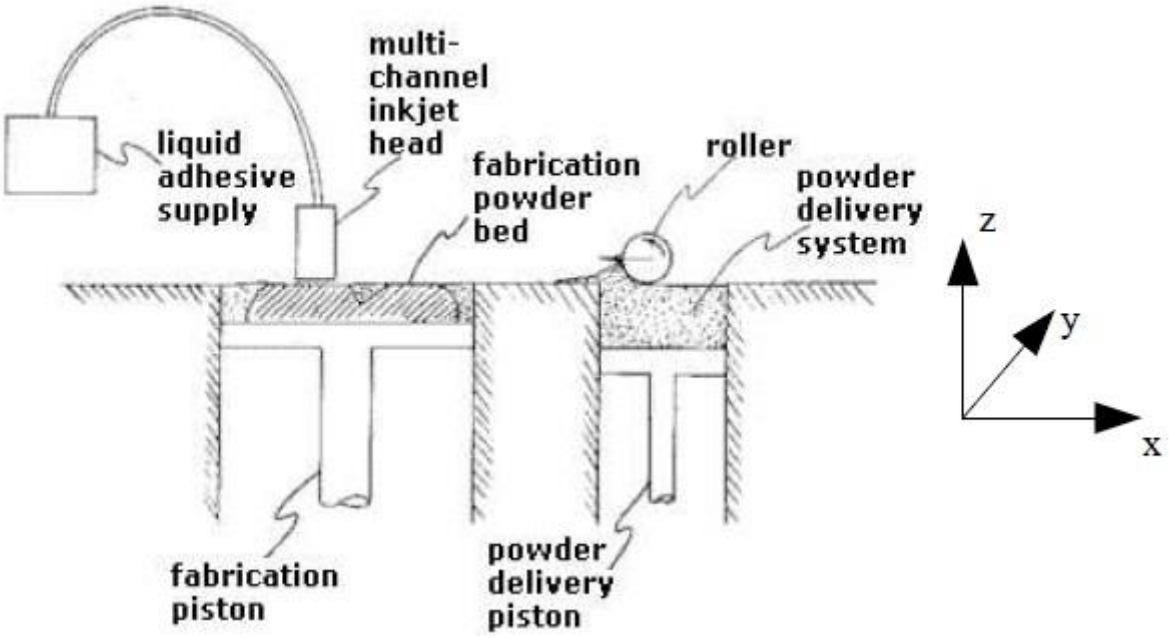

Figure 13. Schematic representation of powder based 3D printing[10]

The main advantages of this technology are that it is very easy to use, versatile, and even very complex shapes are easy to print; also low-melting point materials like pre-ceramic polymers can be used thanks to the low temperatures involved in the process. Printing times are also really short: depending mainly on the surface area, a layer can be printed in 3-5 minutes.

There are also some drawbacks to be taken into consideration: powder has to respect specific dimension and morphology requirements in order to show good flowability and good layer spreading; accuracy and surface finish are in any case worse compared to other techniques; low process temperatures mean also the need of a long post treatment.

Fused Deposition Modeling:

The Fused Deposition Modeling (FDM) was developed first for polymers in 1988 and commercialized after 1992 by Stratasys. Since the beginning of the 21st century there has been a large growth in the sales of these machines, and their price has dropped substantially. It has been speculated that 3D printing may become a mass market item because open source 3D printing can easily offset their capital costs by enabling consumers to avoid costs associated with purchasing common household objects[6,12].

A plastic filament or metal wire is unwound from a coil and supplies material to an extrusion nozzle which can turn the flow on and off. The nozzle is heated to melt the material and can be moved in both horizontal and vertical directions by a numerically controlled mechanism, directly controlled by a CAM software package. The model or part is produced by extruding small beads of thermoplastic material to form layers as the material hardens immediately after extrusion from the nozzle. Stepper motors or servo motors are typically employed to move the extrusion head.

The process can be schematized as follows:

1. The filament passes through the heated liquefier and acts as a piston to extrude a continuous bead of molten material through the nozzle;
2. The bead is deposited on a platform that indexes down after each layer is completed.

Bonding of beads and layers occurs thanks to the adhesiveness of partially molten material, leading to the fabrication of the object.

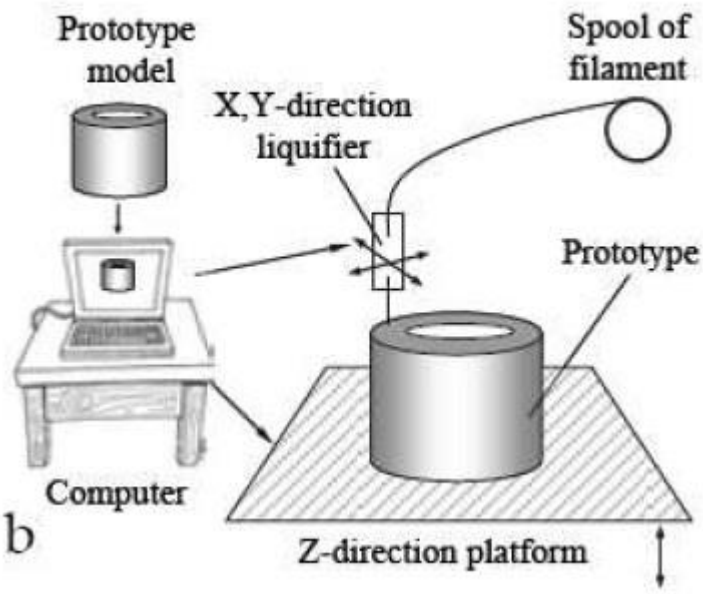

Figure 14. Schematic representation of Fused Deposition Manufacturing[10]

FDM technique leads to good component strength and minimum wastage, but also limited accuracy (function of the nozzle diameter) and general slowness caused by limited extrusion rates.

The Fused Deposition Manufacturing of Ceramics (FDMC) was developed just in 1997 by A. Safari; filaments of about 1.8mm diameter were made of a mixture of ceramic powder (50-55vol%) and a six-component thermoplastic binder system made of polymer, elastomer, pacifiers, wax, surfactant and plasticizer. The process leads to the formation of a green body; then the object is removed from the substrate and a heating treatment is performed in order to eliminate the organic additives.

FDMC, as well as the other technologies specifically designed for ceramics, is usually much more expensive than a printer which is designed for polymers; one of the challenges of this work has been therefore to adapt a commercial FDM printer which has been designed for thermoplastics (ABS, PLA) to make it print a structure made of preceramic polymer; this would decrease dramatically the cost of a ceramic prototype, with great benefits in the biomedical field. The apparatus used for this work, with all its characteristics and limitations, will be described with more detail in the experimental section (see Chapter 4).

CHAPTER 3: BIOMATERIALS AND TISSUE ENGINEERING

The need of materials suitable for surgical implants takes its origins in the ancient times: Egyptians, Greeks and Romans used vegetal fibers and animal derived materials to sew wounds; first prostheses were made of wood and worked surprisingly well. From the last century metals started to be used commonly for dental implants; the rise of stainless steels and alloys made possible to fabricate each kind of prosthesis. Chronologically, various plastic materials, ceramics and composites followed.

With the increasing demand of solutions to improve remedies and illness recovery, collaboration between medicine and materials engineering starts to gain some importance: it is the birth of the tissue engineering, defined by the USA National Institute of Health as "a rapidly growing multidisciplinary field involving the life, physical and engineering sciences that seeks to develop functional cell, tissue and organ substitutes to repair, replace or enhance biological function that has been lost due to congenital abnormalities, injuries, diseases or aging"[13].

Our focus is not on cells and biologic materials but on synthetic materials that can mime and reproduce the functionality of the damaged tissue; according to its IUPAC official definition, "biomaterial is a material exploited in contact with living tissues, organisms, or microorganisms".

From a more practical approach, biomaterials are all materials commonly used to fabricate medical devices like prostheses, bone implants, artificial tissues and organs; they have to operate with an intimate contact with living tissues minimizing eventual reject reactions.

Fundamental requisites of a biomaterial are:

- Biofunctionality: the implanted material has to offer reasonable mechanical properties;
- Sterilizability: material has to be sterilized without losing its biofunctionality;
- Biocompatibility: material has to promote a favorable reaction (or at least no reaction) from the living system for the specific application in which it is involved;
- Biomimic: an ideal implant has to behave like the host tissue: this means that the interface between implant and living tissue has to be made of the same kind of tissue and it has to respond in the same way to the organic stimulus.

Biomaterials can be classified in different ways depending on where the focus is; considering their evolution into the living body, they can be divided into biostable and biodegradable materials.

Biostable materials are not object of substantial chemical and/or physical modifications as time goes by; biodegradable materials, on the other side, bear chemical and/or physical transformations which lead them to disappear after a time.

Focusing on the interaction with the host organism, materials can be:

- Biotoxic: they cause an adverse reaction with the biological tissue due to chemical and/or galvanic processes; examples from this category are some Ni alloys, Cd, V, some steels, carbides and methylmetacrilates.
- Bioinert: they are chemically and physically stable after implantation and show a good coexistence with the organism with minimal interactions with the environment; examples are Ta, Ti, Al and Zr oxides and UHMWPE. Bioinertia can be forced through a morphological fixation with glues or cements which avoid direct bonds between implant and tissues, but it leads to unstable implants and problems in orthopedic and dental applications.
- Bioabsorbable: they gradually degrade into the organism without reject or toxic reactions.
- Bioactive: they are not only bioabsorbable, but they are also gradually replaced by biological tissue; direct biochemical interactions with the organic tissue are favored, so that the tissue can grow on the material surface itself with a strong mechanical bond between natural tissue and prosthesis.

Bioactivity is the most favorable condition in order to design and develop implants with minimal reject and inflammation risks, but absorbance and reactions need accurate design. Materials chemical release kinetics have to be controllable and perfectly synchronized with the modification sequence of cells for wound recovery. If dissolution rate is too high, ion concentration is also too high and therefore ineffective; on the other hand, too low rate means too low concentration in order to stimulate cell proliferation and differentiation.

In the following paragraphs the interactions between material and tissue are analyzed with special attention on bone implants, whose development is one of the goals of this work.

Bioceramics for bone repair:

In order to realize 3D scaffolds for bone repair, polymers are difficult to be used because of their low mechanical strength; therefore bioceramics are gaining more and more interest. Their applications include hips, teeth, tendons, ligaments substitution, maxilla-facial reconstruction, bone fillers after tumor removal operations[14].

Bioceramics are inorganic non-metallic materials characterized by partly covalent ionic interatomic bonds; they can be monocrystals, polycrystals, glasses, glass-ceramics or composites.

What makes an interface favorable for bone cells to attach and proliferate is the mineralization of the implant surface, which permits the formation of a natural bond between living and non-living materials.

To select the proper material for a bone implant, some other studies and classifications have been proposed; Hence has introduced a bioactive index linked to the time needed by the interface to form a bond with the bone tissue with more than 50% of its surface[15]:

$$I_B = \frac{100}{t_{0.5bb}} \quad (1)$$

Materials with $I_B > 8$ (class A) form bonds with both soft and stiff tissues; those with $I_B < 8$ (class B) can just bond with stiff tissues.

In 1994 another biomaterial classification has been proposed:

- Class A: osteoproductive materials. Osteoproduction has been defined by Wilson as "the colonization process of a bioactive surface with free staminal osteoblasts" [16]; it occurs when a material causes both an intra- and extracellular response on its interface.
- Class B: osteoconductive materials. An osteoconductive implant is just a biocompatible surface above which bone cells can migrate, so it causes just an extracellular response.

What causes the strong interaction between biomaterials for bone repair and human tissues is the mineralization of the implant itself. Bone matrix is basically made of organic collagen and inorganic carbonated hydroxyapatite (HA, $Ca_{10}(PO_4)_6OH_2$) with low crystallinity; whose natural analog is the mineral hydroxyapatite. Natural HA does not satisfy the medical standard of chemical purity, and for the same reason HA obtained from animal bones cannot be used without sophisticated preliminary purification. An implant which can develop a HA coating is therefore the ideal solution to stimulate cells to attach and proliferate. In this sense ceramic biomaterials are gaining more and more importance: silicates in glasses and other materials can easily bond with Ca and when merged into human blood plasma (or simulated body fluid) they can lead to HA formation.

Since the 1990s, wollastonite ($CaSiO_3$) ceramics have been studied as artificial materials for artificial bones and dental roots because wollastonite exhibits good bioactivity and biocompatibility[17].

The mechanism of apatite formation on the surface of wollastonite in human blood plasma is basically led by ion exchanges within the implant surface and the solution; in fact, human plasma can be seen as an aqueous solution of proteins and salts, whose exact composition is shown in the table below:

Water	90%
Proteins	8%
Organic substances	1.1%
Inorganic salts ions:	0.9%
Sodium	135-146 mM
Potassium	3.5-5.2 mM
Calcium	2.1-2.7 mM
Carbonate	23-31 mM
Phosphate	0.7-1.4 mM

Table 3. Human blood plasma composition[18]

The ionic activity product (IP) of HA in human blood plasma has been considered to be crucial for the formation of HA; the increase in the calcium ion concentration and pH of the solution can result in the increase in the IP of HA and thus to its precipitation on the surface of the substrate.

HA formation on the wollastonite in human blood plasma is schematically illustrated in the following figure.

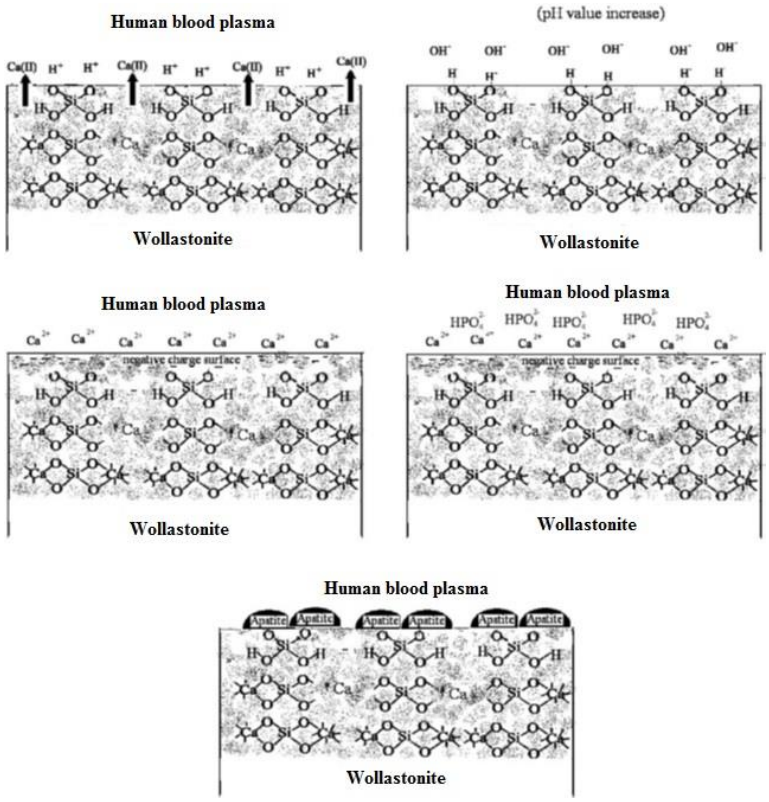

Figure 15. Mechanism of HA formation on wollastonite[19]

The mechanism of HA formation on wollastonite can be interpreted as follows:

1. Calcium ions from wollastonite exchange with H^+ in the solution leading to the formation of silanol ($\equiv Si\text{–}OH$) in the surface layer:

$$\equiv Si - O - Ca - O - Si \equiv \ + 2H^+ \ \rightarrow \ 2 \equiv Si - OH + Ca^{2+} \qquad (2)$$

   Reaction is accompanied by a pH increase and finally by the production of a negatively charged surface with the functional group ($\equiv Si\text{–}O^-$):

$$\equiv Si - OH \ + \ OH^- \ \rightarrow \equiv Si - O^- + H_2O \qquad (3)$$

2. Calcium ions in the solution are initially attracted to the interface with the material. The phosphorus concentration decreases but that of calcium increases with depth. It indicates that calcium accumulation on the silica-rich layer takes place prior to that of phosphorus.
3. Subsequently, the IP of HA at the interface is higher than in the bulk solution and high enough such that HA precipitates on the coating surface.
4. As soon as HA nucleates on the material surface, spontaneous growth occurs and calcium and phosphate ions are consumed from the surrounding body fluid.

After HA formation, growth factor absorption and thus attach, proliferation and differentiation of preosteoblast cells follow.

Two types of interaction between implant and tissue can occur:

- Extracellular interaction led by material surface properties; nanometric porosity and $\equiv Si-O^-$ groups on the surface play and important role in protein and collagen absorption. Absorption is followed by coagulation and cell adhesion system activation; interactions between osteoblasts and their protein ligands contribute on cell adhesion. Another remarkable consequence of protein absorption is proenzymes transformation into active enzymes. All substances on the implant surface have a direct effect on cell differentiation and proliferation: on bioactive ceramics osteoblasts proliferation is favored.
- Intracellular interaction caused for example by soluble Si release; studies showed that it can be a strong growth factor for human osteoblasts leading to a faster bone regrowth.

Osteoblasts create an extracellular matrix (ECM) which mineralizes in nanocrystals and collagen on the implant surface while the bioactive implant itself degrades with time. It is really important to tailor the implant solubility and bioreactivity in order to develop new materials for in situ regeneration and tissue engineering.

Bone tissue engineering:

Tissue engineering is a promising approach for reconstruction and regeneration of tissues and organs damaged or lost because of trauma, injuries, illnesses or aging; it can also offer a solution for the lack of tissues and organs as transplantations[14].

Actually the best alternative in reconstructive medicine consists of autograft, where the patient's tissue is removed from a donator site and implanted on the damaged zone; other options are allografts and xenografts. Where organ transplantation is not needed, artificial prostheses are chosen.

All orthopedic implants in use in these days lack in the three most important living tissues properties: auto-repair, correct blood amount and response to environmental stimuli like mechanical loads. Moreover, their limited duration leads to the need of later interventions which can be expensive and dangerous.

Tissue engineering approach intends to overcome these limitations through the use of biomaterials designed to stimulate the patient's own cells: they should be withdrawn from the patient and seeded on a synthetic scaffold which would act as a guide and would stimulate tissue growth creating a living biocomposite, then is could be implanted in the patient; the scaffold should reabsorb in the body releasing non-toxic substances with the same rate as cells produce their ECM.

Bone formation:

In order to regenerate a bone, the scaffold should mimic the own structure of the bone and stimulate new bone growth if seeded with osteoblasts.

Starting point for new bone formation is preosteoblasts mitosis, which is activated by chemical stimuli from the environment; each cell cycle begins after the previous mitosis is completed. After this transition from G0 to a critical growth stage G1, the cell starts to synthesize DNA and duplicate chromosomes (stage S). After an accurate control by DNA repair enzymes, followed by a critical mass increase and by the synthesis and activation of various growth factors (stage G2), another mitosis process occurs. If the environment does not permit G1 or G2 completion the cells proceed with a scheduled death called apoptosis.

Figure below shows preosteoblasts changes in presence of biological active ions.

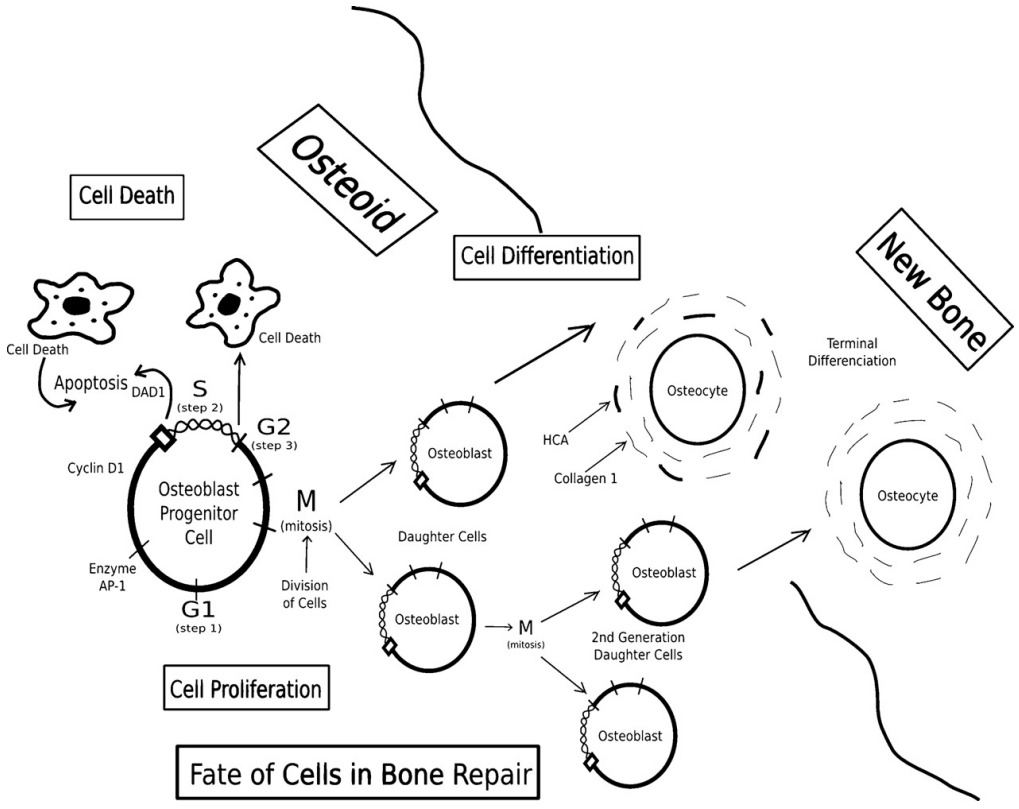

Figure 16. Schematic of osteogenic progenitor cells cycle[15]

Class A materials like bioactive glasses are the only ones able to force a rapid bone formation *in vivo* through osteoproduction process. Class B osteoconductive materials like synthetic HA do not produce the proper conditions to form new mineralized bone but lead to structures similar to scar tissue ones; what lacks is the release of critical concentrations of bioactive ions with the proper rate. For this reason implants made of class B materials are promising but have to be proper designed and functionalized with growth factors etc. in order to be effective for bone repair applications.

Cell cycle however not only forms the structure for their own proliferation but also determines functions and differentiation of some existing cells; osteoblasts are responsible for Type 1 collagen production, osteocytes for ECM production and mineralization, the last one being a crucial step because of the importance of HCA-collagen bond for the bone mechanical properties.

To sum up, bone tissue formation follows several steps:

1. Non-differentiate mesenchymal cells activation and migration through chemotaxis;
2. Cell fixing on matrix through fibronectin;
3. Mitosis and mesenchymal cells proliferation led by growth factors;
4. Cartilage mineralization;
5. Vascular initialize and chondrolysis;
6. Osteoblast differentiation and bone matrix deposition;
7. New tissue mineralization.

For all these steps to be completed, there is the need of:

- An osteoconductive signal;
- a substrate able to receive the signal and to be the support for bone formation;
- non-differentiate cells able to become osteoblasts, fibroblasts and cementoblasts.

Bone structure:

Bones are constituted of highly specialized connective tissue in which osteocytes and a particularly stiff intercellular substance stand out; stiffness is due to the presence of microscopic mineral crystals of calcium phosphate, calcium carbonate and lower quantities of magnesium phosphate and calcium fluoride. Bone is made for the 85% of needle-like HA crystals with 20-40 nm length and 1.5-3 nm thickness; also other apatites (like fluorine apatite) are present[20-22].

These crystals are merged in a collagen fibrils matrix. From a structural point of view, compact bones and spongy ones (with alveolar structure) can be distinguished; focusing of collagen fibers dimensions and disposition, bone tissues divide into fibrous and lamellar. Most of bones are made of lamellar tissue: collagen fibers are organized into overlaying concentric lamellae forming large hollow fibers of about 200 μm diameter named osteons. Haversian canals, cylindrical pores in the osteon center, contain blood vessels which nourish the tissue. Pores and lacunae in the lamellae provide space for the osteocytes; from the lacunae radiate the canaliculi, very fine channels which build a continuous cavity system in which metabolic and gas exchanges between blood and cells are possible.

These specific structural features have been associated with various physical properties: stiffness of bone arises from the composite structure of mineral microcrystals and protein fibers. Slow creep results from slip at cement lines between osteons; the cement lines act as weak interfaces imparting toughness to the bone. The pore structure of bone is essential in maintaining its viability and consequently its ability to adapt to mechanical stress.

Figure below shows a schematical of bone hierarchical structure.

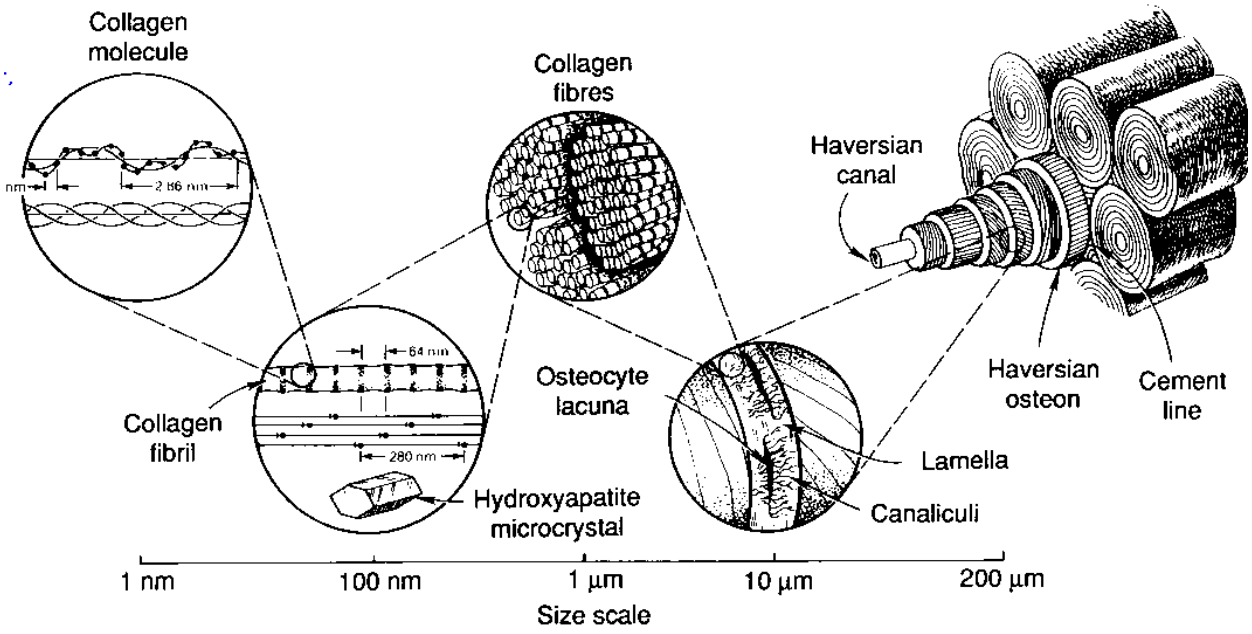

Figure 17. Hierarchical structure of human compact bone[20]

Scaffolds for bone repair:

An ideal scaffold mimics the host tissue ECM working as a 3D template for the cells to attach, proliferate and migrate; criteria to be satisfied in order to have bone restoration are:

- material biocompatibility;
- 3D growth promotion;
- Interconnected macropores network with pores bigger than 100 μm to allow cell penetration, tissue growth, vascularization and nutrients transport;
- Mesopores with a diameter between 2 nm and 50 nm to promote cell adhesion;
- Osteoconductive material: scaffold should bond with the host tissue without forming scar tissue;
- Proper surface morphology: it promotes cell adhesion through protein absorption on the scaffold surface, which is a critical step during implantation;
- Proliferation and differentiation promotion;
- Degradation rate equal to tissue restoration rate and releasing of non-toxic and easy to eliminate products;
- Bone shape match;
- Proper mechanical properties;
- Commercially producible and sterilizable.

CHAPTER 4: EXPERIMENTAL PROCEDURE AND CHARACTERIZATION METHODS

Before giving a detailed description of all the operations performed in each experiment, it is important to highlight which guide lines lead the whole work and to present an overview of the followed procedure; thus, a brief description of basilar steps involved in the transformation from polymer and filler to bioceramic is given.
Moreover, measuring techniques and instruments used to obtain quantitative data, images and graphs are introduced; characterization methods used (and therefore presented) are Melt Flow Index, X-ray diffraction (XRD), scanning electron microscopy coupled with energy-dispersive X-ray spectroscopy (SEM-EDX) and bioactivity tests.

Experimental procedure:

The aim of the first part of the work is to develop a mixture of preceramic polymer, filler and eventually additives in order to obtain a material which can be extruded in form of sticks and with proper viscosity and thermal and mechanical characteristics to be formed through Fused Deposition Modeling; finally, it has to overcome a heating treatment at more than 800°C keeping its shape and transforming into wollastonite.

First step is the calculation of the weight ratios between all the active components in the mixture; for this purpose it is taken into account:

- desired final composition, this means wollastonite composition;
- filler (calcium carbonate) stoichiometry;
- filler oxide yield;
- polymer (silicone) ceramic yield.

After that, the need of a plasticizer is also considered. It is necessary to keep in mind that the developing material is meant for biological applications, so each additive should be at least bioinert; because of that, Carnauba wax is chosen and mixtures with different wax amounts are prepared in order to find the proper combinations of strength and viscosity to make the material be printable but also let it maintain its shape during heating treatment.
Calculations are detailed reported in the following chapters (see Chapter 6) for all the experimented mixtures.

Next step is mixing and homogenization of precursors; dry mixing is performed, this means that no solvent is added. This method can be applied because the silicone used is a solid powder at room temperature. In order to achieve a high homogenization degree without adding solvents, mixing process is supported by heating: silicone is fused while mixing is performed and the resulting mixture is milled in order to obtain powder again.

The instrument used is a Brabender® Mixer W 50 EHT equipped with roller blades; polymer, filler and eventually plasticizer powders are poured into the mixer chamber and electric temperature conditioning with compressed air cooling is set. The rotor speed ratio of 2 : 3 (driven to non-driven) results in a high torque resolution; rotors shape, as well as the tight clearance between rotors and mixing chamber, guarantee an intensive, high shear mixing. Individual mixing steps can be switched as a function of speed gradients. Table below offers an overview of mixer technical data.

Mixer W 50 EHT	
Application	Thermoplastics
Volume of mixer bowl approx. [cm^3]	55
Sample weight [g]	40-70
Heating/cooling	el. heating /air
Torque max. [Nm]	200
Speed ratio driven : idle blade	2 : 3
Operating temperature max. [°C]	250 / 500

Table 4. Brabender® mixer W50EHT technical data

Exact powder amounts, temperature sets and speed programs are descripted in detail in the following chapters (see Chapter 6) for all the mixtures experimented.

After mixing and milling, the resulting powder has to be formed into small rods in order to be printed. One method could be extrusion, but previous experiments have showed that it can be risky because of silicone thermosetting behavior: if silicone reticulates in the extruder chamber, then it is really difficult to remove it.

Because of that, it is chosen to adapt a Karg® Melt-Index Tester type MeltFloW basic, normally used for rheological measurements, in order to produce rods of dense material with an appropriate diameter. A melt-index tester is a device to check the flow characteristics (Melt Mass Flow Rate [g/10min] or Melt Volume Flow Rate [cm^3/10min]) of thermoplastic

materials (granules, powder or grinding) in the molten state. According to ASTM D-1238 standard, the material is poured into a vertical chamber in which temperature is set and kept by two thermocouples (one at the top and one at the bottom); a piston loaded with a testing mass is positioned at the top of the chamber and forces the molten material to exit through a nozzle at its bottom. Each 10 minutes the wire is cut with a manual cutting device; then the Melt Mass Flow Rate (MFR) is calculated by weighting the wire pieces obtained with an analytical precision balance.

Table 5 offers an overview of the instrument technical data.

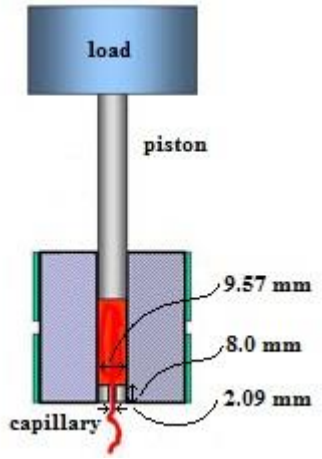

Figure 18. MFI tester parameters

Karg® Melt-Index Tester type MeltFloW basic	
Temperature range	room temperature / 400°C
Testing mass limit	21,6 kg

Table 5. Karg® Melt-Index Tester type MeltFloW basic technical data

For the purpose of rods realization, no MFI measurements are needed; the mixture powder is poured into the Melt-Index tester chamber and molten and the loaded piston forces it to exit through the nozzle in form of a wire which is cut into rods. In order to obtain rods with a diameter which can be compatible with the 3D-printer, a new nozzle with a bigger diameter is designed and mounted in the tester. An accurate description of temperature, load and quantity sets can be found in the following chapters (see Chapter 6).

Once the rods are ready, the preceramic mixture can finally be used as a feeder for the 3D-printer in order to realize samples and scaffolds with a simple geometry.

For this purpose, Itis3D® Maxit 3D-Printer is used. It is a Fused Deposition Manufacturing device able to produce quickly and accurately models and parts directly from 3D digital data; using additive processes, it deposits material, one layer at a time, and can create intricate 3D physical forms. 3D Printing is the term commonly used for low cost (under 10000€) technology. The two key aspects of 3D Printing are that it involves a layering process and that it is additive, not subtractive; the additive nature of 3D printing means that there is very little waste of materials, making it a much 'greener' technology, as no plastic is wasted.

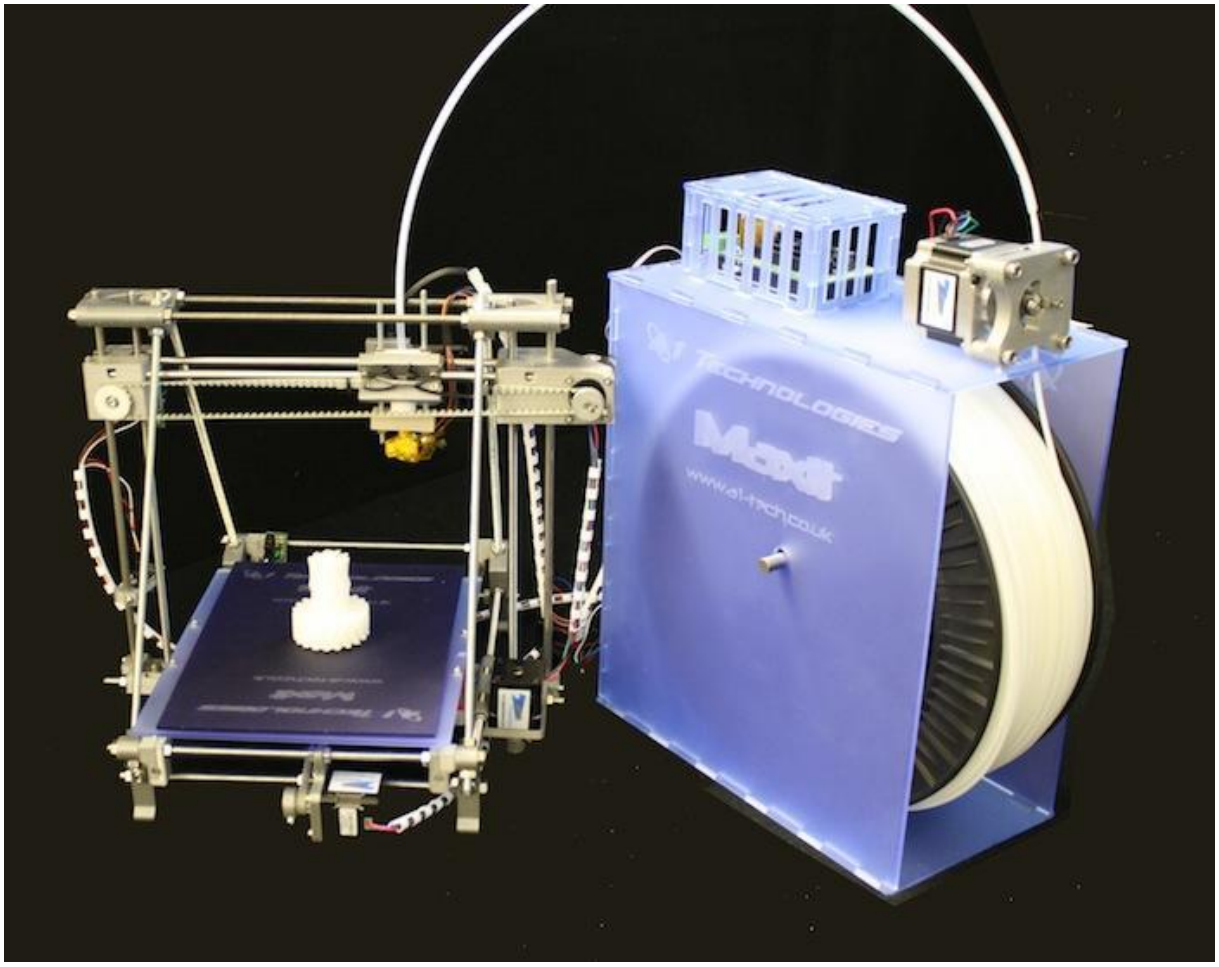

Figure 19. Maxit 3D Printer

The Maxit is a self-assembly 3D printer kit; this allows it to be one of the cheapest 3D-printers on the market. It works with ABS or PLA wires and is able to support uninterrupted and consistent printing operations of complex 3D objects and parts.

Its main features are:

- Low cost;
- Self-assembly;
- Dedicated Graphical User Interface (GUI);
- Plastic parts on Maxit are printed on Maxit printers; this means that if a component breaks, it can be reprinted by the printer itself;
- Quick, reliable and consistent printing;
- Extruder motor remote from the hot end; this allows the printing head to be much lighter with lower inertia and leads therefore to faster printing.

Maxit 3D-printer technical data are summed up in the table below.

Maxit 3D Printer	
Printable area	210 x 160 x 100 mm
Printing speed	Up to 100 mm/s
Layer thickness	0.125 – 0.3 mm
Nozzle size	0.5 mm
Filament size	3 mm
Temperature control	±1°C

Table 6. Maxit 3D Printer technical data

Before printing, a 3D model of the desired component has to be provided: in this work some of the models used are created using Netfabb® Studio Basic 4.9, an open-source CAD software; others are provided by the Maxit kit itself or with the courtesy of Andrea Zocca of BAM Federal Institute for Materials Research and Testing, Germany.

After CAD modeling, the 3D file (.stl format) has to be sliced in layer (.gcode format) in order to be printed by the Maxit; Repetier-Host V0.34® software provided by Itis3D® not only controls printing operations but also converts files through Slic3r® or Skeinforge® software.

Maxit 3D-Printer is not designed for preceramic printing, nor even for silicone printing; one of the main challenges of this work is to customize such a low-cost device in order to print other materials with completely different viscosity, thermal and mechanical behavior.

One of the biggest problems is printer feeding: the extruder motor normally works turning a cogwheel whose teeth hook the plastic filament pushing it in the hot end; preceramic mixture rods are not suitable for the hook because of their high toughness, so a new method has to be found.

Toughness also causes many problems in entering the hot end, so the use of a properly chosen lubricating agent is taken into account. Another important issue is the setting of proper printing parameters, e. g. temperature, extruding and feed rates, pauses and retractions and more. Finally, it is also difficult to remove the samples from the heating bed: to solve this issue, the objects are printed directly on refractory blocks which can overcome the later heating treatment.
All these aspects will be discussed in detail in the following chapters (See Chapter 6).

Once samples are printed, they have to overcome a heating treatment in order to first reticulate and then convert from polymer to ceramic through pyrolysis.
Usually, reticulation is achieved through a separate heating treatment at temperatures between 150°C and 250°C; its aim is to keep the shape of the object during pyrolysis. In this case, there is no need of a separate treatment; that is mainly due to three factors:

- Filler ratio covers more than 50 wt% of the mixture providing structural stability also without an important reticulation;
- During printing process, preceramic material is heated at more than 100°C and kept at this temperature for a while;
- Pyrolysis process is performed with an extremely low heating rate in order to limit pores and cracks formation (due to decomposition gas release).

Thanks to these factors, a unique heating treatment at relatively high temperature is performed in a Naber® oven; the choice of an oxidizing atmosphere (air) allows carbon to be burned. Heating treatment is also presented with more details in the following chapters (see Chapter 6).

Characterization methods:

Density measurements:

For the later rheological measurements an estimation of preceramic rod density is needed; it is performed by dividing the mass of a piece of rod, weighted on an analytical balance, and its volume. In order to evaluate it, the piece of rod is considered as a truncated cone: it is not a cylinder due to gravity action during its formation; its length and diameters are measured with a digital caliber.

Rheological measurements:

In order to define speed and temperature ranges of the printing process, it is important to have in mind the flow characteristics of the preceramic polymer. An extended characterization of the used precursor has been already performed[23] and is reported in the following chapter (see Chapter 5); nevertheless there is no information about the preceramic mixture chosen. A first qualitative analysis of its flow characteristics is therefore performed with Karg® Melt-Index Tester type MeltFloW basic descripted before.

Input data of a MFI test are piston load mass m_{load} and material density ρ; measurements give the mass flow MFI as a result. From this data, viscosity η can be evaluated through:

$$Q = \frac{MFI}{\rho} \tag{4}$$

$$\Delta P = P_{appl} - P_0 = \frac{m_{load} \cdot g}{\pi R^2} - P_0 \tag{5}$$

$$\eta = \frac{\pi r^4}{8Q} \cdot \frac{\Delta P}{\Delta L} \tag{6}$$

Where P_0 is atmospheric pressure, R is chamber radius and r and ΔL are nozzle radius and length respectively.

Shear rate can be calculated from:

$$\dot{\gamma} = \frac{4Q}{\pi r^3} \tag{7}$$

Tests are performed at different temperatures and different loads are applied for each temperature in order to vary the shear rate[24].

X-ray diffraction (XRD):

XRD spectra are performed with Bruker® AXS D8 diffractometer, with Cu-Kα radiation and θ-2θ configuration.

Phase identification is done with the help of Crystal Impact GbR® Match! Phase Identification from Powder Diffraction program and ICDD® PDF-2 Powder Diffraction File.

Samples are therefore finely milled and powders are accurately positioned in a specific sample holder.

Bruker AXS D8 ADVANCE	
Configuration	Theta/2 Theta geometry
Measuring circle diameter	435, 500, and 600 mm
Angle range	360°
Max. usable angular range	-110° < 2 Theta ≤ 168°
Angle positioning	Stepper motors with optical encoders
Smallest addressable increment	0.0001°
Reproducibility	} 0.0001°
Maximum angular speed	30°/s

Table 7. Bruker® AXS D8 technical data

Diffraction is the interference suffered by the electromagnetic radiation diffusing from an object on the radiation path; this phenomenon takes its origins from the coherent sum of electromagnetic waves diffused from atoms belonging to the same reticular plane family.

Rays reflected in one specific direction are reinforced (constructive interference) when the optical path difference between rays ($2d \sin\theta$) satisfies Bragg's law, e.g. it is an integer multiple of the incident monochromatic radiation wavelength.

$$n\lambda = 2d \sin\theta \tag{8}$$

Where n is an integer number, λ the radiation wavelength, d the distance between crystallographic plans and θ the incident angle.

A schematic representation is shown in figure below.

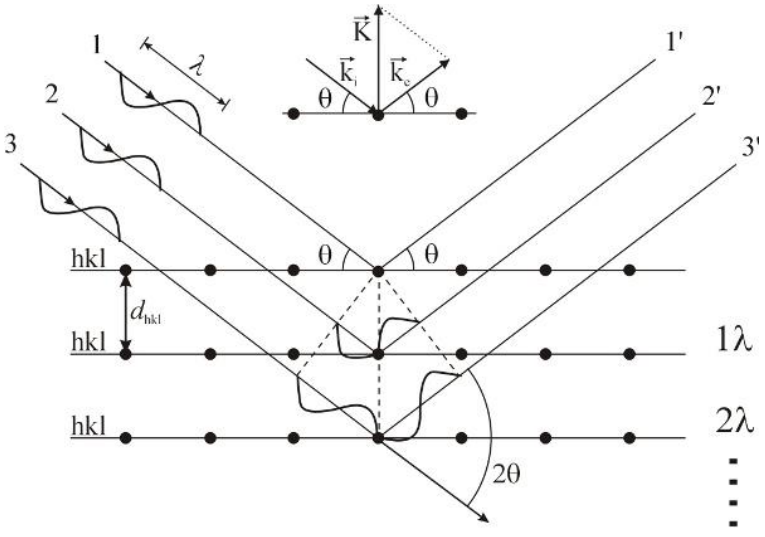

Figure 20. Schematic of X-ray diffraction from a crystal reticulate[25]

Diffractogram shows intensity of the reflected rays as a function of diffraction angle 2θ; it has the shape of a peaks series. From the peaks position it is possible to deduce the present phases; from their intensity and width quantitative composition and crystallite dimension respectively can be estimated.

Scanning Electronic Microscope coupled with Energy-Dispersive X-Ray Spectroscopy (SEM-EDX):

SEM micrographs are obtained with a JEOL® JSM-6490 and permit the study of sample morphology; EDX spectra obtained from IXRF SYSTEMS 500 equipment allow an elemental analysis and chemical characterization of the samples.

Images are produced by bombarding the sample surface with an incident electron beam and acquiring the information from the produced electron beam. The types of signals produced by a SEM include secondary electrons and characteristic X-rays.

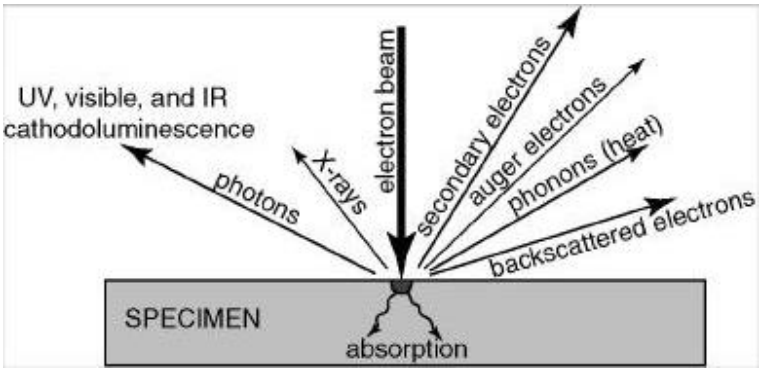

Figure 21. Effects produced by electron-beam interaction with the sample

Secondary electron imaging can produce very high-resolution images of a sample surface. Due to the very narrow electron beam, SEM micrographs have a large depth of field yielding a characteristic three-dimensional appearance useful for understanding the surface structure of a sample. Characteristic X-rays are emitted when the electron beam removes an inner shell electron from the sample, causing a higher-energy electron to fill the shell and release energy. These characteristic X-rays are used to identify the composition and measure the abundance of elements in the sample.

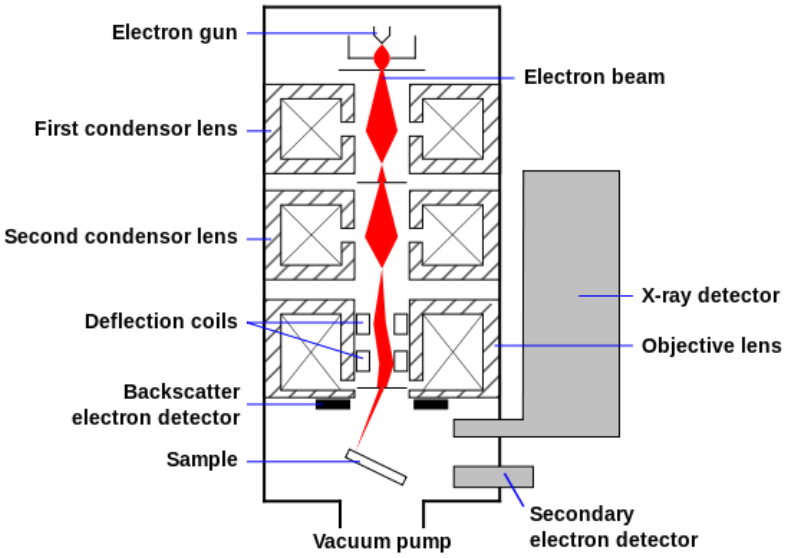

Figure 22. Schematic of a SEM

Bioactivity tests:

Bioactivity tests performed on the pyrolyzed structures. They represent the first of a long series of steps that a biomaterial has to pass in order to be certified and commercialized.

Samples are introduced in a solution with an ion concentration analog to that of human blood plasma and kept at a constant temperature of 37,5°C. Samples are removed from the simulated body fluid (SBF) after different time lapses and HA precipitation on the surface is evaluated.

These tests are performed at the Institute of Biomaterials of Friedrich-Alexander Universität Erlangen-Nürnberg with the help of Professor Aldo Boccaccini and Valentina Miguez Pachego. Environmental conditions are kept stable in an IKA® KS 4000 i control incubator shaker.

This phenomenon is the essential requirement for a synthetic material in order to bond with the natural bone; for this reason such tests permit to make a prevision on material bioactivity. Nevertheless, it is important to remember that even if there is a clear link between HA formation on the material surface and ability to bond with the bone tissue *in vivo*, this method cannot lead to sure and quantitative information but just on qualitative one.

At the end of the SBF immersion time lapse, samples are dried and then characterized through SEM-EDX; it is important to calculate Ca/P ratio in the sample and to confront it with HA ratio which is 1.67.

CHAPTER 5: MATERIAL SYNTHESIS AND CHARACTERIZATION

A detailed description of the reagents chosen for the preceramic mixture is presented in this chapter; particular attention is given to silicone resin, whose physical and rheological properties are discussed in detail in order to fix the limits on its processability and formability. Recipes and detailed steps followed in order to produce the preceramic rods are then discussed; three mixtures with different weight ratios are designed and realized and their differences are highlighted in terms of processability and final ceramic composition in order to choose the best combination of properties. The winner is then characterized through rheological investigations.

Silicone resin:

As already introduced in the previous chapters, silicone resin used in this work is Silres® MK produced by Wacker Chemie GmbH®. It is a solvent-free, solid (powder) methyl silicone resin with high reticulation degree and heat resistance and has a really high SiO_2 content; the use of an oxidizing atmosphere favors SiO_2 formation rising silica yield compared to pyrolysis in inert atmosphere: in the first case there is a 84 wt% yield, in the second a 64 wt% yield (after complete oxidation, expressed in terms of solid resin [DSC]). It is soluble in aromatics, esters, ketones and selected paraffins and chlorinated hydrocarbons.

According to the producer, other special features are:

- very high binding strength;
- little smoke evolution on pyrolysis;
- excellent thermal stability;
- ideal for producing non-stick mixtures like prepregs with excellent storage stability.

The resin is said to be permanently stable up to 300°C. Above 350°C and as the temperature rises, the methyl silicone resin undergoes oxidative degradation to silica, carbon dioxide and water. Very little smoke evolves during this thermal degradation and soot-like decomposition products are not formed. The SiO_2 backbone left behind after decomposition joins the fillers into shapes of high mechanical strength. The heat resistance of products ceramified in this way is limited by the fillers and support materials employed.

Silres® MK can be cross-linked both thermally (T > 150°C) or through a proper catalysis.

Silres® MK	
Class	Methyl-polysilsesquioxane
Physical form	Solid - Powder
Apparent density (kg/m^3)	500
Water solubility	Insoluble at room temperature
Glass transition temperature (°C)	35-55
Thermal decomposition temperature (°C)	>350
Main ceramic phase / inert atmosphere	SiOC
Composition (at%) (1000°C in N_2)	$SiO_{1.52}C_{0.64}$
Main ceramic phase / oxidizing atmosphere	SiO_2
Ceramic yield (wt%) (at 1000°C in N_2/air)	64/84

Table 8. Silres® MK technical data

In order to process the material through 3D printing, it is important to know other properties that are not mentioned in the previous report like temperature- and shear rate-dependent viscosity, and reticulation kinetics. Viscosity and extrusion feasibility of silicones have been widely investigated[26-33]. In a previous work have been already performed some investigations through DSC and rheological tests in order to extrude a similar mixture of MK and fillers[23]; results are shown here below.

DSC measurements:

Samples of 5-10 mg weight have been analyzed in a TA Instruments® DSC Q200; temperature has been equilibrated at 20°C, then temperature gradients of 20, 15, 10, 5°C/min to a final temperature of 300°C have been set; after 1 min permanence at 300°C, cooling with 40°C/min rate to 20°C has been set. It has been marked that silicone completely reticulates at about 220-250°C depending on the heating rate and undergoes no state transformations during the cooling stage; this second part of the graph is therefore omitted. Permanence at 300°C is needed to assure that all the material is reticulated also with the faster gradients.
Resulting graphs are presented in Figures 23-26.

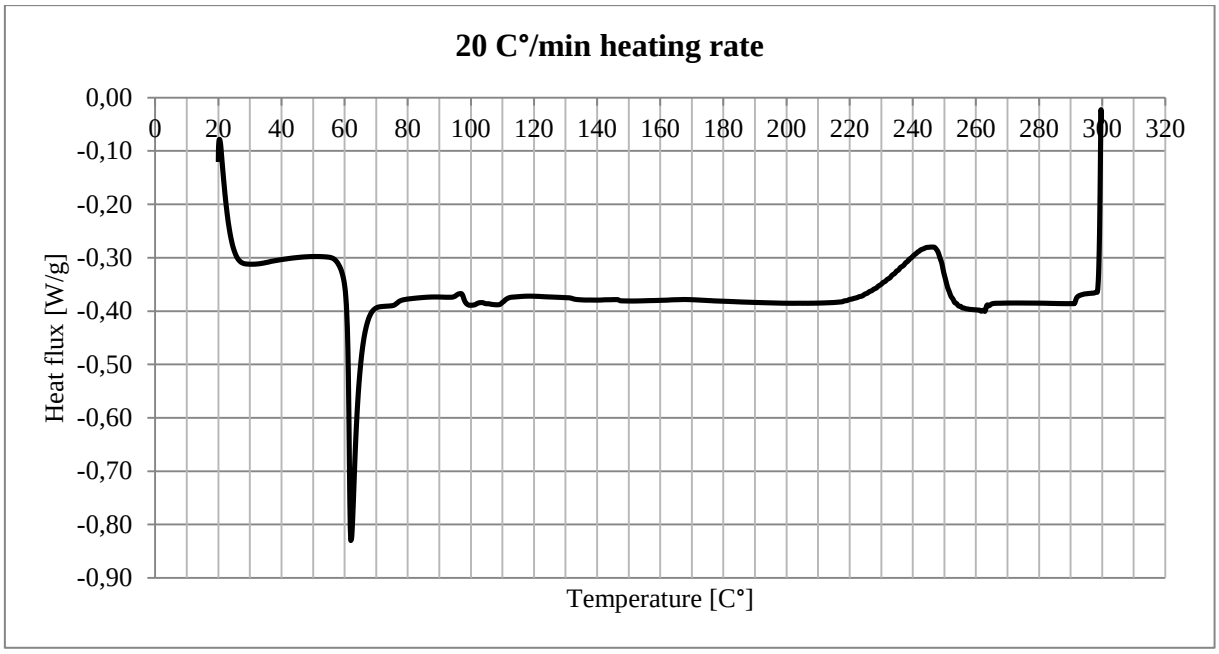

Figure 23. Silicone DSC at 20°C/min heating rate[23]

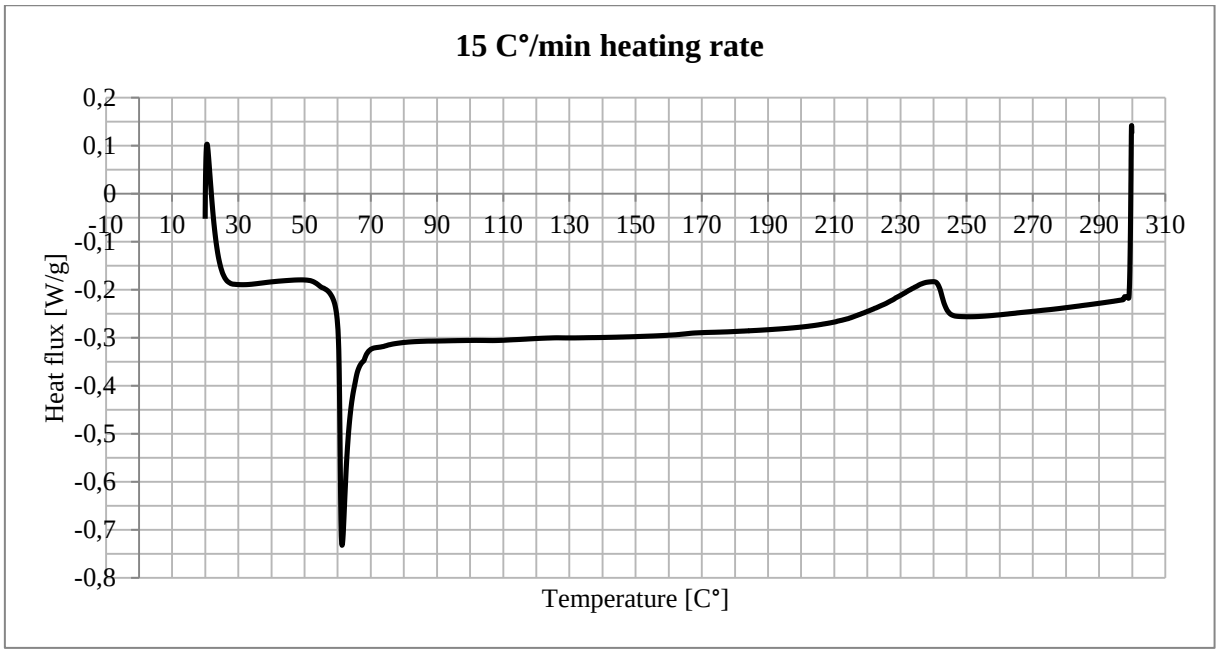

Figure 24. Silicone DSC at 15°C/min heating rate[23]

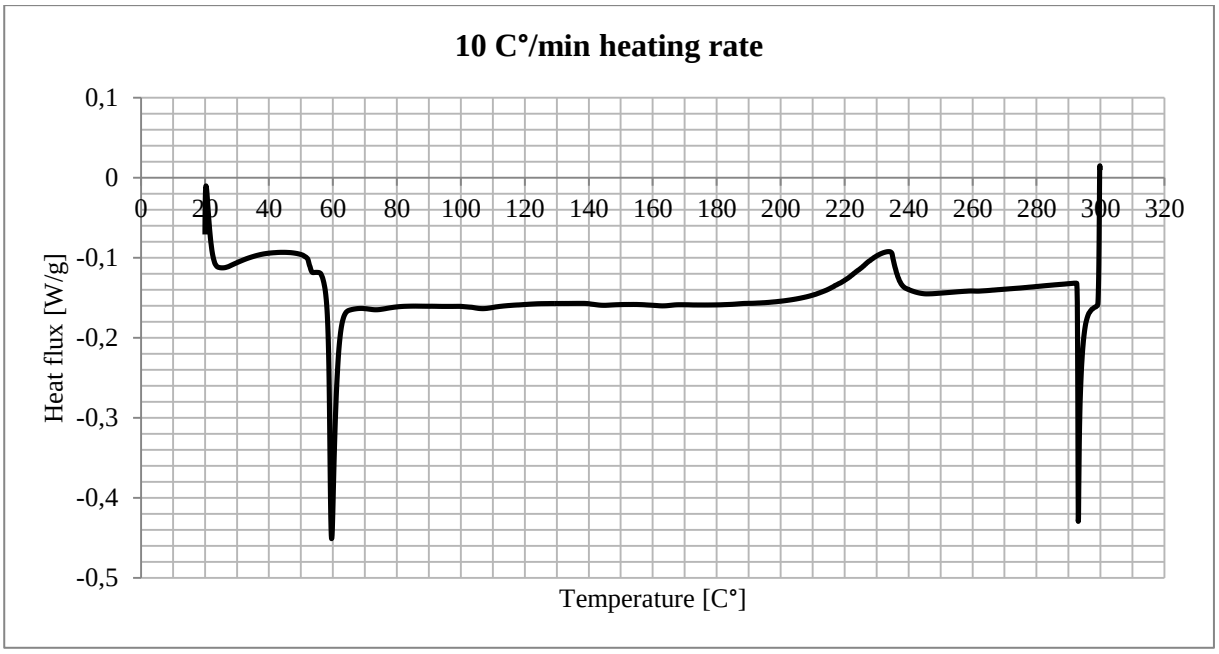

Figure 25. Silicone DSC at 10°C/min heating rate[23]

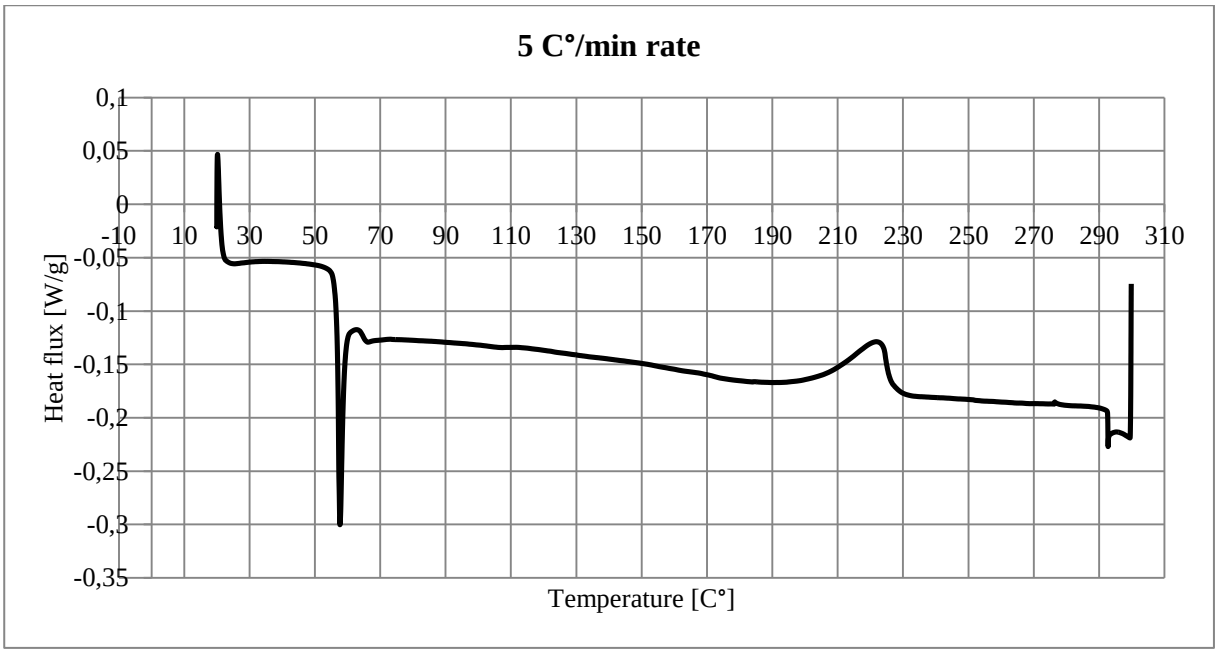

Figure 26. Silicone DSC at 5°C/min heating rate[23]

In all the graphs presented, fusion and reticulation peaks are present; they are shifted at lower temperatures with the decrease in heating rate because of thermal and chemical inertia.

These preliminary tests already show that there is a favorable temperature window for the printing process to occur. Nevertheless, it is better to be sure that reticulation is not too fast at around 200°C in order to prevent mixer, M-I tester and printer from blocking; for this reason other tests have been performed with a higher heating rate (30°C/min) focusing on permanence at high temperature.

Results are shown in Figures 27-30.

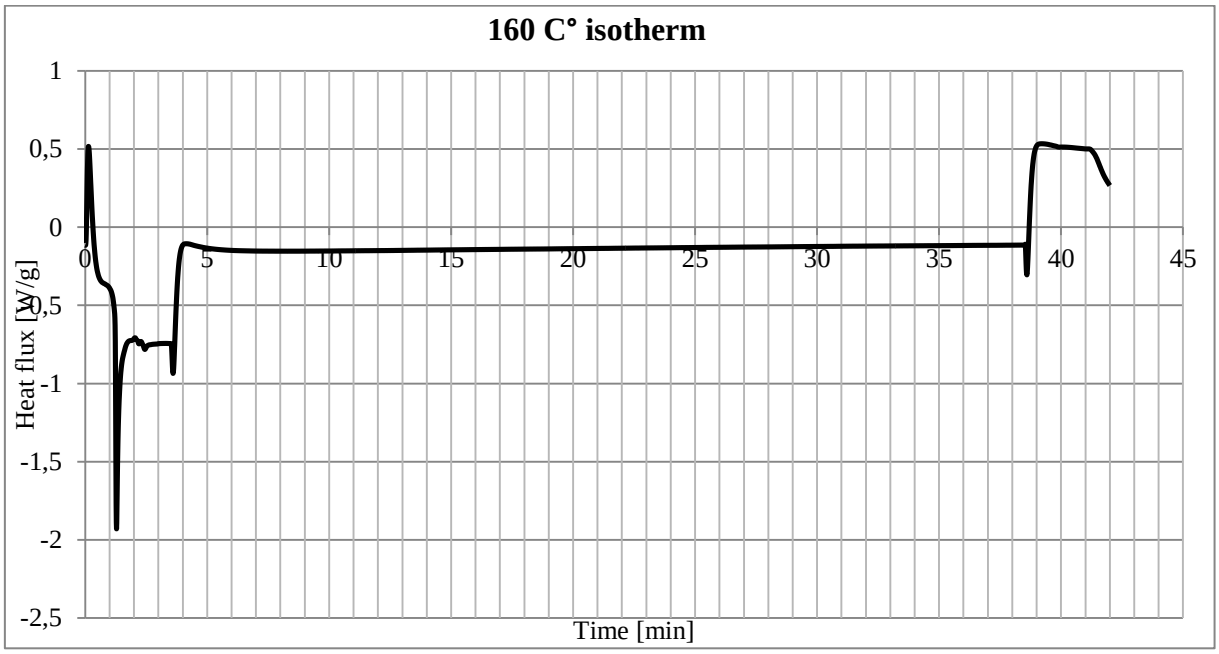

Figure 27. Silicone DSC 160°C isotherm[23]

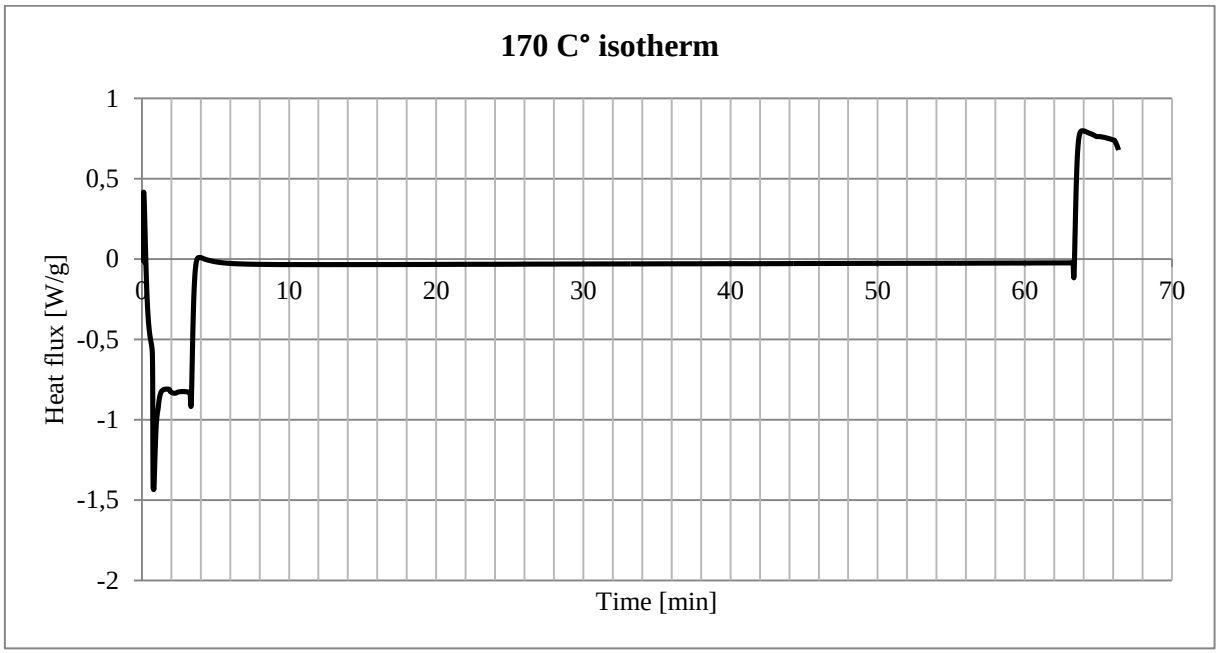

Figure 28. Silicone DSC 170°C isotherm[23]

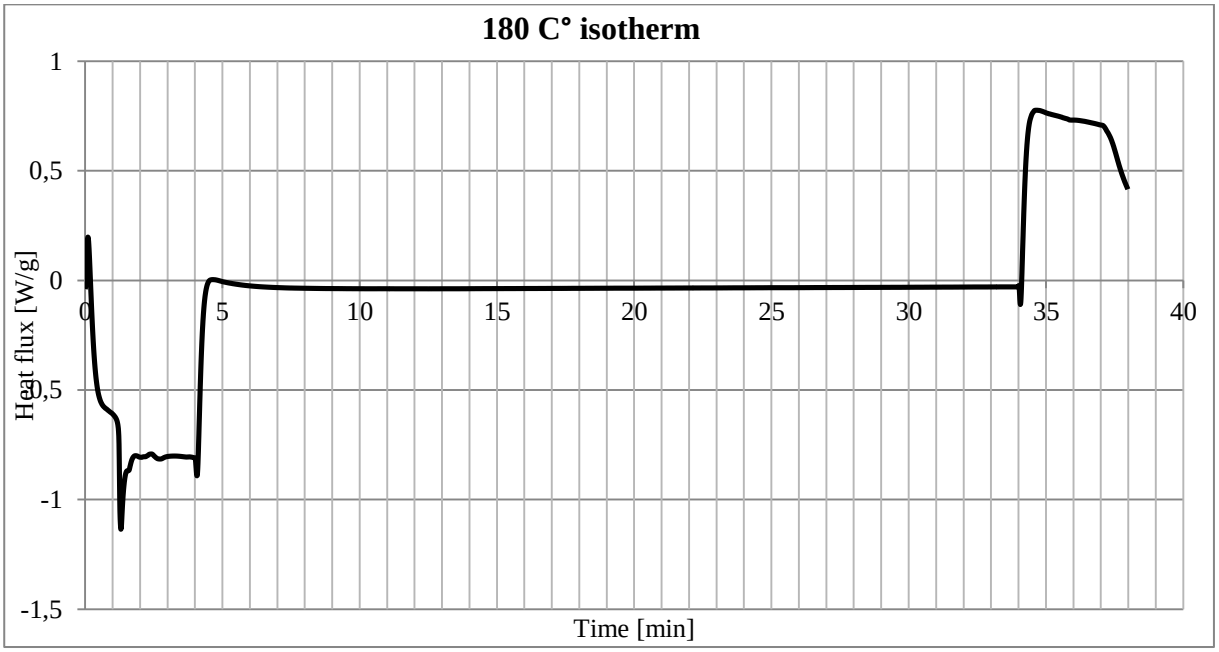

Figure 29. Silicone DSC 180°C isotherm[23]

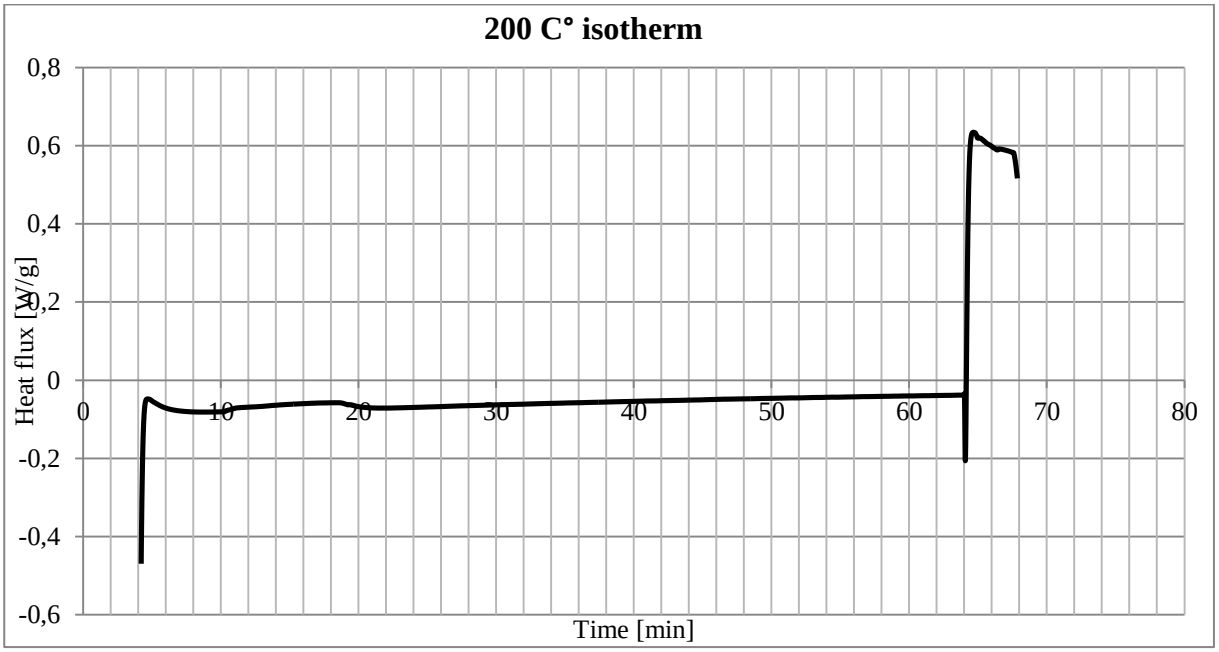

Figure 30. Silicone DSC 200°C isotherm[23]

From these graphs results that just at 200°C reticulation occurs after 5 minutes and in a time lapse of 10 minutes; at lower temperatures no reticulation occurs also after 1 hour. These results allow proceeding with the experimental steps in project without excessive worry about the instruments in use.

Rheological tests:

Rheological tests have been performed in a TA Instrument® ARES parallel disk rotational rheometer; 4 different temperatures have been chosen: 80°C, 100°C, 120°C, 140°C. Silicone viscosity minimum has been found to be at around 120°C[26,30], so this temperature range is the favorite candidate for a forming process.

Measuring steps have involved: calibration of temperature and dishes gap, introduction of the sample, melting and recalibration of the same gap (with exceeding material removal); the shear rate has varied from 10^{-2} to 10^{3} s^{-1} in order to investigate the whole Newtonian plateau. Results are shown in Figures 31-34.

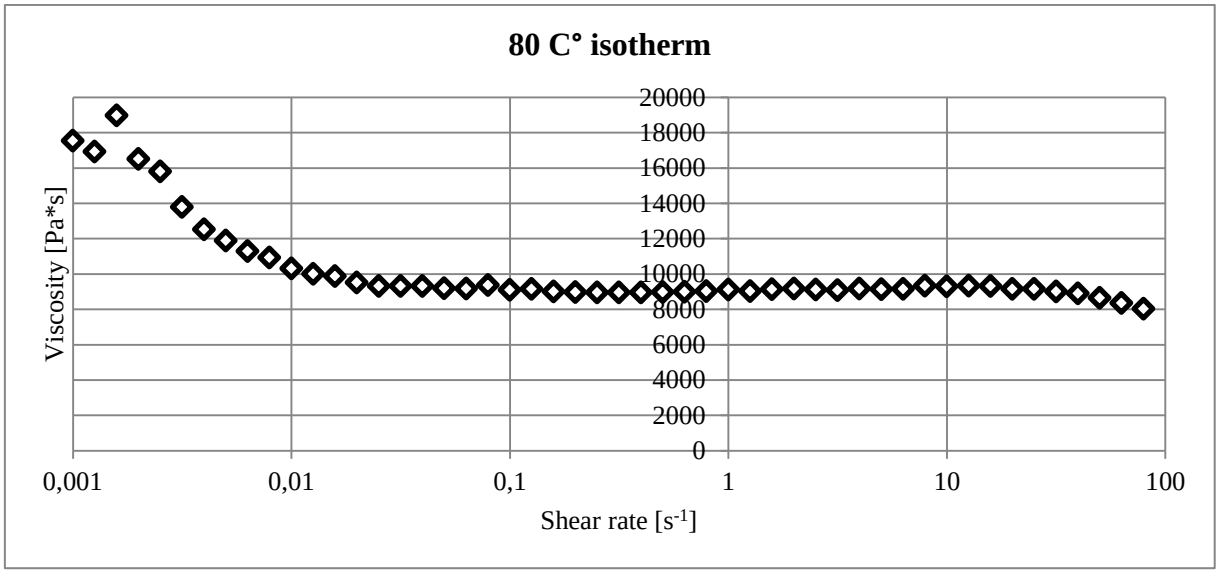

Figure 31. Silicone rheometer 80°C isotherm[23]

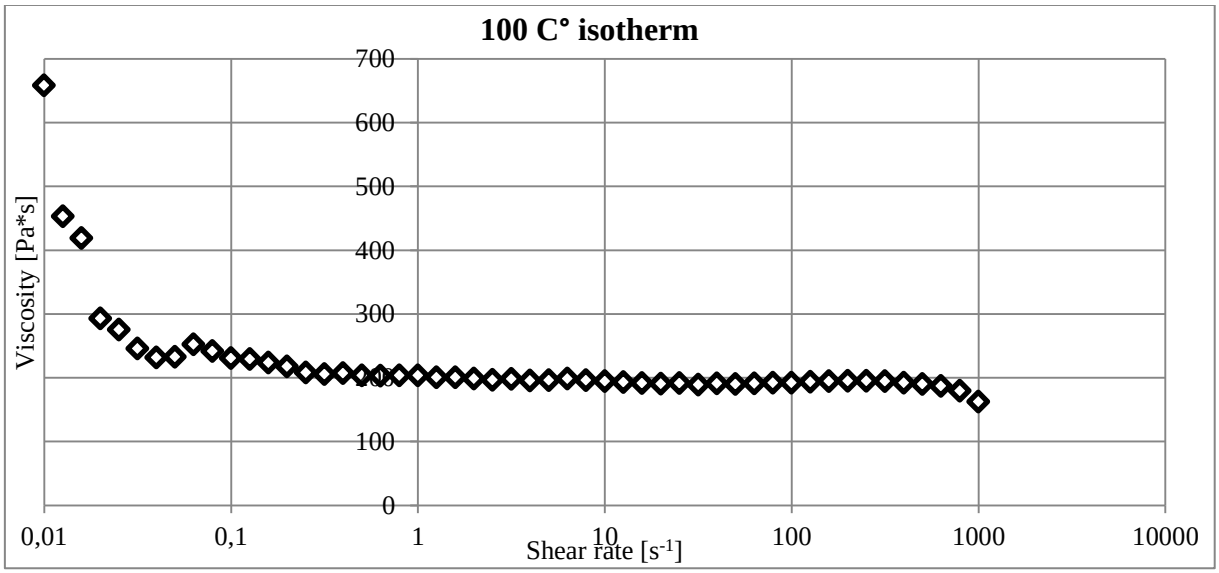

Figure 32. Silicone rheometer 100°C isotherm[23]

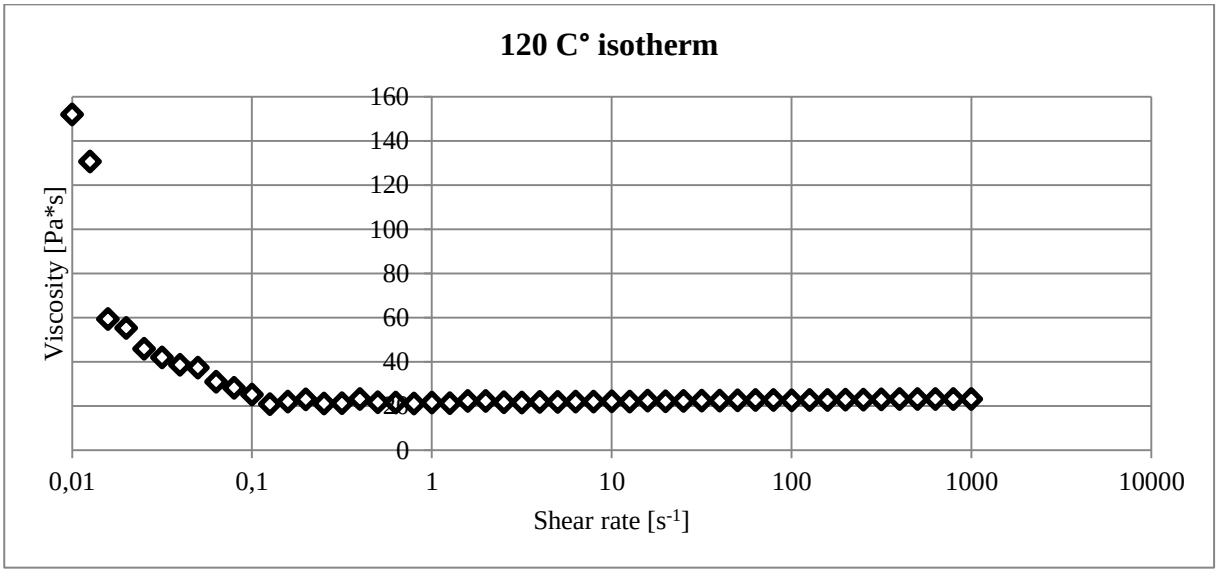

Figure 33. Silicone rheometer 120°C isotherm[23]

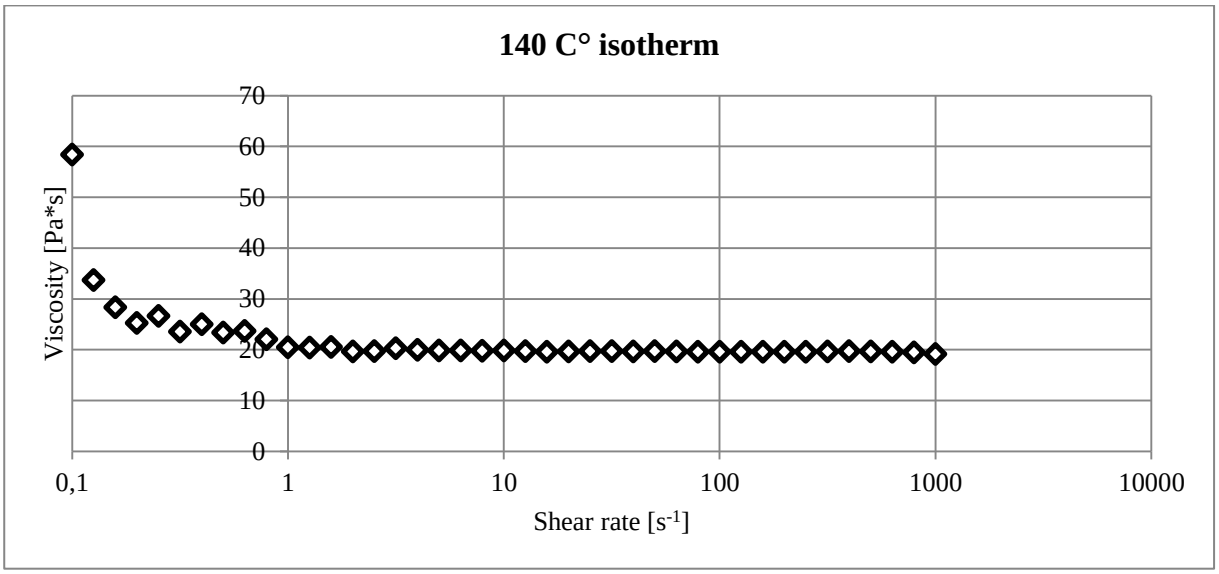

Figure 34. Silicone rheometer 140°C isotherm[23]

At each temperature the Newtonian plateau can be easily detected; from these data an average value of $\eta_0$has been extrapolated for each test. Viscosity as a function of temperature has been evaluated using William-Landel-Ferry (WLF) equation:

$$\eta_0 = D_1 e^{-\frac{A_1(T-T^*)}{A_2+(T-T^*)}} \quad (8)$$

Where A_1, A_2, D_1 are material-dependent constants extrapolated from the data and T^* is the reference temperature.

Fitting parameters and viscosity values are indicated in Tables 9 and 10, followed by the resulting viscosity-temperature graph (see Figure 35).

D_1 (Pa*s)	A_1	A_2	T^* (°C)
$1.75401*10^{18}$	42.23772	5.52955	60.61102

Table 9. WLF fitting parameters[23]

T (°C)	η_0 exp (Pa*s)	η_0 calc (Pa*s)
80	9173	9353
100	196	144
120	22	29
140	20	12

Table 10. experimental and calculated viscosity values[23]

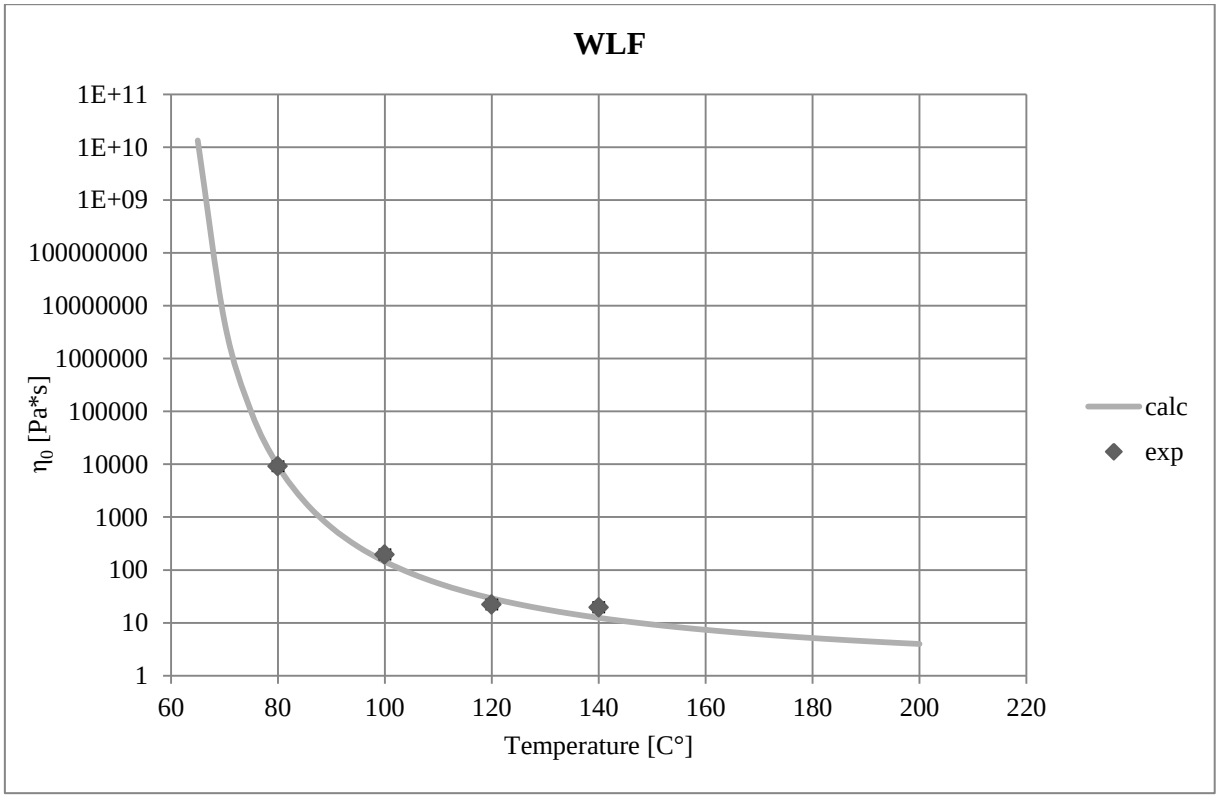

Figure 35. Silicone WLF[23]

WLF equation allows estimating the polymer viscosity in the whole formability range and thus it is really important in order to control the forming process.

Mixture with calcium carbonate ($CaCO_3$):

In order to obtain wollastonite from silicone through pyrolysis, it has to be mixed with an active filler able to evolve as calcium oxide (CaO) which will react with SiO_2 during pyrolysis giving $CaSiO_3$.

A first mixture of just Silres® MK and micrometric $CaCO_3$ powder is prepared following the stoichiometric wollastonite CaO/ SiO_2 ratio; calculations are here reported.

Wollastonite: $CaSiO_3 = CaO \cdot SiO_2 \rightarrow CaO/SiO_2 = 1$

SiO_2 molecular weight: $56.08\ g/mol$

CaO molecular weight: $60\ g/mol$

CaO/SiO_2 weight ratio: $(CaO/SiO_2)_w = \frac{56.08\ g/mol}{60\ g/mol} = 0.93$

For 100 g of SiO_2, 93 g of CaO are needed.

MK silica yield (when pyrolyzed in oxidizing atmosphere): 0.84

In order to have 100g of SiO_2, $\frac{100g}{0.84} = 119\ g$ of MK are needed.

$CaCO_3$ molecular weight: $100.09\ g/mol$

$CaCO_3$ CaO yield: $\frac{56.08g}{100.09g} = 0.56$

In order to have 93 g of CaO, $\frac{93g}{0.56} = 166g$ of $CaCO_3$ are needed.

Weight ratio: $(CaCO_3/MK)_w = \frac{166g}{119g} = 1.4$

Brabender® mixer has a maximum capability of 50g; MK and $CaCO_3$ amounts used are indicated in the table below.

$1.4\ g_{CaCO_3} : (1 + 1.4) g_{tot} = m_{CaCO_3} : 50\ g_{tot} \rightarrow m_{CaCO_3} = \frac{50g * 1.4g}{2.4g} = 29.17g$

$m_{MK} = 50g - 29.17g = 20.83g$

$\frac{29.17g}{50g} 100 = 58.3\%_w\ CaCO_3$

Mixing is performed at a constant temperature $T = 90°C$; initial rotating speed $\omega_i = 10\ rpm$ is increased of 10rpm each minute until a final speed of $\omega_f = 100\ rpm$ is reached and kept for 1 minute; total mixing time is therefore $t = 10min$.

It is important to monitor torque (it should be lower than 100 N*m) and temperature (it should stay lower than 100-120°C) during the process in order to avoid excessive stresses on the roller blades and reticulation inside the mixer chamber.

After mixing process is completed, just 41 g of compound can be recovered from the mixing chamber because of its adhesiveness.

The material is then milled manually with an agate mortar to obtain a coarse powder; then it is used to charge the Melt-Index tester (nozzle used is the standard one provided with the instrument). Temperature is set at 90°C and nozzle is left closed for 3 minutes to allow powder packing; then small rods with a length of about 100 mm and an average diameter of 1.2mm are extruded. Dimensions are not remarkable at this point because these first rods will be used not to print but just to perform chemical and rheological characterization. Note that the help of testing loads is needed in order to extrude the rods because of the material high viscosity.

Adding a plasticizer:

First recipe shows some troubles during mixing and extruding steps; they are mainly due to adhesiveness and viscosity of silicone. It is likely to find the same difficulties during the printing process, which is a much more critical perspective. In order to improve the material processability, the use of a plasticizer is therefore needed; but it is also important that the compound maintains its biocompatibility. Because of that, choice falls on Carnauba wax.

Carnauba wax is an exudation of the Brazilian palm Copernicia cerifera, which produces the wax in the cuticula of its fronds. The leaves are harvested from the wild growing trees by cutting the leaves, trying in the sun and threshing. The crude wax is refined in different variations for cosmetic and food applications.

Carnauba wax consists of:

- 75-85% aliphatic & aromatic (cinnamic acid based) mono- and di-esters;
- 3-6% free wax acids;
- 10-15% free wax alcohols;
- 2-3% lactides;
- 1-2% hydrocarbons;
- 4-6% resins.

Carnauba wax shows a density $\rho = 0.97\ g/cm^3$ an extremely narrow melting curve with a melting point of approx. 84°C; the wax is of high crystallinity and of high contraction, very hard and brittle. It has very good emulsification properties and provides slippery surfaces; it can be added as plasticizer in hot-melts and chewing gums and as lubricating agent in pencils and metal working[34].

Being an edible plasticizer and melting at less than 100°C, Carnauba wax seems to be a good candidate for the preceramic mixture; a compound with 10% wax is therefore prepared, of course respecting the same stoichiometric calculations and instrument limitations presented before.

$m_{tot} = 50g$

$m_{wax} = 10\% \cdot 50g = 5g$

$m_{MK+CaCO_3} = 90\% \cdot 50g = 45g$

$m_{MK} = 1g \cdot \frac{45g}{2.4g} = 18.75g$

$m_{CaCO_3} = 45g - 18.75g = 26.25g$

$\frac{26.25g}{50g} 100 = 52.5\%_{CaCO_3}$

Mixing is performed with the same parameters set before; the resulting compound is much less adhesive and almost all the material is easily removed from the chamber and blades.

Also rods extrusion has to be adapted to the new mixture; at $T_1 = 90°C$ material flows too fast to cut the rods properly, so extrusion is performed at $T_2 = 80°C$.

Pyrolysis and XRD characterization:

Rods made of the two compounds are thermally treated in oven in order to verify if the recipes will convert to wollastonite and if they provide the desired shape stability.

Heating program is set as follows:

1. Heating from room temperature to 900°C with a heating rate of 2°C/min;
2. Permanence at 900°C for 1 hour;
3. Slow cooling in oven.

It is important to underline that no permanence at a mid-temperature (350-450°C) is set for cross-linking; the high filler amount, together with the settled really slow heating rate, are supposed to guarantee enough to reach shape maintenance.

Treatment is performed in a platinum melting pot to avoid contaminations from the pot itself; air is chosen as oxidizing atmosphere.

After treatment, samples are finely milled through an agate mortar and XRD measurements are performed.

Pictures of the treated samples as well as resulting XRD spectra are presented in the following figures.

Figure 36. (a) MK + 58.3% $CaCO_3$ and (b) MK + 52.5% $CaCO_3$ + 10% wax rods after pyrolysis

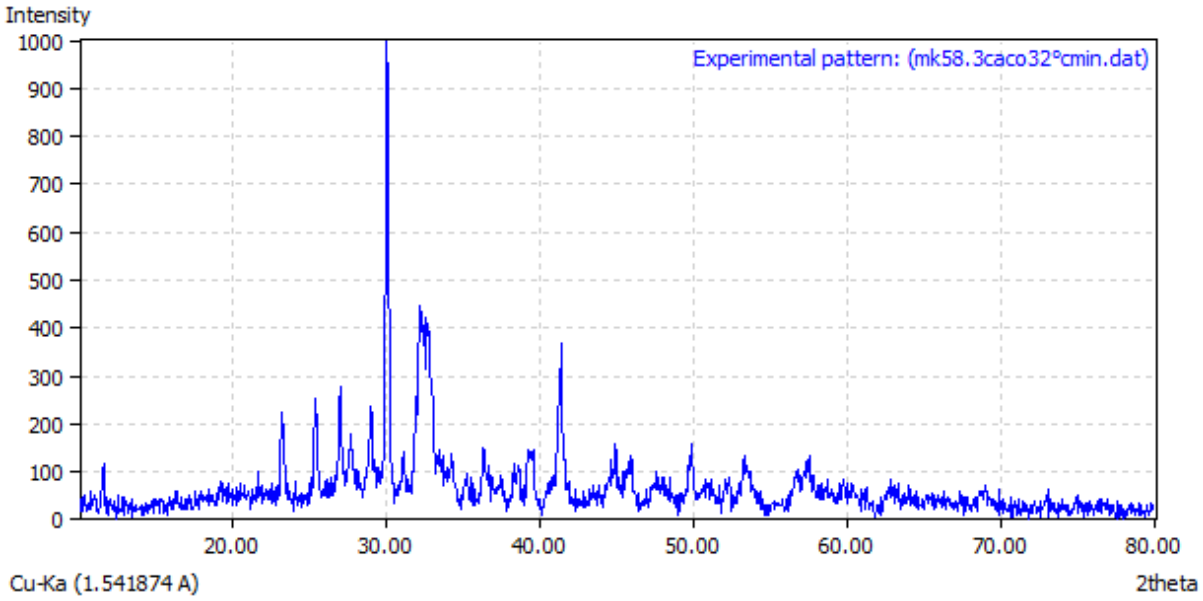

Figure 37. XRD spectrum of MK + 58.3% $CaCO_3$ after pyrolysis with 2°C/min heat rate

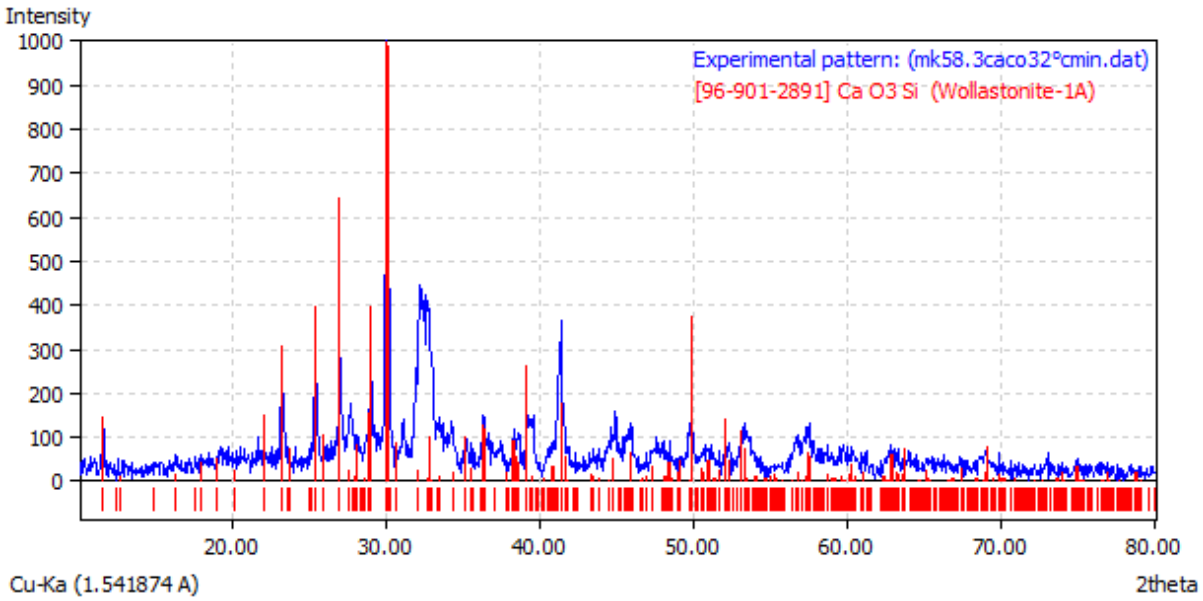

Figure 38. XRD spectrum of MK + 58.3% $CaCO_3$ after pyrolysis with 2°C/min heat rate compared to wollastonite

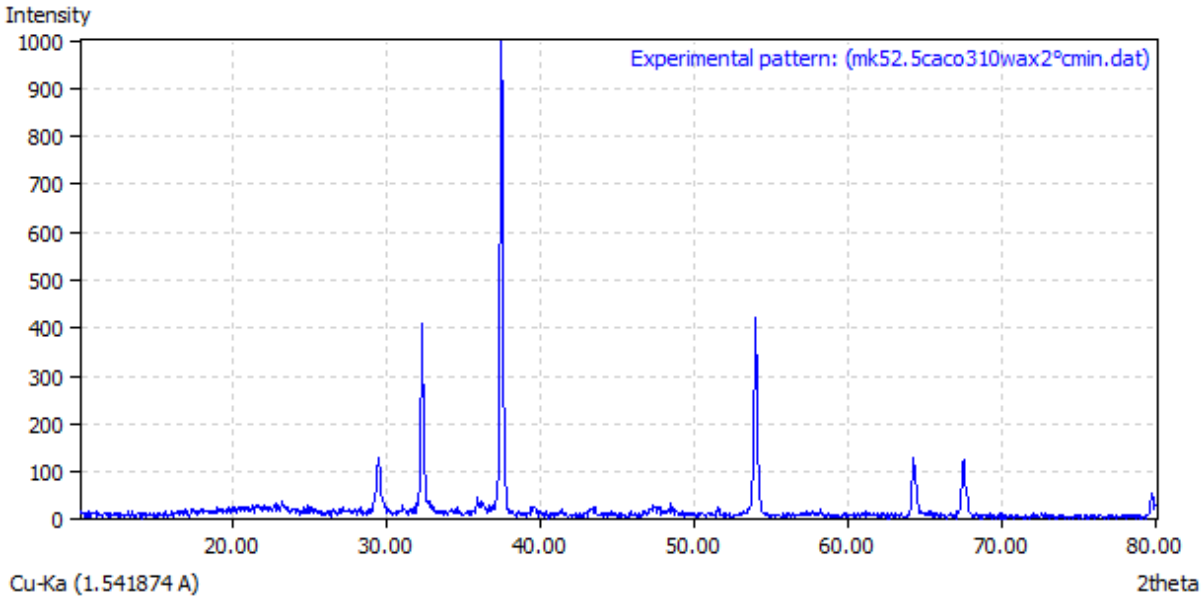

Figure 39. XRD spectrum of MK + 52.5% $CaCO_3$ + 10% wax after pyrolysis with 2°C/min heat rate

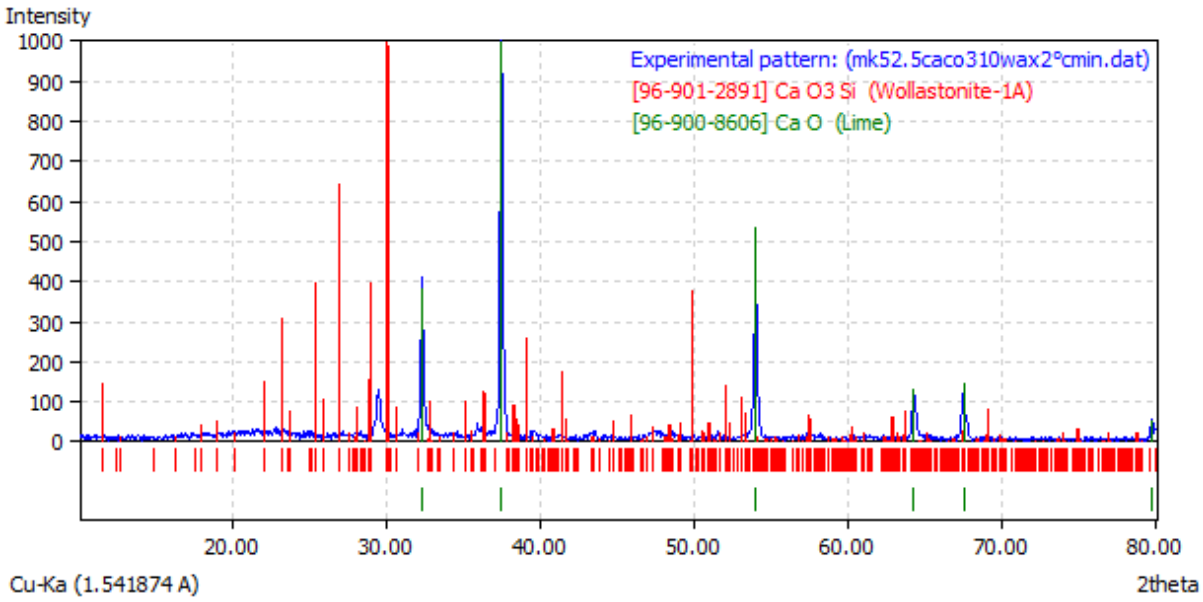

Figure 40. XRD spectrum of MK + 52.5% $CaCO_3$ + 10% wax after pyrolysis with 2°C/min heat rate compared to wollastonite and lime

From the XRD spectra it can be easily seen that no wollastonite forms after pyrolysis of rods with 10% wax; it seems that just calcium oxide has formed. On the other hand, in rods without wax the respect of stoichiometric accounts has easily led to the desired ceramic. Peaks between 31-33° are not ascribable to wollastonite but to Ca_2SiO_4 (larnite). Moreover, during heat treatment the structure of the rods containing wax overcomes a complete collapse; rods without wax keep their form, but they are broken in several parts.

Results shown discourage the use of Carnauba wax in the preceramic mixture; it seems that the wax avoids the contact between silicone and calcium carbonate and thus wollastonite formation. On the other hand, the processability problems discussed above still exist.

Tailoring plasticizer amount:

A new attempt is therefore performed by projecting a third recipe which contains less plasticizer: calculations are presented below.

$m_{tot} = 50g$

$m_{wax} = 3\% \cdot 50g = 1.5g$

$m_{MK+CaCO_3} = 97\% \cdot 50g = 48.5g$

$m_{MK} = 1g \cdot \frac{48.5g}{2.4g} = 20.21g$

$m_{CaCO_3} = 48.5g - 20.21g = 28.29g$

$\frac{28.29g}{50g} 100 = 56.6\%_{CaCO_3}$

Mixing is performed with the same parameters set before; the resulting compound shows a behavior which is an average of the first two recipes; it is still pretty easy to remove the mixture from the mixer blades and chamber. Mixture is then milled and rods extrusion is performed in the same way as before (at $T_2 = 80°C$).

New rods are subject to pyrolysis; for this second attempt, there is a chance that slowing down the heating rate to 1°C/min might solve structural problems.

Also rods of the second compound (MK + 52.5% CaCO3 + 10% wax) are treated together at the slower heat rate in order to see if their structure resists with a slower decomposition and gas release.

Results are shown in the following figures.

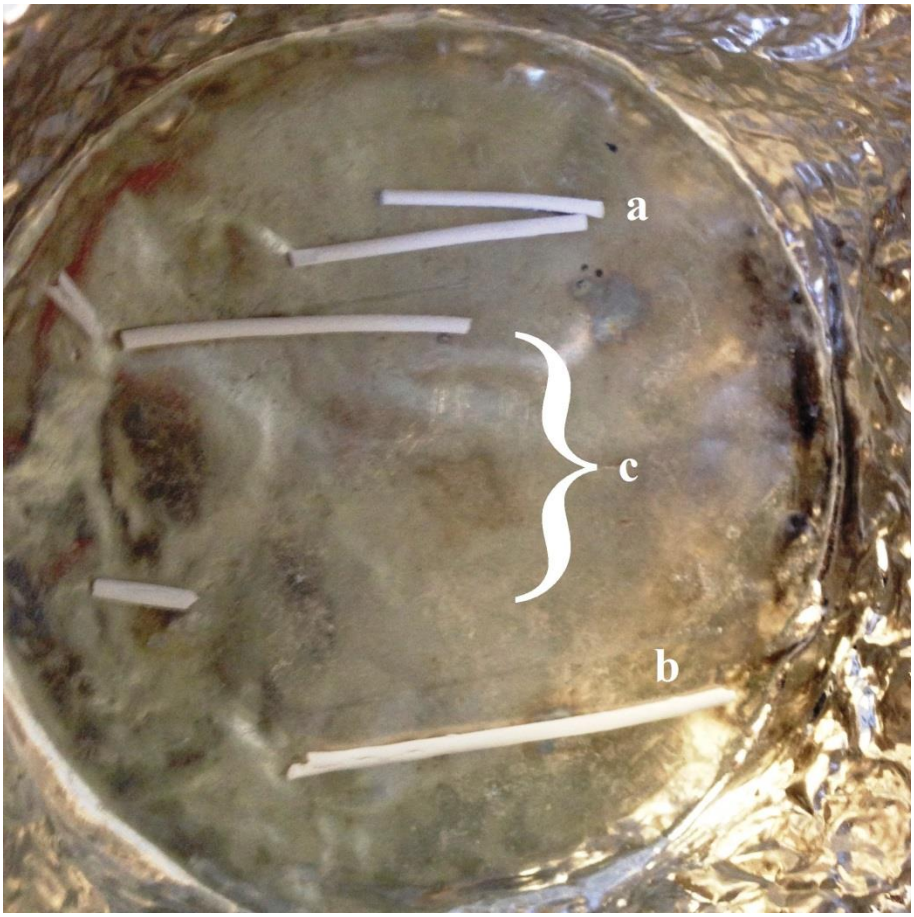

Figure 41. (a) MK + 58.3% $CaCO_3$, (b) MK + 52.5% $CaCO_3$ + 10% wax and (c) MK + 56.6% $CaCO_3$ + 3% wax rods after pyrolysis with 1°C/min heat rate

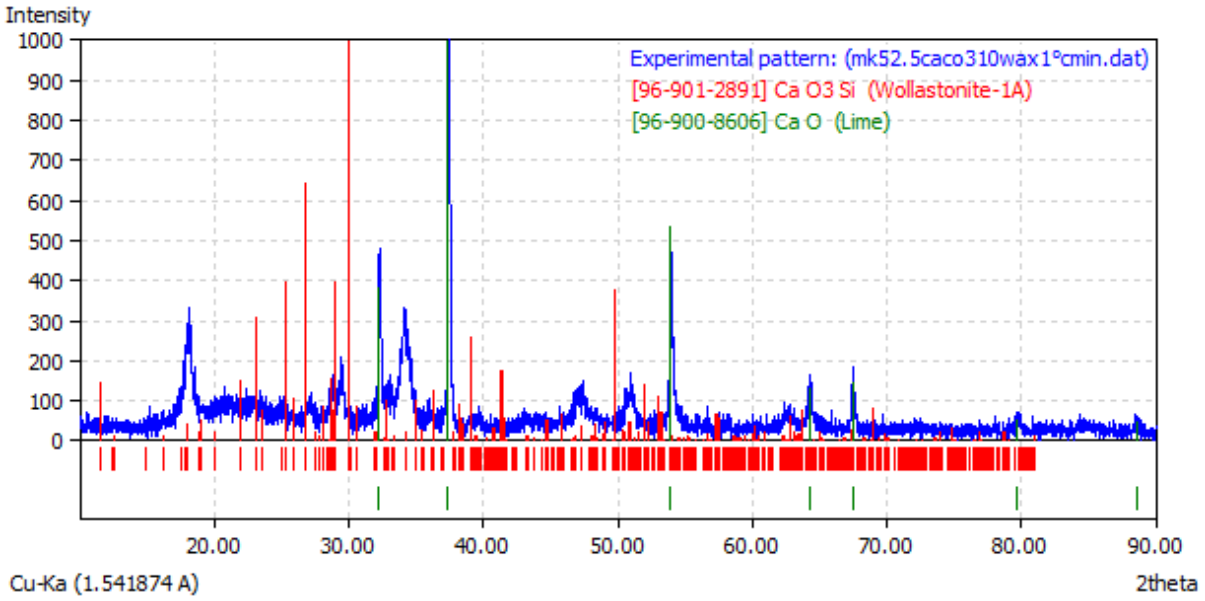

Figure 42. XRD spectrum of MK + 52.5% $CaCO_3$ + 10% wax after pyrolysis with 1°C/min heat rate compared to wollastonite and lime

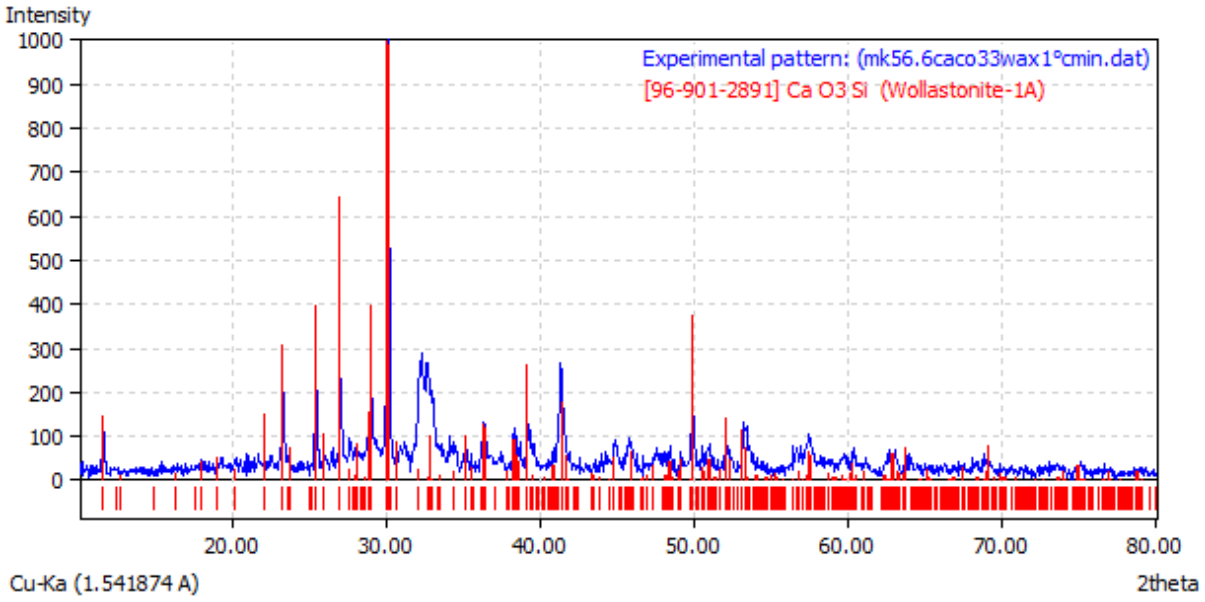

Figure 43. XRD spectrum of MK + 56.6% $CaCO_3$ + 3% wax after pyrolysis with 1°C/min heat rate compared to wollastonite

Structural damages cannot be detected in (a) and (c) specimens and just a little crack is visible in (b) rods; this fact proofs that compound characteristics, together with the really low heat rate, make an additional cross-linking step unnecessary.

XRD measurements are performed on all samples; (a) rods results are not shown because they are not relevant (wollastonite has already been detected in the previous measurements).

Spectra of the other two compounds show significant differences: (b) rods (10% wax) do not form wollastonite even with a lower heat rate; the detected calcium oxide is not suitable for biomedical applications. (c) rods (3% wax), on the other hand, present almost the same spectrum of rods without wax with easily detectable wollastonite peaks.

Third mixture respects ceramic transformation requirements while considerably improving material processability and formability; therefore it wins the selection process and will be used for the later printing attempts.

In order to set up the proper process parameters, a deeper investigation on its rheological properties is needed.

Density measurements:

In order to study the mixture rheological behavior, an estimation of its density is needed. Diameters and length of a piece of rod are measured with a digital caliber and its weight is registered by an analytical balance; then volume and density are calculated.

As stated before, one piece of rod can be schematized as a truncated cone because of gravity action during extrusion; volume is calculated as follows:

$$V = \frac{\pi}{3} h(R^2 + rR + r^2) \tag{9}$$

Where h is cone height, R its bigger radius and r its smaller one.

Measurements and results are reported in the table below.

h (m)	**R (m)**	**r (m)**	**V (m^3)**	**m (kg)**	**ρ (kg/m^3)**
$75.29*10^{-3}$	$1.08*10^{-3}$	$0.50*10^{-3}$	$1.54249*10^{-7}$	$6.52151*10^{-5}$	422.79

Table 11. Rod density measurements

Rheological measurements:

Powder of the selected mixture is prepared in the same way as the one used for rod extrusion and several MFI measurements are performed by varying both the shear rate and the temperature. Temperature is set at 80°C, 100°C and 120°C; shear rate is tailored by adding different testing loads on the piston. Because of the small amount of powder and of the rapidly decreasing viscosity of the material with temperature and shear rate, mass flow rate is measured by weighting with an analytical balance the amount of material extruded in 1 min (or even less) and not in 10; more than a measure is taken for each temperature and shear rate.

From the measurements performed and knowing the M-I Tester geometry an attempt of evaluating shear rate and viscosity is performed (by applying formulae (4)-(7)). Results are summarized in Tables 12-14.

M-I test at T = 80°C			
Testing mass (kg)	**Mass flow rate (g/min)**	**Viscosity (Pa*s)**	**Shear rate (s^{-1})**
3,8	0,0698	8869,7822	3,07002
	0,0725	8539,45928	3,18877
5	0,125	6897,07099	5,49788
	0,1248	6908,12399	5,48908
6,2	0,1791	6170,61391	7,87736
	0,1759	6282,87067	7,73662
8,8	0,306	5332,37565	13,45881
	0,3213	5078,453	14,13175

Table 12. M-I test at T = 80°C

M-I test at T = 100°C			
Testing mass (kg)	**Mass flow rate (g/min)**	**Viscosity (Pa*s)**	**Shear rate (s^{-1})**
1,2	0,7732	119,71133	34,00769
	0,8348	110,87781	36,71705
2,16	3,6133	79,42304	158,92394
	4,3109	66,57061	189,60651
3,36	6,6135	80,13946	290,88187
	8,3057	63,81188	365,30997

Table 13. M-I test at T = 100°C

M-I test at T = 120°C				
Testing mass (kg)	**Extruded mass (g)**	**Time (s)**	**Viscosity (Pa*s)**	**Shear rate (s^{-1})**
1,2	2,1089	60	43,89056	92,75584
	2,1917		42,23242	96,39764
2,16	8,0821	20	11,836	1066,4261
	7,2987		13,10641	963,05715
3,36	11,1032	15	11,93355	1953,41017
	10,5142		12,60206	1849,78612

Table 14. M-I test at T = 120°C

From these measurements average values of viscosity and shear rate are estimated and plotted on graphs which show viscosity as function of applied shear rate. All results are reported in Figures 44-46 and discussed in the following paragraph.

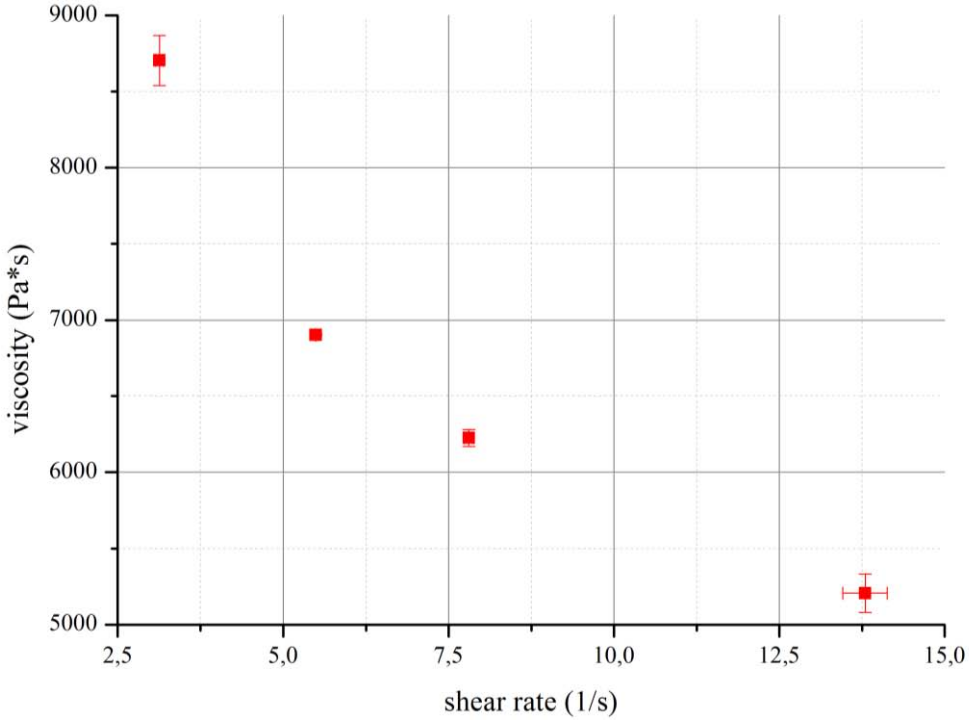

Figure 44. Viscosity as shear rate function at T = 80°C

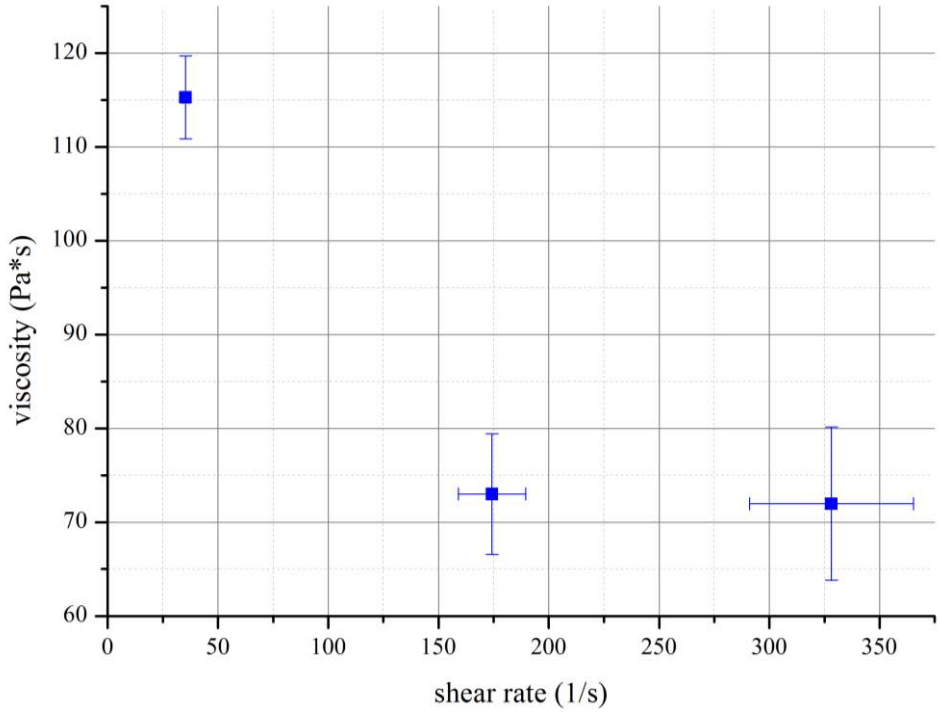

Figure 45. Viscosity as shear rate function at T = 100°C

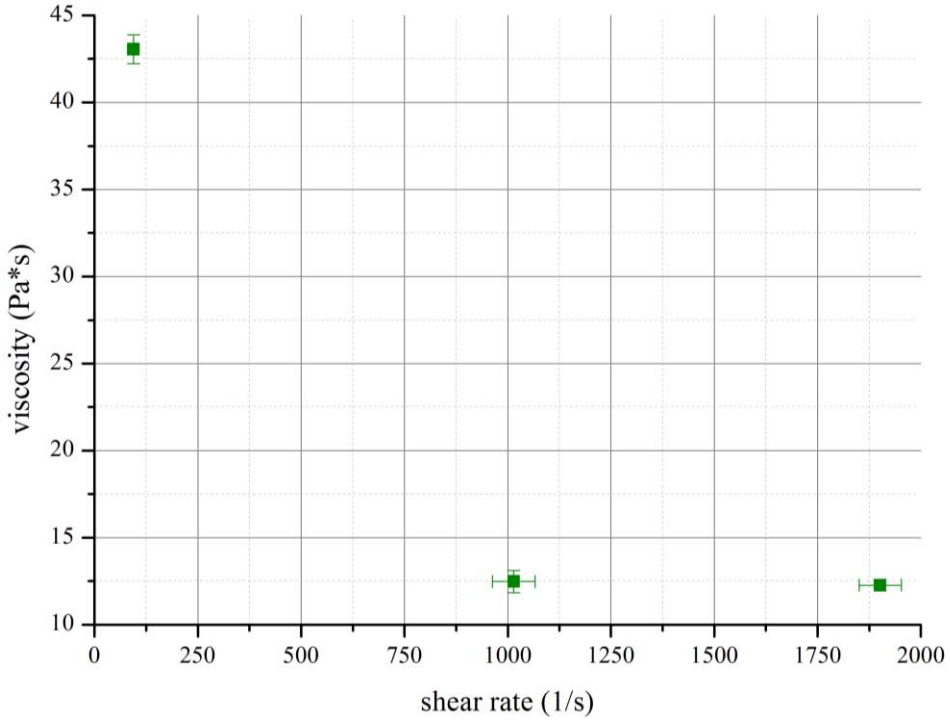

Figure 46. Viscosity as shear rate function at T = 120°C

A logarithmic equation, which is function of both shear rate and temperature, tries to fit the experimental data:

$$\ln \eta = a_1 + a_2 \ln \dot{\gamma} + a_3 (\ln \dot{\gamma})^2 \quad (10)$$

Where a_1, a_2 and a_3 are temperature dependent parameters.

Fittings are plotted in a double logarithmic graph together with experimental data (Figure 47).

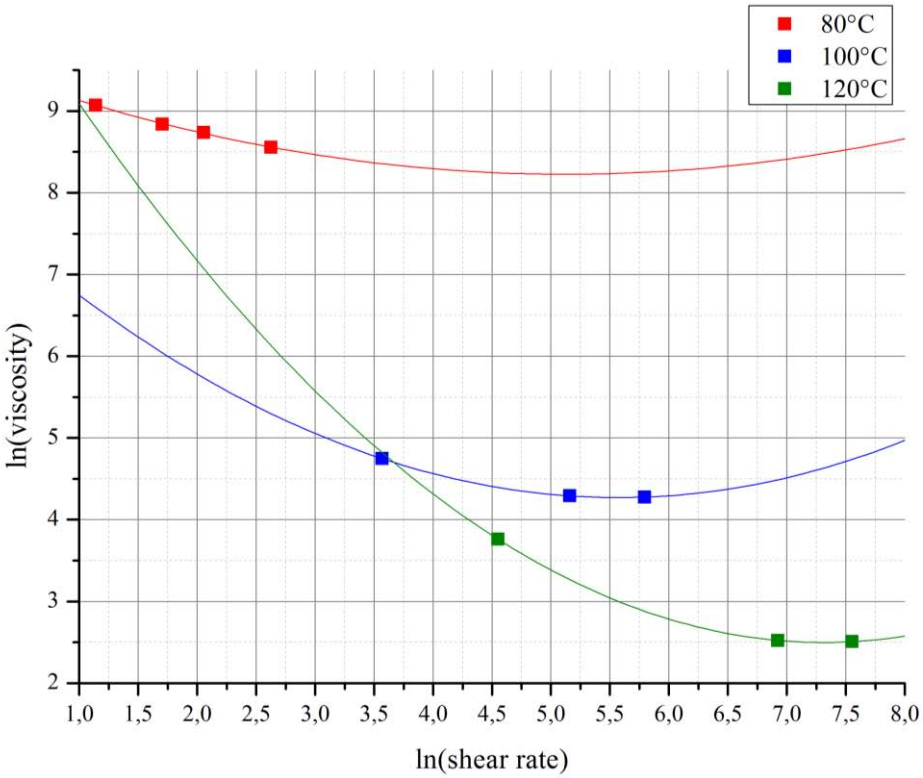

Figure 47. Viscosity as function of shear rate logarithmic fittings

Some considerations should be done on this graph; first, as expected, preceramic mixture behaves like a pseudoplastic material and measurements performed fall into the window of non-Newtonian behavior: decrease of viscosity with shear rate is a proof of this property. The fact that viscosity is not constant at a given temperature means on one hand that it can be tailored by changing process shear rate; on the other hand, selecting an optimal setting of the printing process becomes more difficult.

Another aspect to be highlighted is that viscosity decreases evidently with temperature: differences of various orders of magnitude are detectable in a 40°C range; this is also in accordance with a pseudoplastic behavior. Nevertheless, it is important to keep in mind that MK is a thermoset polymer: if compound is left at high temperature for some time, it will cross-link increasing its viscosity at really higher values.

Negative aspects of performed measurements are also clearly visible from the graph: data campaign is too poor to have a statistically relevant fitting, so temperature dependence cannot be modeled; the whole process is too subjective and exposed to human mistakes to be accurate and precise enough. Finally, chamber dimensions and extremely rapid flow at higher temperature make wire extrusion really difficult to be controlled.

Comparing these results with measurements performed on pure silicone, some differences can be noticed:

- At the same temperature and shear rate taken into consideration, pure silicone viscosity seems to have already reached the Newtonian plateau; silicone filled with $CaCO_3$ and wax is still showing a decrease in viscosity. Filler and/or plasticizer can be responsible for this plateau shift.
- Viscosity values at same temperature and shear rate are of the same order of magnitude, but a decrease in value can be detected for compounds; this can be the effect of Carnauba wax acting as a plasticizer as expected.

To conclude, M-I tests can give a forecast of the changes from the pure silicone to the preceramic mixture and of its behavior in the printing process window helping setting proper printing parameters; but measurements are not suitable for absolute quantitative evaluations.
Further investigations with other rheological instruments such as capillary or rotational rheometers are strongly recommended.

CHAPTER 6: PRINTING ATTEMPTS AND CHARACTERIZATION

The main goal of this work is to investigate the feasibility of adapting a low cost rapid prototyping technology suitable for thermoplastic polymers in order to produce ceramic items. This possibility would open a new road in bone tissue engineering, going in the direction of a massive diffusion of affordable 3D scaffolds.

The state of the art is still far away from it: low cost 3D printers have hit the market since just one or two years and studies on their technical features are still at a preliminary stage. Because of that, first attempts with Maxit 3D Printer in this work are performed by using PLA provided by Itis3D® in order to evaluate precision and accuracy limits and to understand how process parameters shall be varied to produce optimal porous structures.

The next step is to adapt printer and process in order to produce structures with preceramic rods; considerations and attempts regard not only parameter settings but also hardware adapting.

Structures obtained through this process are finally pyrolyzed and characterized in terms of chemical composition, morphology and bioactivity.

Porous structures:

Maxit 3D Printer is a basic low-cost 3D printer; it has a unique heating head able to print one material at a time. Head can move in x and z directions thanks to motors and end stops mounted on a steel structure; printing bed moves in y direction. Independency of movements in the two plane directions x and y provides a simpler (and therefore lighter) support structure and faster prints. Head contains a heating resistance and is fed with a plastic wire thanks to an extruder motor: it puts a cogwheel in rotation and hooks the wire pulling it into the heated chamber forcing the molten material to exit. The extruder motor is not located on the printing head but on the wire holder apart from the structure in order to lower head inertia.

Printer is controlled through Repetier-Host® software; it allows not only to set all process parameters but also to position and modify 3D models on the printing bed and to create the "layered model" (.gcode) for the printer to be printed. This model is created by Slic3r® or Skeinforge® software, both distributed together with the printer.

Plastic material used to feed the printer for these first attempts is polylactic acid (PLA); printer is designed to work with it or with ABS as well, but PLA is chosen because of its ecosustainability (it has vegetal origins and it is fully biodegradable) and its lower melting temperature. In order to understand its behavior during process and its similarities and differences compared with preceramic compound, its physical and rheological properties are also taken into consideration.

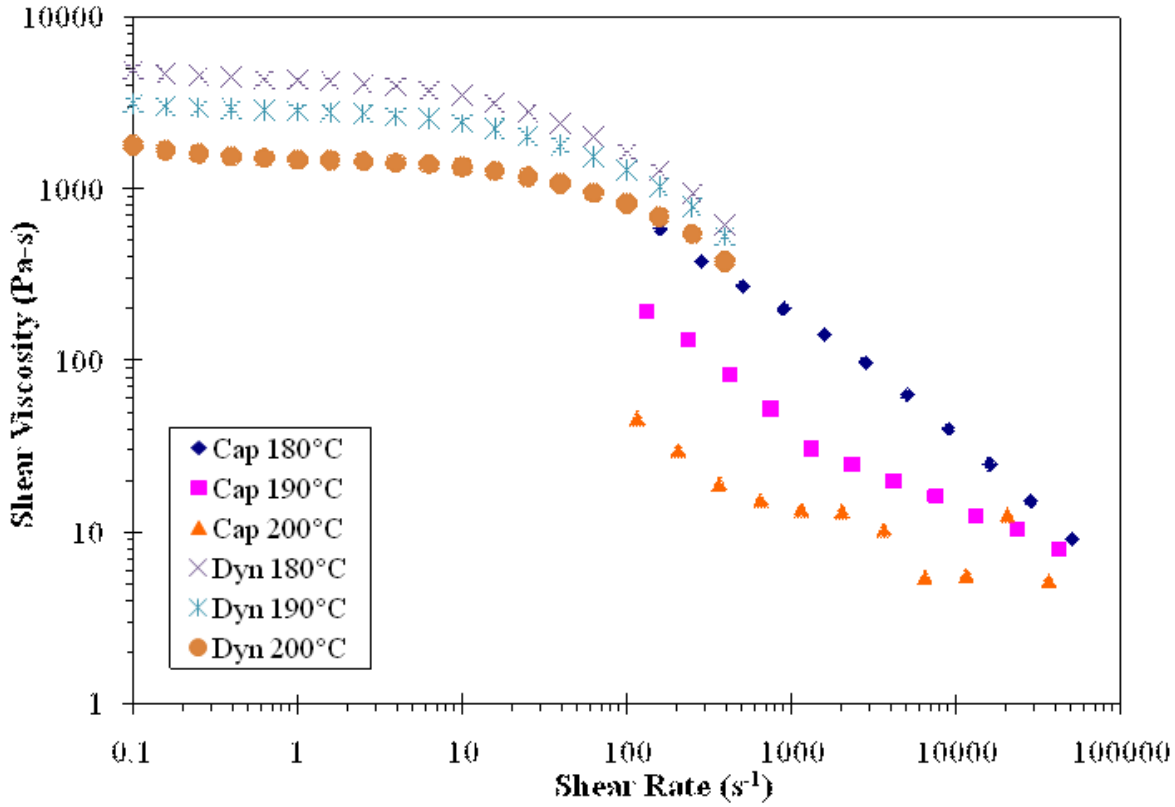

Figure 48. Capillary and dynamical rheology results for PLA at 180°C, 190°C and 200°C[35]

PLA melt temperature varies between 150°C and 160°C[35]; Maxit user manual suggests setting a printing temperature of 200°C. Viscosity values registered for PLA at that temperature in the non-Newtonian region (capillary rheology data) cover almost the same region as compound ones registered between 100°C and 120°C. η oscillates between 50 and 5 Pa*s for shear rates between 100 and 50000 s^{-1} for PLA; same viscosity range is covered for shear rates between 50 and 2000 s^{-1} by the preceramic compound. So, if applied forces and printing rates are optimally set for PLA printing, parameters for preceramic printing should be reasonably similar.

Some first printing attempts are performed using test files provided with the printer and simple models like cubes and cones created with Netfabb® Studio Basic 4.9. Both Slic3r® and Skeinforge® software are tried to understand which is best for our objectives; Slic3r® is more immediate and simple and allows a better comprehension of the resulting .gcode file, but Skeinforge® is much more customizable and also more precise in z direction. This can be non-relevant for the first simple models, but it definitely is for complex porous structures. So it is chosen to work with Skeinforge® and porous structures are printed using models made by Andrea Zocca of BAM Federal Institute for Materials Research and Testing, Germany.

Skeinforge® settings are optimized in all its features to guarantee highest precision and accuracy in printing bulk but especially hollow structures:

- temperature is set at 200°C as recommended.
- feed and flow rates, controlling head and extruder speed respectively, are both set at 45 mm/min; same rate means neither accumulation nor lack of material during printing.
- layer thickness is set at 0.4 mm.
- perimeter width is set at 0.4*1.8=0.72 mm.
- clip, comb, retraction and all other options are already optimized by the software distributor to assure the highest quality.

As clearly visible from the settings, there are some technological limits to precision and accuracy: even if perimeter width, which is the width of the thinner wall printable, was set to 0.4*1 = 0.4 mm (which would mean that a wall would be made of a single layer), it could not be thinner than 0.4 mm. This is also the minimum distance between layers to print them separate: porosity cannot be smaller than 0.4 mm and a porosity of maximum 0.5 mm is needed for biomedical applications; micropores are in any case unrealizable. Producing biomedical scaffolds with this apparatus is thus possible but really challenging.

For this first feasibility evaluation it has been decided not to push the printer over its limits but to optimize the process for bigger porous structures; hollow objects realized show porosity with at least 1-2 mm.

3D models and corresponding printed PLA objects are reported in the following figures. Both bulk and hollow structures shapes correspond perfectly to the models; surface shows clearly its wire packing structure meaning that surface finish has to be improved.

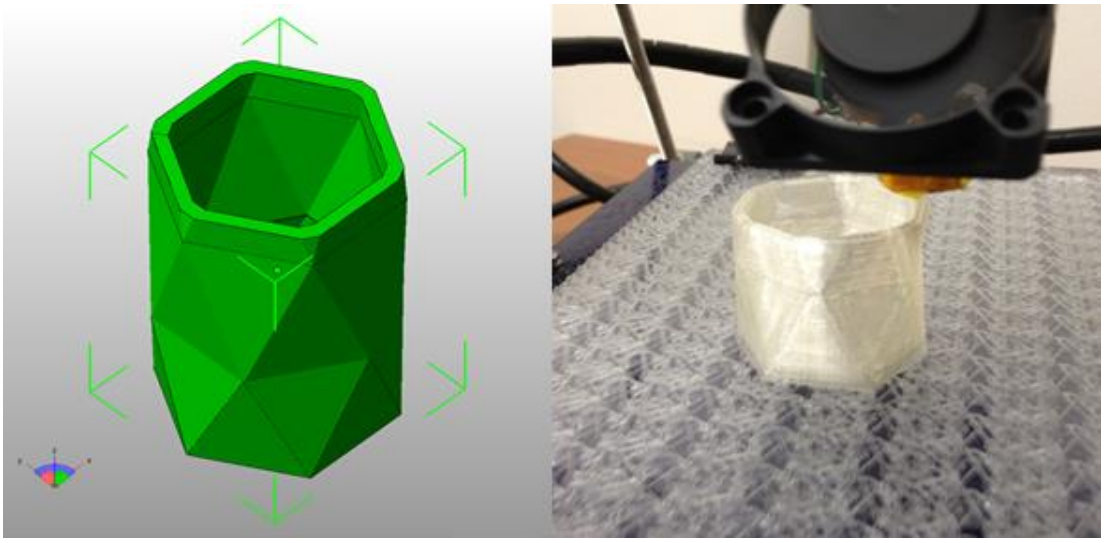

Figure 49. Hexagonal vase - 3D model and printed object (during printing)

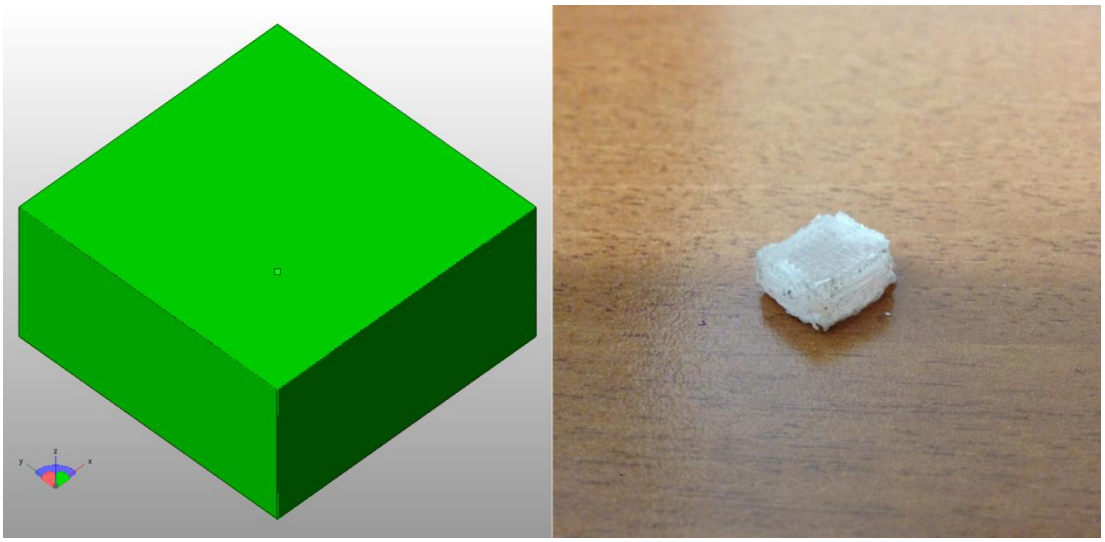

Figure 50. Parallelepiped - 3D model and printed object

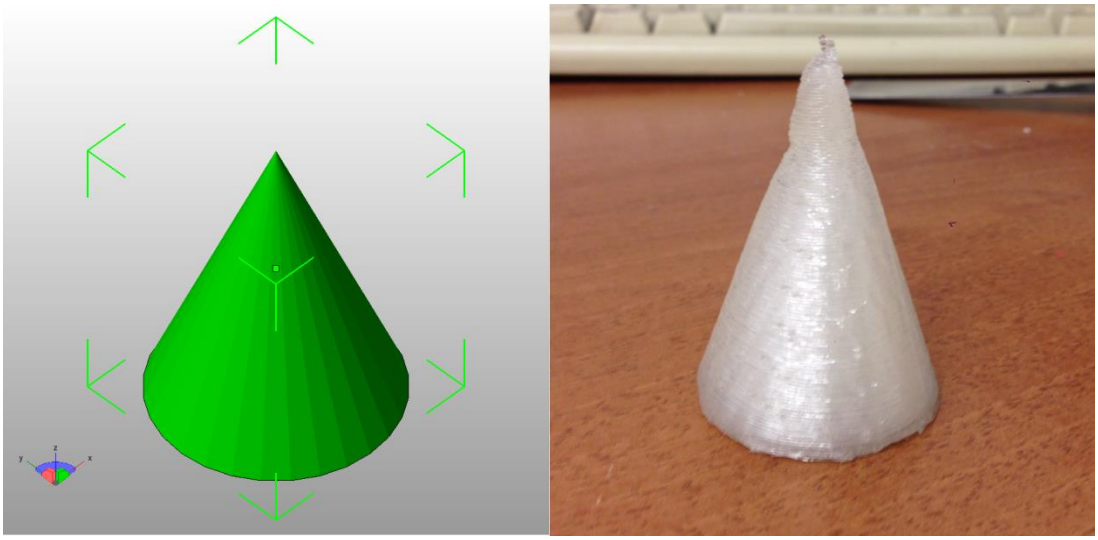

Figure 51. Cone - 3D model and printed object

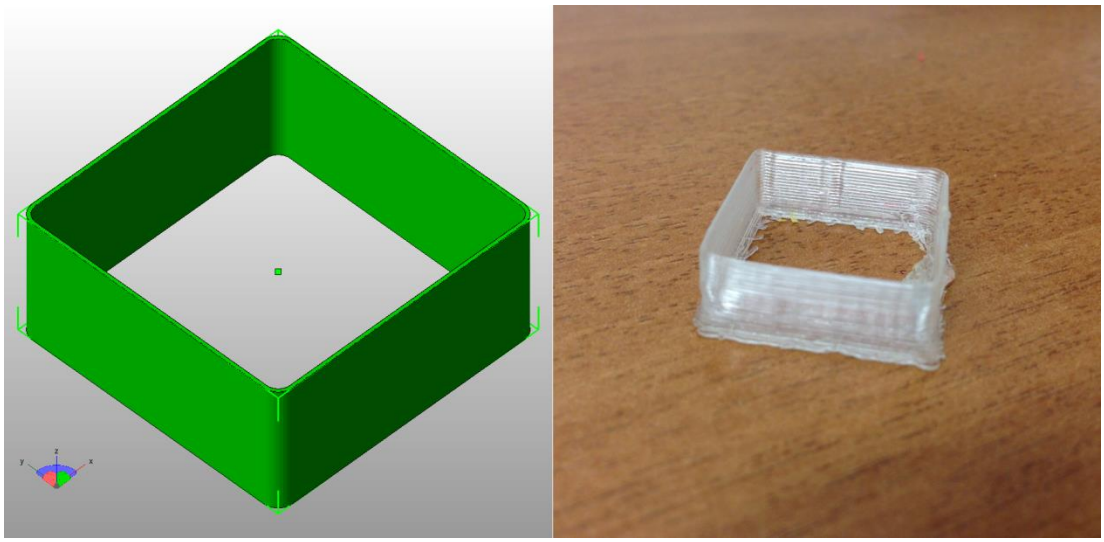

Figure 52. Single wall fence - 3D model and printed object

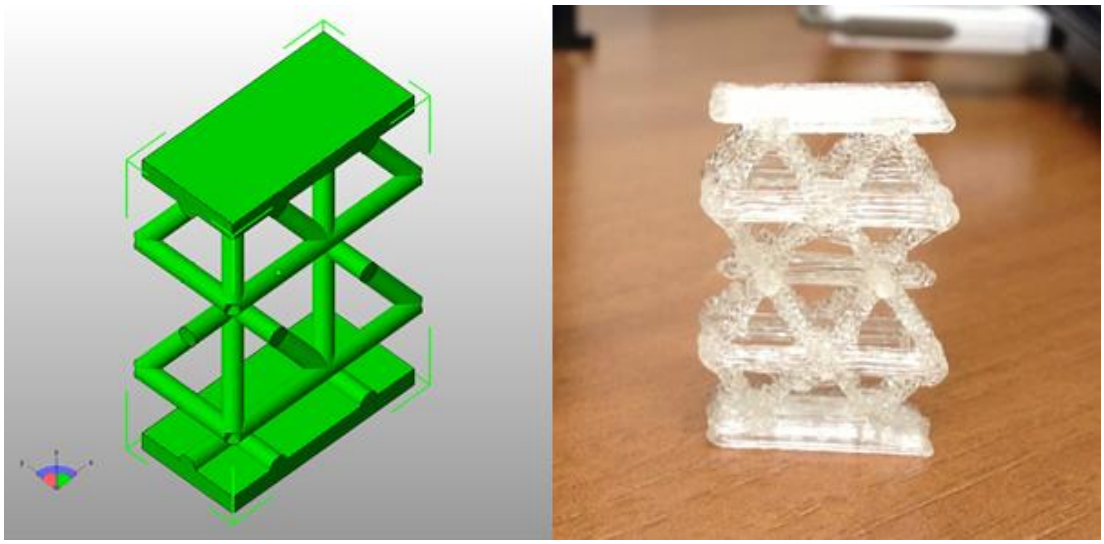

Figure 53. Octahedral structure - 3D model and printed object

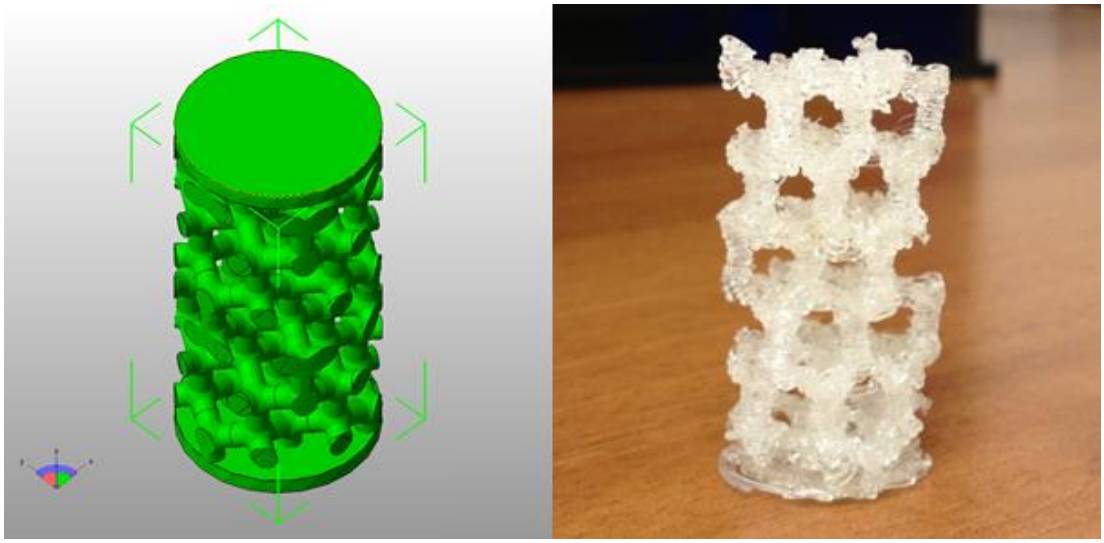

Figure 54. Diamond cylinder - 3D model and printed object

Printing with preceramic compound:

Though it is now known that printer cannot resolve layers and pores smaller than 0.4 mm, it is chosen to keep on with the established experimental procedure to verify if dense and porous structure made of preceramic compound can be realized through this process. A brief discussion over main parameter settings and experienced troubles is here reported.

Extruding force:

A remarkable difference between PLA wire and preceramic rods makes extruding process really arduous: while the first is flexible and elastic, the second shows a really fragile behavior; if not supported by a frame and pushed with an axial force into the chamber, rods fracture forming a coarse powder which obstructs both feeding tube and heated head.

Even if a rigid frame was produced and installed on the printing head, rods fragility would still be a problem: extruder motor cannot be used directly on them because gear cogs would break the rod at the first contact. Moreover, extruder motor is located apart from the printing head but preceramic rods cannot be longer than 15 cm because of M-I tester configuration.

First solution investigated is extruder motor substitution with a system made up of a metal tube and a piston loaded at its top; gravity force application would maintain flow rate constant but not controllable (unless the load is changed). Setup is represented in Figure 55.

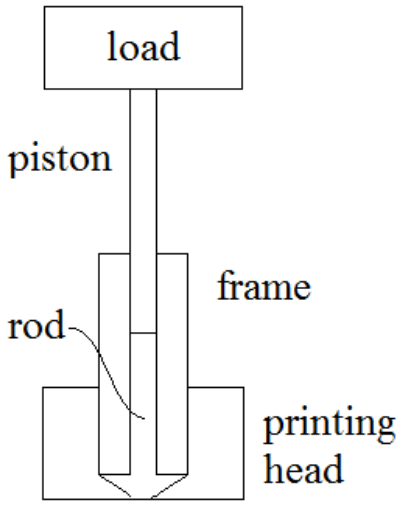

Figure 55. Loaded piston system for material extrusion

This configuration does not work for several reasons: first, in order to load a reasonable amount of material, frame and piston have to be longer than 10 cm; second, frame has to be thinner than 3 mm to fit in the heated chamber and piston has to be thinner than 2 mm to fit into the metal frame; third, a load of some kg is needed to let the material flow. These limitations lead to a really unstable structure above printing head with a too high inertia to let the mechanism move.

The only way to push the material with the necessary force without increasing head inertia is to use a motor; it also permits to tailor force and therefore flow rate. This consideration gives birth to the second idea: to make PLA wire act as a piston. Wire is pushed into the feeding tube by the present extruder motor; preceramic rods are loaded from a cut approximately 10 cm before the printing head; when PLA wire meets the rods, it pushes them into the heated chamber and forces the molten material to exit.

The new configuration is schematized in Figure 56.

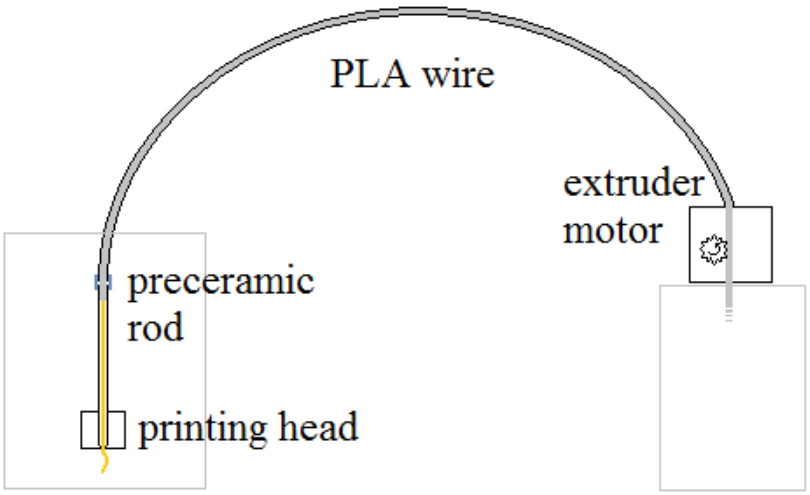

Figure 56. Schematic of new extruding configuration

This second solution works reasonably well with a minimum intervention on the printer hardware; before starting to print, however, some other feeding improvements have to be adopted.

Feeding:

Extruded rods produced for previous characterizations have a diameter of about 2-2.1 mm; standard PLA wire has a diameter of 2.8-2.9 mm and fits the heated chamber entrance perfectly. Smaller diameter coupled with material fragility leads to buckling and consequent fracture and powder accumulation inside the heated chamber; for this reason feed rods have to be specifically extruded to perfectly fit into the heated chamber entrance.

A new nozzle for the M-I tester is realized by the mechanical workshop of the Industrial Engineering Department with a diameter of 3 mm; new rods extruded through the bigger nozzle have a diameter of 2.8-3.1 mm (oscillation are due to gravity and swelling phenomena) and can be used to feed the printer.

To avoid breaks and obstructions which still occur during process because of the non-perfect alignment of piston and rod, rods are merged into silicone oil before use; a generous amount of silicone oil is also poured into the feeding tube.

Printing temperature and feed and flow rates:

As mentioned before, preceramic mixture heated at 100°C-120°C shows a viscosity as function of shear rate diagram which seems to be compatible with PLA one at 200°C. After some confirming tries performed varying both temperature and rates, Skeinforge® software is set at a process temperature of 120°C and at a feed and flow rate of 45 mm/min.

Other software parameters:

Layer thickness, perimeter width, clip, comb and all other options are left unvaried in Skeinforge® because they are already optimized to print structures with porosity.

A special mention goes to retraction: normally when there are pauses or gaps, or while heating head is going up in z direction, PLA wire is retracted of some mm by the extruder motor; this trick avoids material accumulation in some points and emptying of the heated chamber due to gravity.

With the new printer asset, retraction is not possible: if the extruder motor tries to retract the wire, just PLA “piston” will follow leading to a gap between piston and rod and thus to a hole in the following section.

No retraction means more difficulties in creating porous structure, but at the moment it is a necessary choice.

Printing bed:

Even if the whole printing process is redesigned and optimized to try out the new feeding material, this does not mean that the printer can actually build an object. What most affects print success is the first layer adhesion: if the first layer does not adhere to the support bed properly, there will not be a stable basis for the successive layers to fix on. From this point of view, provided polyimide support seems to be perfect: silicone compound adheres strongly to its surface.

On the other hand, at the end of the printing process object has to be removed from the bed to be treated in oven; in fact, plastic bed cannot stand a temperature of 900°C. But high fragility of preceramic compound passes on also to the printed structure and when it is tried to be removed it breaks into pieces.

If the object overcomes heat treatment, then it will be much more resistant and it will probably lose its adhesiveness to the support (organic functional groups will decompose).

A good solution can be therefore the use of a different printing bed, which of course promotes adhesiveness but can also be easily mounted and removed from the printer and can withstand thermal treatment at high temperature.

Choice is fallen on refractory bricks: they are specifically meant to resist at high temperatures and can be mounted as supports on the printing bed by simply fixing them with some synthetic rubber. Once printing process is ended, bricks can be removed and directly transferred into the oven. Their light weight does not affect bed movement and, most important, their porous structure allows a resistant adhesion of silicone compound on them.

Results and characterization:

Porous structures:

Some criticalities in porous scaffold printing process have already been highlighted in the previous paragraphs; several attempts are performed tailoring both temperature and rates but no porous structure can be printed.

First, temperature effect has to be considered: some printing attempts are performed at 80°C, but this temperature is definitely too low; high viscosity leads to head blocks, non-continuous material flux and thus undesired holes in printed structure. Moreover, material cools too fast to strongly adhere to the substrate. This problem not only regards porous structures but also dense ones, in particular in case of thin walls; an example is shown in the picture below.

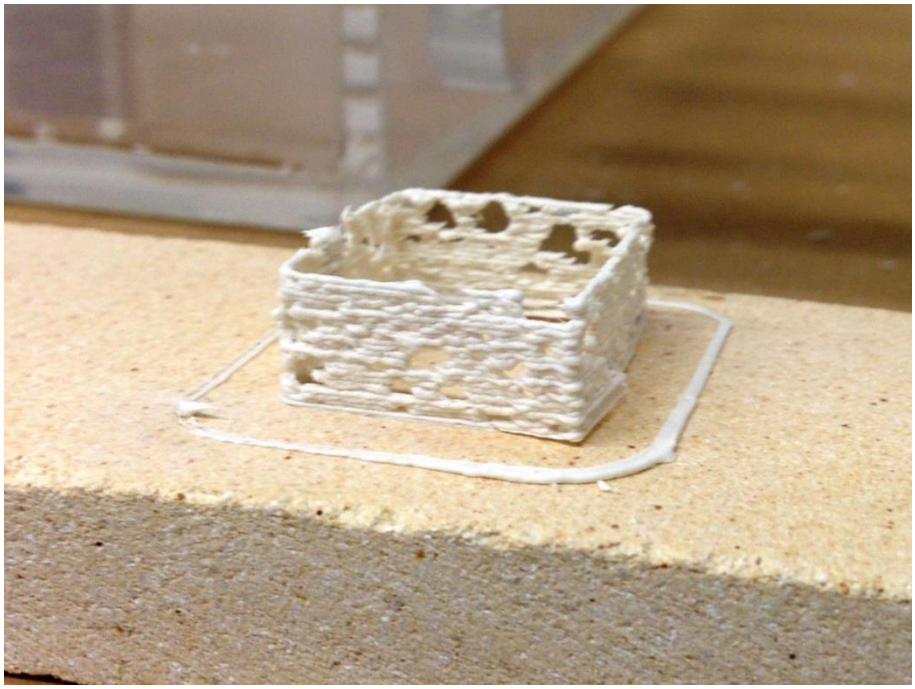

Figure 57. Thin wall preceramic printed sample

Setting temperature at a value which is high enough to assure a decrease in viscosity and thus a correct flow of material makes the cooling rate decrease as well. This is not a problem for dense structures because shape is stable even when the deposited wire is still warm; in case of porous structures too slow cooling unfortunately means that bridges over pores will not maintain their shape but will drip down making the structure collapse.

No picture is taken to show this phenomenon because the printing process does not come to an end.

Softening and dripping processes are caused not only by a too high temperature but also by the use of a huge amount of silicone oil: if it is necessary to assure good flowability, on the other hand it penetrates in the preceramic rods softening them; this makes the compound flow faster than the piston does, leading to undesired material accumulation in some regions and uncontrolled flow and printing rate.

For these reasons, the idea of printing porous structures is abandoned at the moment; focus is transferred on printing simple geometries in order to lead the experimental procedure to end; thermal treatment has to be performed and resulting ceramics have to be characterized in terms of morphology, chemical composition and bioactivity. It is important to notice that bioactivity will be tested just as a really preliminary stage: no protein or cell tests are programmed; to see if the ceramic material obtained is suitable for cell attachment and proliferation porosity is not needed.

Dense structures:

In order to simplify the printing process the easiest geometry has been chosen: a small parallelepiped with 1 cm * 1 cm square basis and 0.5 cm height; several attempts are performed and the best 8 samples are chosen to go on with the experimental procedures. Figures 58-59 show some of the samples.

Figure 58. Printed preceramic parallelepiped

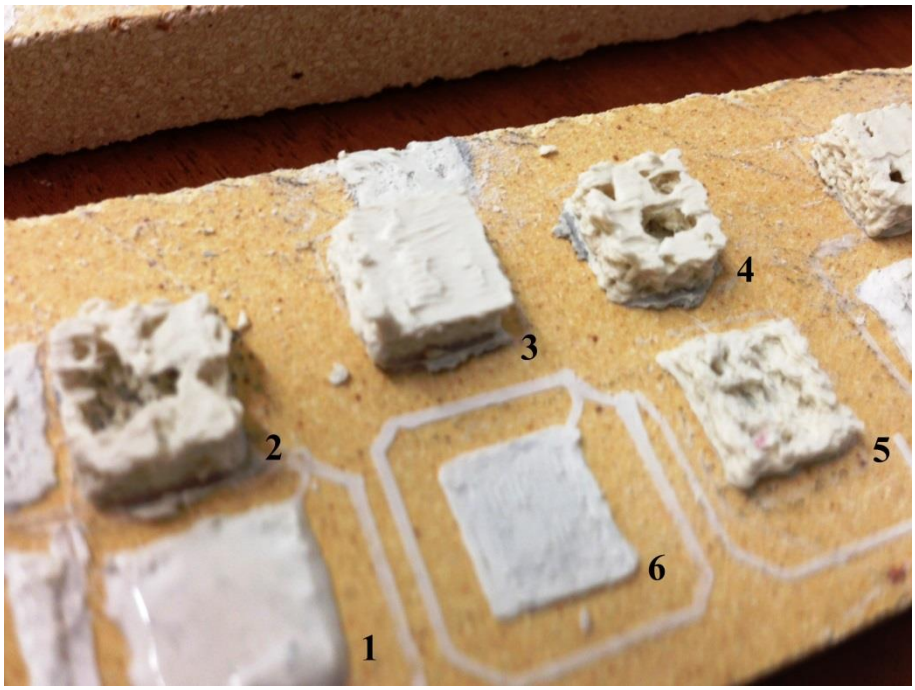

Figure 59. Printed preceramic parallelepipeds – attempts

As it clearly appears from pictures, even printing simple geometry with fixed optimized parameters gives really aleatory results; this does not happen when PLA wire is used. Parallelepiped shown in figure 58 is satisfactory: its dimensions are quite precise and there are no holes in its structure; just some surface roughness on lateral walls is visible. In figure 59, on the other hand, just sample 3 can be considered a good result. Sample 1 is dripped down, probably because of an excessive permanence in silicone oil; sample 2 and 4 are completely printed but adhesion problems in the central region have caused more than a hole; printing of sample 5 and 6 is suspended before end because of head block. Many attempts are therefore needed to achieve acceptable results.

Pyrolysis:

Selected printed samples are then brought into the oven and they withstand heating treatment at 900°C in oxidant atmosphere; modalities are illustrated in Chapter 5. During thermal treatment, organic functional groups decompose and are released in the atmosphere and newborn silica and calcium oxide bond together to form wollastonite.

Pyrolyzed samples are shown in Figure 60.

Figure 60. Pyrolyzed ceramic parallelepipeds

Pyrolysis seems not to affect samples geometry: no shrinkage is detected on samples, whose height, length and width is the same measured before treatment. This is mainly a beneficial effect of using active fillers; adhesion vincula on the refractory substrate also help.

Organic groups release does not affect dense and cohesive structures: no additional cracks are detected in samples 1, 3, 7 and 8; additional cracks appear in samples 2 and 4, whose structures were already damaged due to holes presence.

XRD characterizations performed on the compound (see Chapter 5) confirm that there is wollastonite formation.

It can be concluded that thermal treatment chosen is optimal to achieve ceramic conversion to the desired composition without shrinkage or cracking; this conclusion is really promising in terms of development of a net shape process.

SEM and EDX characterizations are also performed on pyrolyzed structures to investigate surface morphology and to verify that wollastonite has formed; results of these measurements are discussed later in this work in comparison with samples treated for bioactivity tests.

Bioactivity:

Biomaterial behavior in application conditions has to be evaluated in a long term perspective in order to guarantee its safety and efficacy; FDA, CE etc. have to approve and certificate its usage.

Experimentation is developed into subsequent steps at the end of each just approved materials can proceed to the next; in this way just a minimal part of candidates has access to the market. Procedure can be schematized as follows:

1. Physical and chemical characterization: data are collected from the starting material to verify if its properties are subjected to changes after succeeding steps.
2. In vitro tests: before implanting materials in animals or humans, they have to withstand:
    a. Immersion in simulated body fluid: it highlights ion release and surface modifications occurring on the implant when poured into a solution which simulates human blood plasma; it is crucial for bone implants because HA formation is detectable.
    b. Bacteria tests: check whether bacteria survive or die on material surface.
    c. pH test: verify if pH in SBF remains suitable for cell attachment and proliferation.
    d. Protein adhesion: growth factors adhesion on material surface is verified.
    e. Cell tests: performed with cells and tissues from mammal donators.
3. In vivo tests: implants are tested on selected animal models, trying to limit animal suffering and sacrifice at a minimum; sometimes alternative methods are possible (silicon trials on informatics simulators).
4. Clinical experimentation on volunteers.

Wollastonite has already been characterized in its chemical and physical properties; as discussed above, there is no sense in testing printed dense structure with bacteria and cells, because a specific porosity is needed for them to be rejected/attach.

What is interesting is to verify if wollastonite samples obtained by 3D printing of the selected preceramic compound gives HA formation when poured into SBF; it is already known that it is a biocompatible material, but its composition has also to be taken into consideration. There is no phosphorus in its structure and just calcium ions can be released, so a reaction like the one seen with bioglasses cannot be expected; but HA formation is still possible, as highlighted in Chapter 4.

SBF tests are performed with the help of Professor Aldo Boccaccini and Valentina Miguez Pachego at the Institute of Biomaterials of Friedrich-Alexander Universität Erlangen-Nürnberg.

1 L SBF is prepared following a recipe firstly developed by Kokubo and his colleagues in 1990[18,36]. It is a metastable solution containing calcium and phosphate ions already supersaturated with respect to HA. Ion concentrations of SBF and human blood plasma are given in table below.

Ion	Concentration (mmol/L)	
	SBF	Human blood plasma
Na^+	142.0	142.0
K^+	5.0	5.0
Mg^{2+}	1.5	1.5
Ca^{2+}	2.5	2.5
Cl^-	147.8	103.0
HCO_3^-	4.2	27.0
HPO_4^{2-}	1.0	1.0
SO_4^{2-}	0.5	0.5

Table 15. Ion concentrations of SBF and human blood plasma

pH has to be adjusted to 7.25 at 36.5°C using 50 mM of tris(hydroxymethyl)aminomethane and approximately 45 mM of HCl.

SBF preparation steps are follows:

1. Cleaning: all bottles are cleaned first with diluted HCl solution, then with a sterilizing agent and finally with ultra-pure water.
2. Dissolution of chemicals:
    - 750 mL of ultra-pure water are put into a 1 L beaker and stirred at a constant temperature of 36.5°C with magnetic stir with heater.
    - Each chemical given in table below until the 8th is added into the water one by one in the order given after each reagent is completely dissolved. Chemical has to be weighted with a weighting bottle and added in water, then remaining chemical on the bottle has to be washed with ultra-pure water and solution has to be added in water.

- 9th reagent ($(CH_2OH)_3CNH_2$) has to be added little by little in order to avoid local increase in solution pH.

Order	Reagent	Amount
1st	NaCl	7.996 g
2nd	$NaHCO_3$	0.350 g
3rd	KCl	0.224 g
4th	$K_2HPO_4 \cdot 3H_2O$	0.228 g
5th	$MgCl_2 \cdot 6H_2O$	0.305 g
6th	1 kmol/m^3 HCl	40 cm^3
7th	$CaCl_2$	0.278 g
8th	Na_2SO_4	0.071 g
9th	$(CH_2OH)_3CNH_2$	6.057 g
10th	1 kmol/m^3 HCl	Appropriate amount for adjusting pH

Table 16. Reagents for preparation of SBF (pH 7.25, 1 L)

3. Adjustment of pH: pH meter is calibrated with fresh standard buffer solution, temperature is checked and pH meter electrode is placed in the solution. pH is measured while temperature is at 36.5°C; it is about 7.5. By adding HCl solution little by little pH is adjusted to 7.26.
4. Refill: ultra-pure water is added to the solution to reach a volume of 1 L and flask is well shook; when the bottle reaches room temperature (20°C) volume is adjusted and bottle shook again.

After SBF solution is ready, samples are poured into separate test tubes full of solution and loaded in the incubator shaker which keeps them stirred and at a constant temperature of 37.5°C.

Due to the lack of available time in Erlangen to perform these tests, samples are extracted just soon after immersion: once after 1 day and once after 3 days. However, it has been reported that HA formation should start soon after less than a day, so it should already be detectable in these samples after immersion.

After their permanence into the SBF, ceramic samples are rinsed with ultra-pure water, dried and then analyzed using SEM imaging and EDX. Pictures and significant results are presented in the following figures.

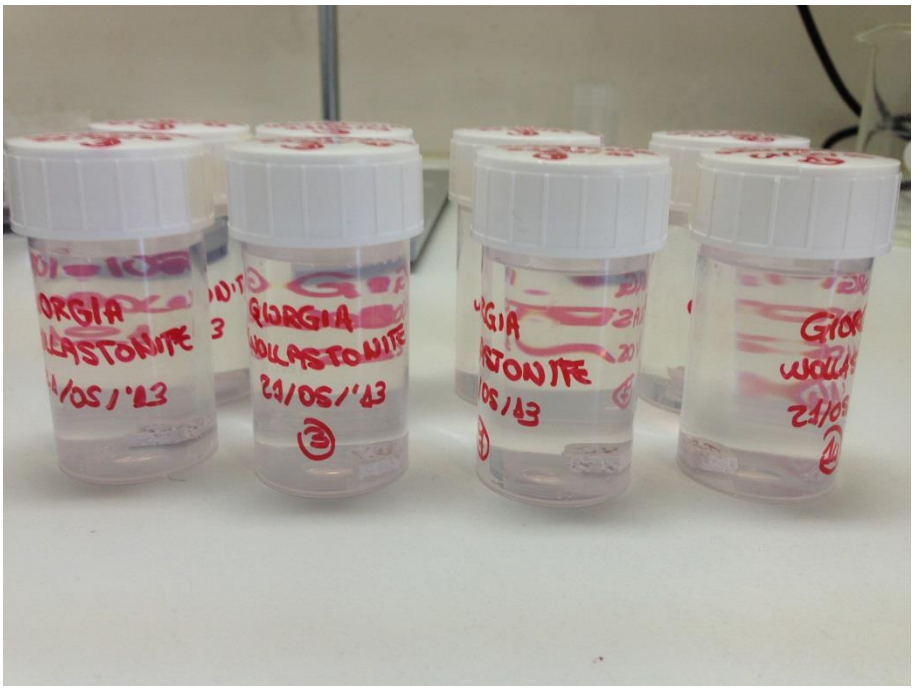

Figure 61. Samples poured in SBF solution

Figure 62. Ceramic printed samples after immersion in SBF solution

Figure 63. Selected samples after immersion and drying (already mounted on SEM sample holder)

One sample per each time point is mounted on SEM sample holder; a piece of the thin wall fence, which has been just pyrolyzed, is also mounted in order to have a SEM image of just wollastonite. Thin wall fence is chosen instead of parallelepiped because it is also interesting to see the morphology of lateral walls of structures, in which deposited wires are still visible. SEM images are collected at different magnifications (50x, 500x, 2000x) and average EDX spectra of sample surfaces are detected. Results are shown here below.

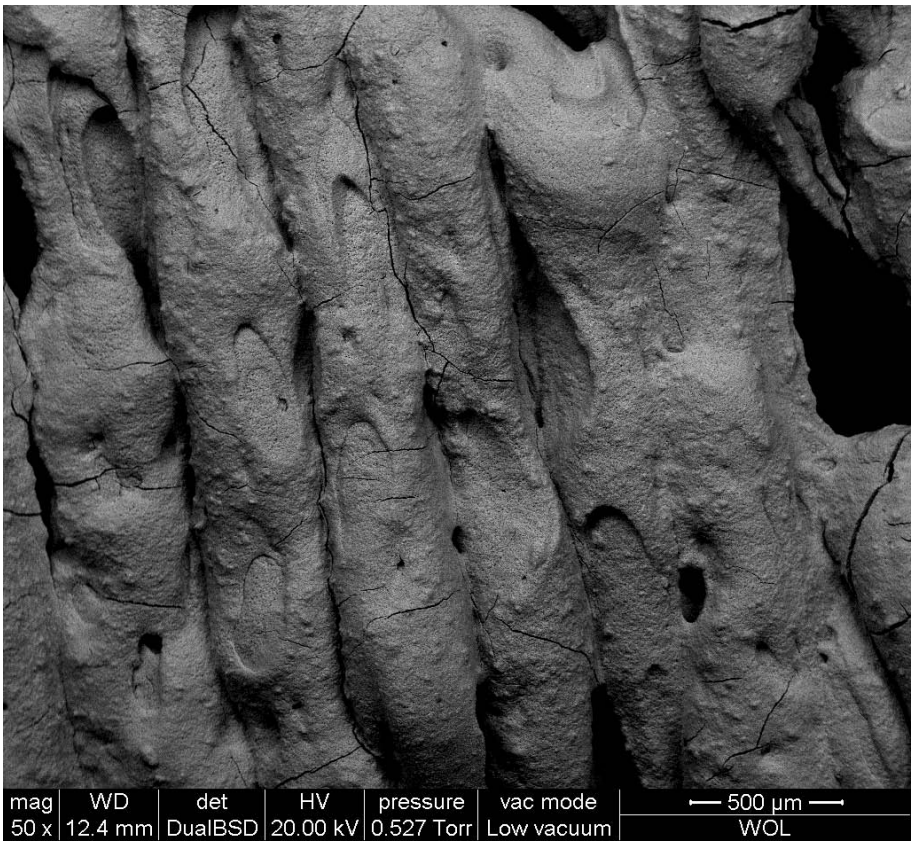

Figure 64. 50x SEM image of ceramic thin wall after no immersion

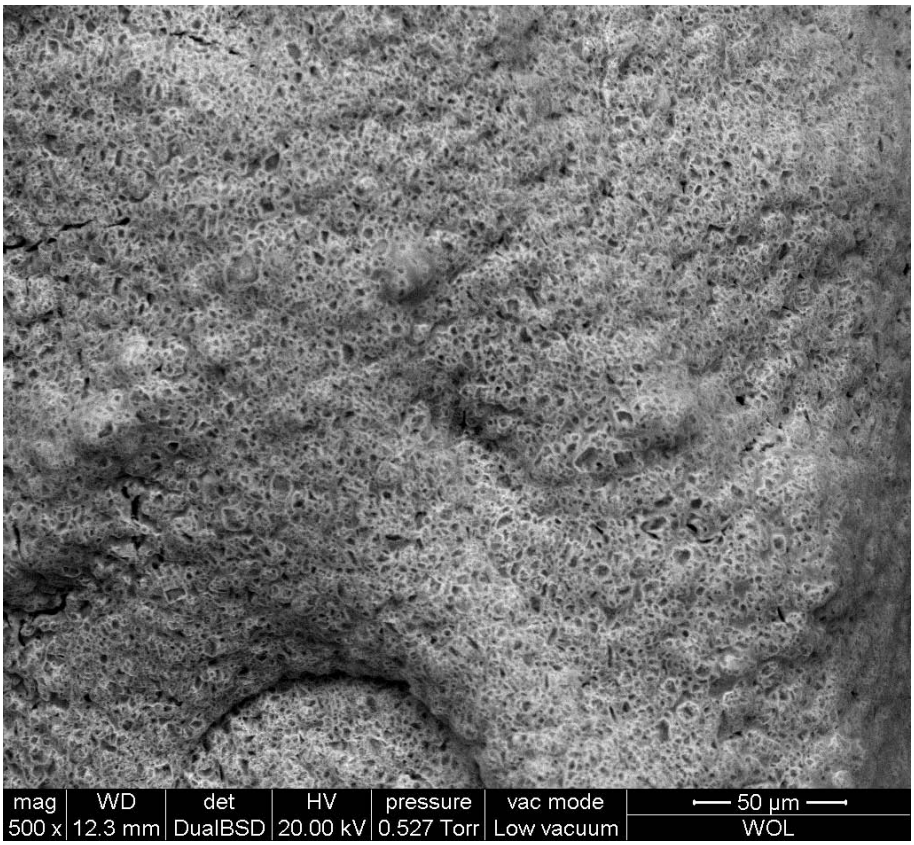

Figure 65. 500x SEM image of ceramic thin wall after no immersion

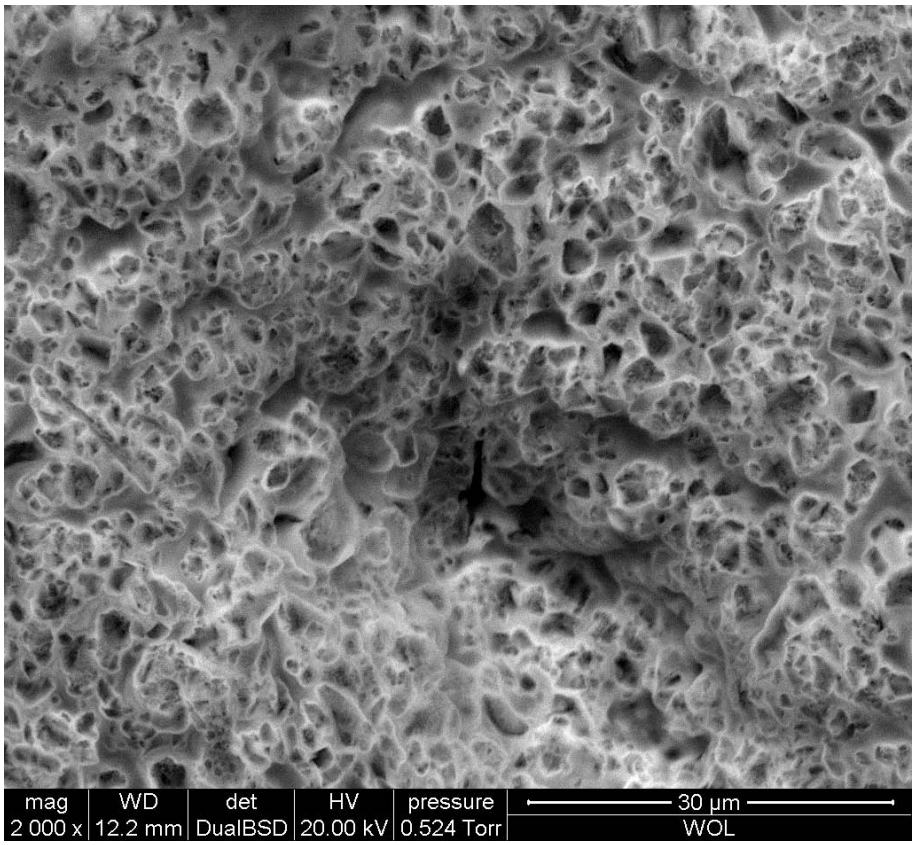

Figure 66. 2000x SEM image of ceramic thin wall after no immersion

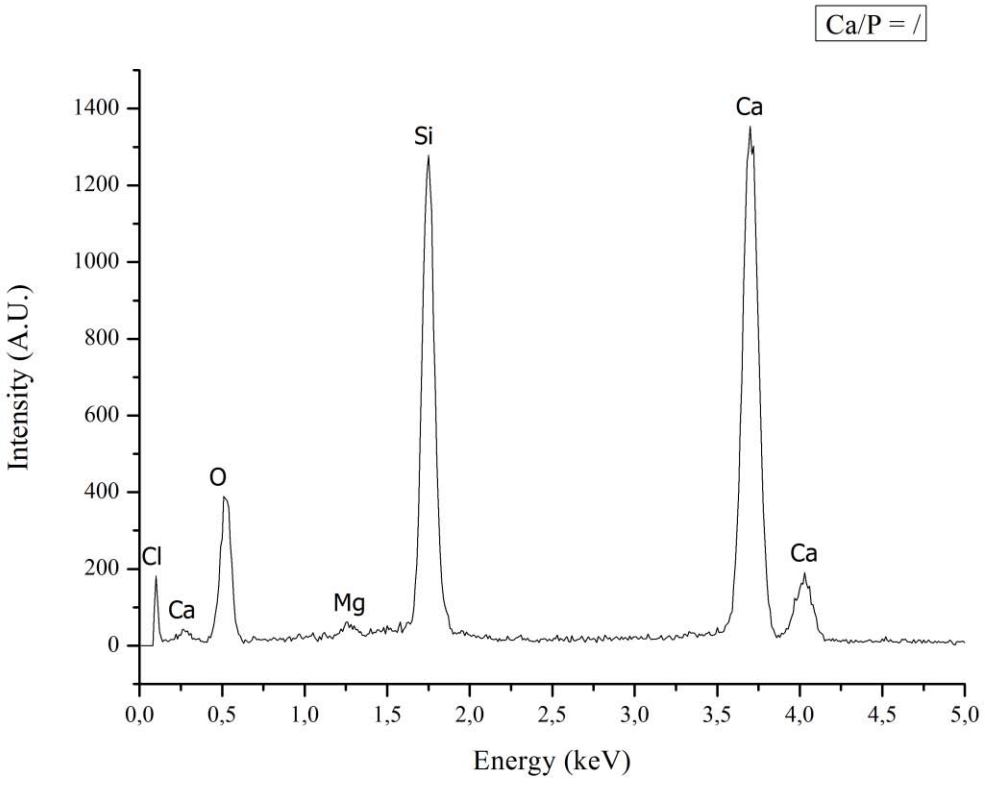

Figure 67. EDX spectrum of ceramic thin wall after no immersion in SBF

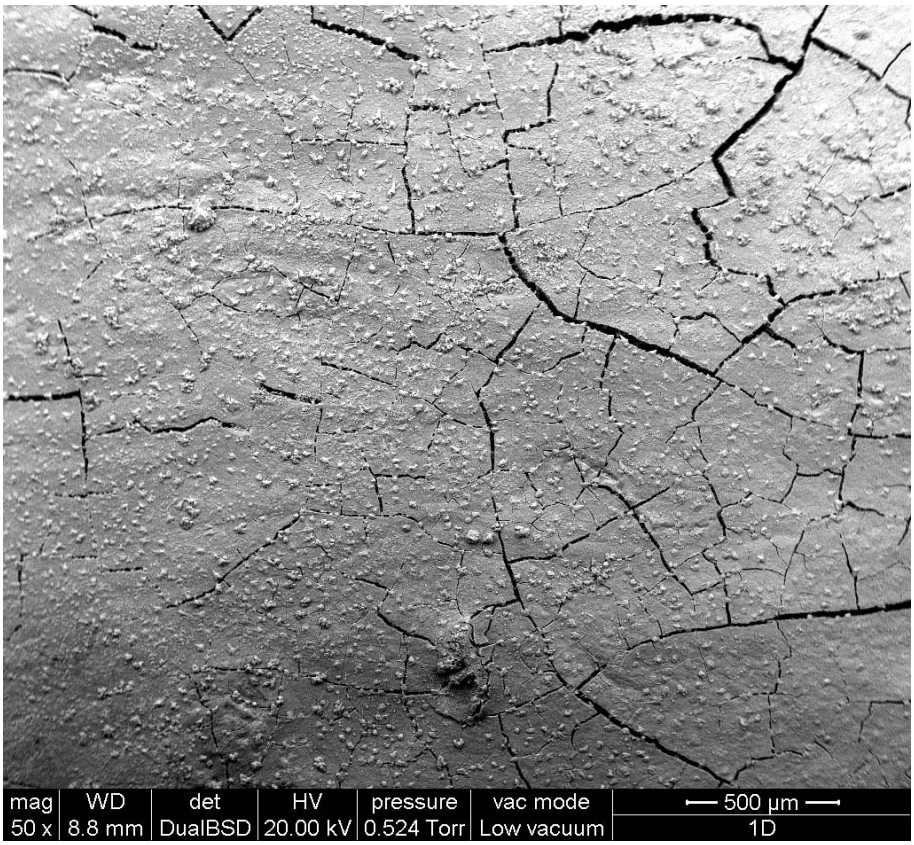

Figure 68. 50x SEM image of ceramic sample after 1 day of immersion in SBF

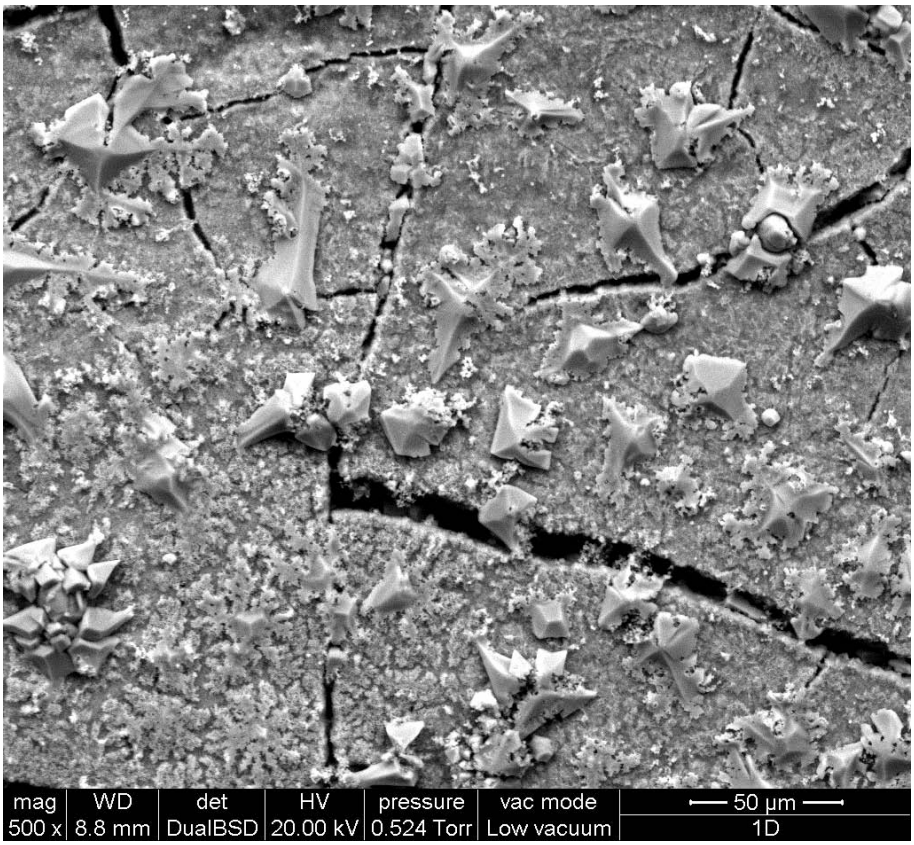

Figure 69. 500x SEM image of ceramic sample after 1 day of immersion in SBF

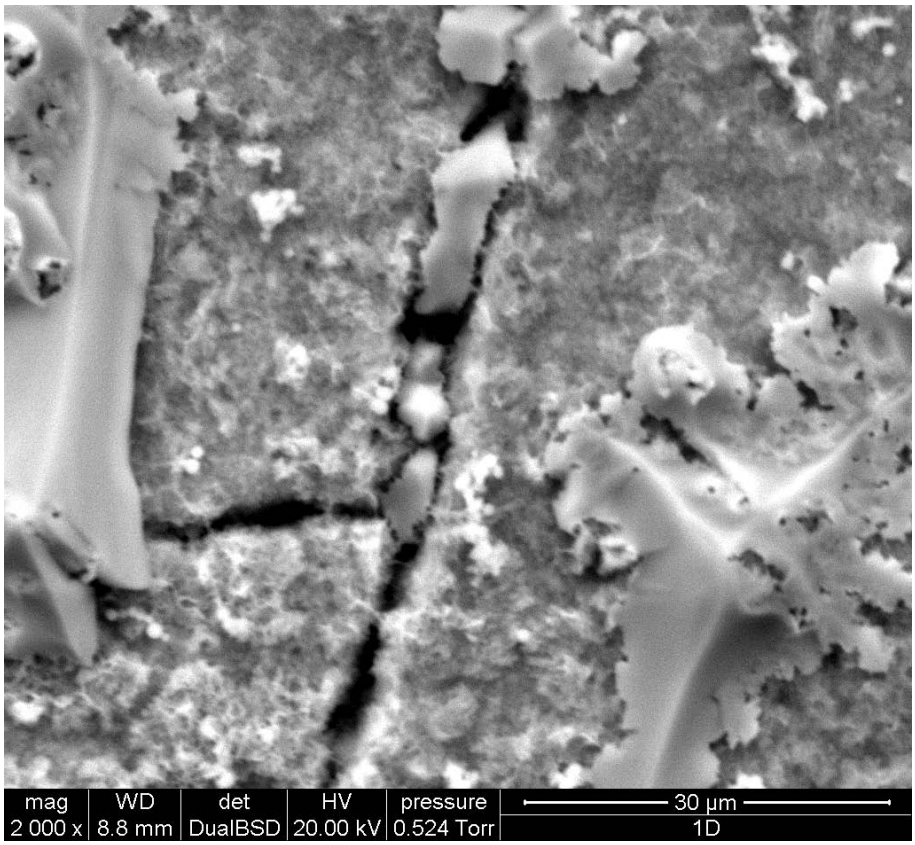

Figure 70. 2000x SEM image of ceramic sample after 1 day of immersion in SBF

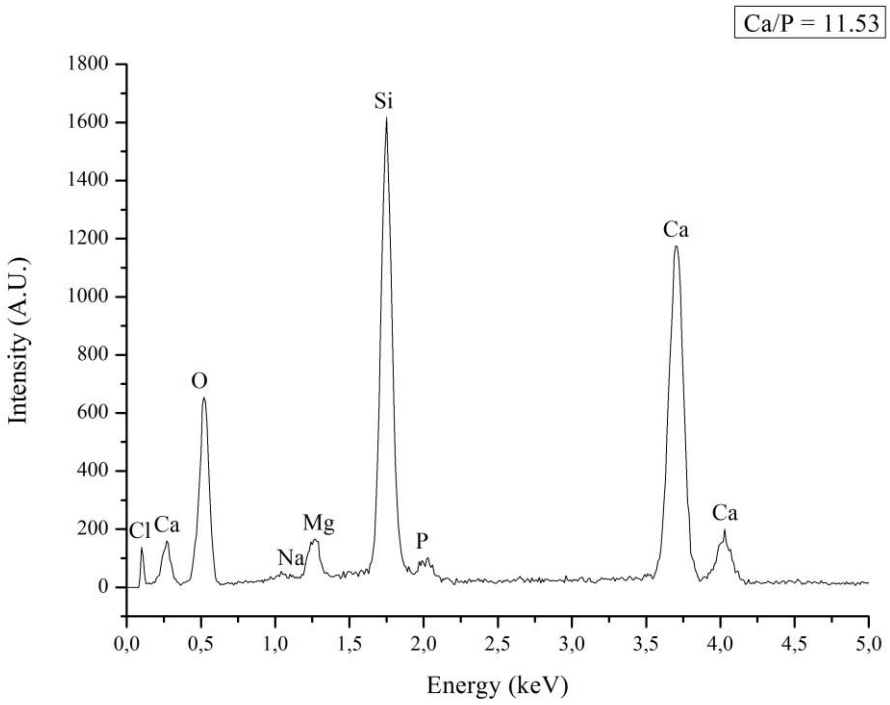

Figure 71. EDX spectrum of ceramic sample after 1 day of immersion in SBF

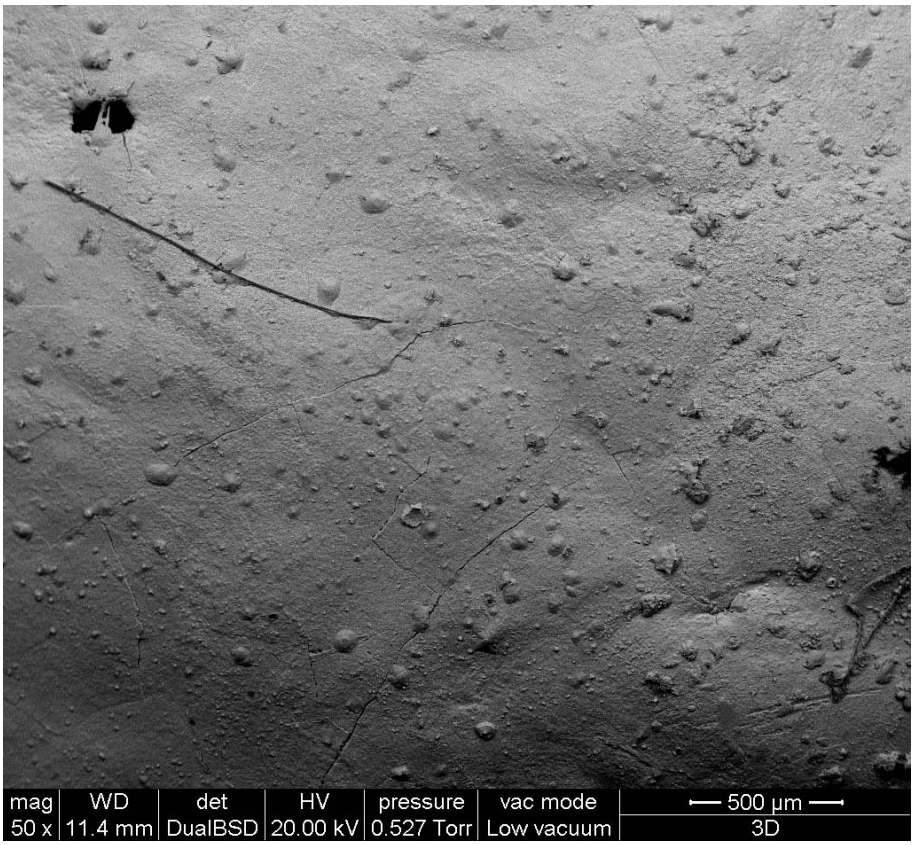

Figure 72. 50x SEM image of ceramic sample after 3 days of immersion in SBF

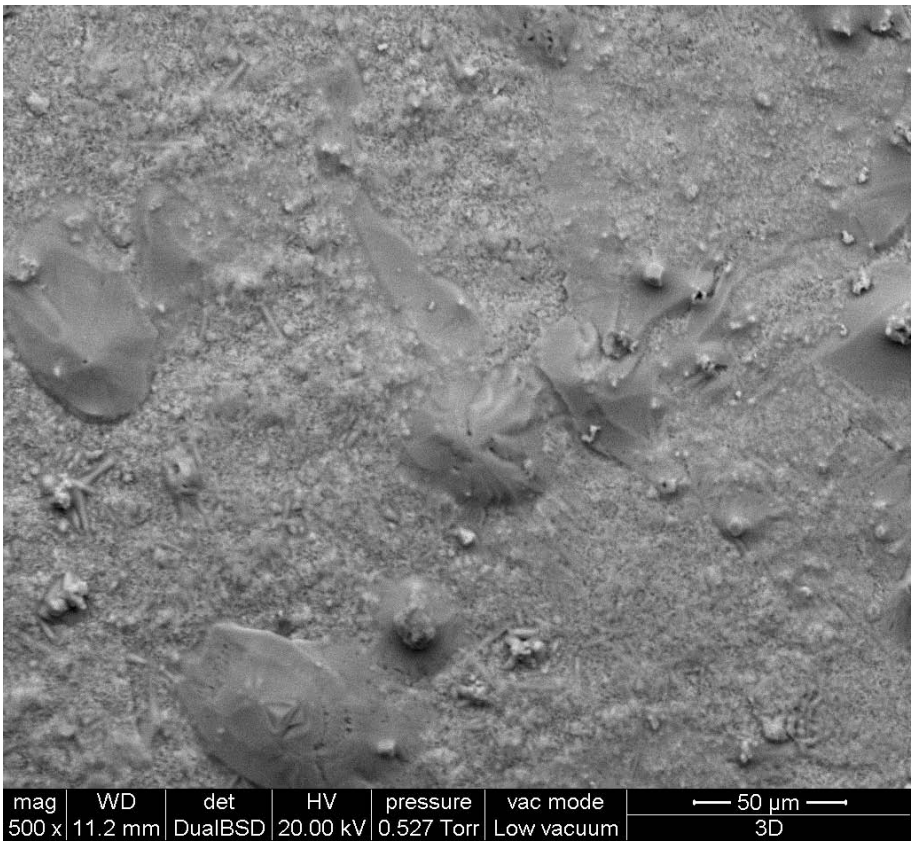

Figure 73. 500x SEM image of ceramic sample after 3 days of immersion in SBF

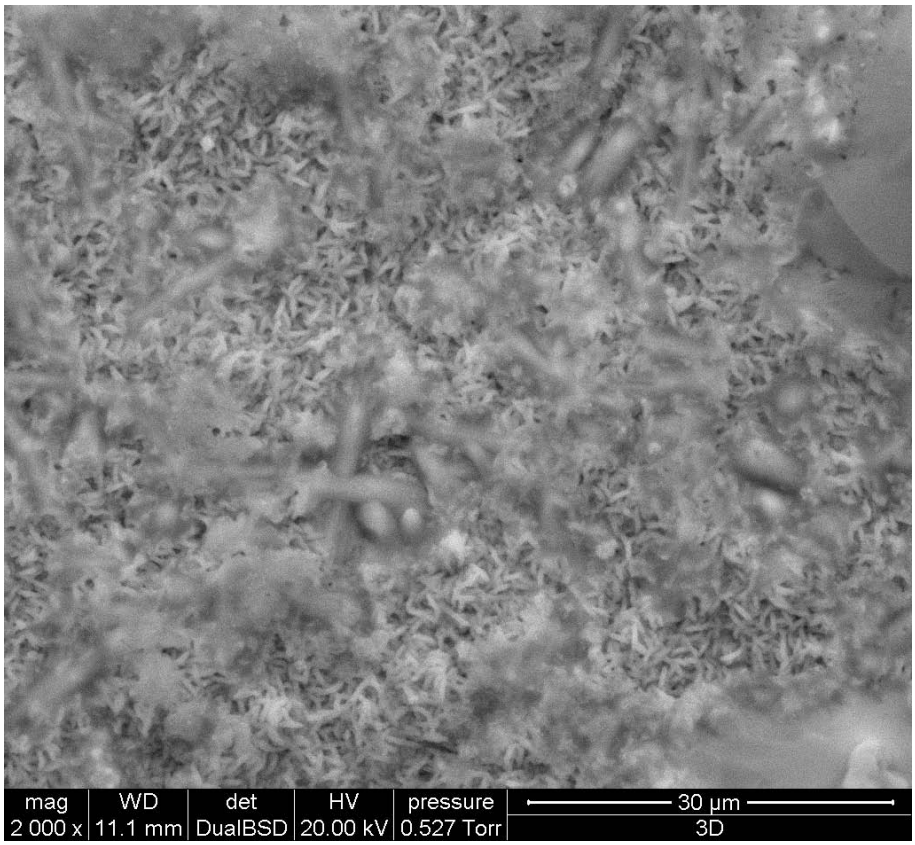

Figure 74. 2000x SEM image of ceramic sample after 3 days of immersion in SBF

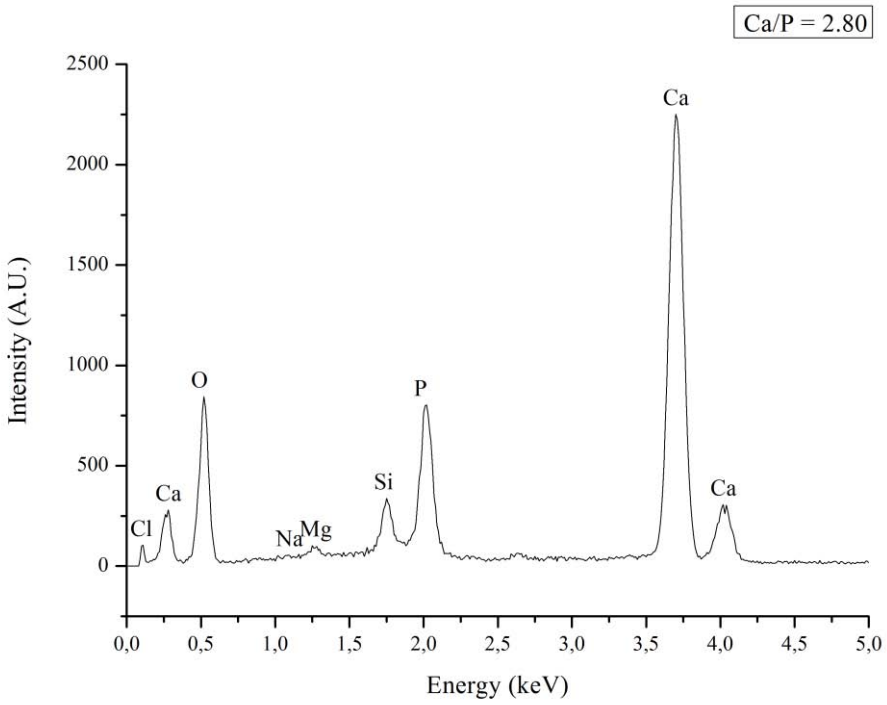

Figure 75. EDX spectrum of ceramic sample after 3 days immersion in SBF

Figures 63-65 show the surface of a ceramic thin wall printed with MK – $CaCO_3$ – wax preceramic compound and subjected to pyrolysis. In the first one (50x) wires extruded by the printer are clearly visible; as mentioned before, they have an average diameter of 0.4 mm; holes due to printing difficulties highlighted before are also present.
Several cracks are detected on sample surface; according to previous works[37], they can be caused by micrometric $CaCO_3$ powder accumulation during mixing process which leads to local pressure increasing during pyrolysis and decomposition to CO_2.
Higher magnifications (500x and 2000x) show an amorphous structure with a huge amount of micropores with an average diameter of about 2-3 μm.
EDX spectrum of sample surface confirms that wollastonite has formed: peaks of Ca, Si and O are rising above other elements; some tracks of Cl and Mg are found, probably due to contamination from refractory substrate; however, they do not hack material biocompatibility.

Figures 67-69 are about sample aspect after 1 day of immersion in SBF under controlled conditions; cracks are visible also on its surface.
Micropores are not visible anymore neither at 500x nor at 200x magnifications; they were probably due to non-optimal printing parameters, but their origin needs further investigations in order to be explained.
Surface appears as a homogeneous amorphous sheet which starts to be covered by crystalline inflorescences; EDX spectrum detects an average increase in Ca/Si ratio. If sample is analyzed in more detail, it can be noticed that inflorescences are particularly rich in Ca; according to HA formation theory discussed in Chapter 3, Ca ions are enriching the outer surface. Bulk phase results enriched in Si; a timid presence of P is also revealed: looking at 200x magnification image (Figure 69), aciform crystals attributable to HA appear.

Surface represented in figures 71-73 shows a significant evolution from the previous one: after 3 days of immersion in SBF, Ca accumulations seem to agglomerate and surface remaining is almost completely covered by aciform complexes, as clearly visible at 2000x magnification.
EDX spectrum shows an exponential increase in P peak intensity. Ca/P ratio is still not the stoichiometric one expected from HA (2.80 versus 1.67) but this can be explained by two facts: the presence of Ca agglomerates on the surface which increase Ca peak intensity and the incomplete covering of the sample surface with HA crystals. Just after 3 days in SBF printed material seem to stimulate well HA formation and thus to be suitable for bone repair.

CONCLUSIONS

As mentioned at the beginning of this work, the focus of the study has been on feasibility of 3D printing of a preceramic material based on silicone in order to produce a simple scaffold; after pyrolysis, resulting ceramic material should be biocompatible for applications in bone tissue engineering.

Specific objectives of the study have been:

- selection and characterization of an optimal mixture of preceramic, filler and plasticizer in order to obtain a material formability window suitable for 3D printing technique;
- reconfiguration and setup of a printer in order to use preceramic material instead of PLA or ABS;
- realization and pyrolysis of samples and their characterization in terms of chemical structure, morphology and biological behavior.

First objective has been satisfactory fulfilled: choice of Carnauba wax as plasticizer guarantees biocompatibility maintenance on one hand and flowability improvements on the other hand. To achieve these results by assuring green body shape stability and wollastonite formation has required several tries with different amount of wax.

Rheological measurements on the selected composition show that its viscosity around 100°C and 120°C is comparable to PLA one around 200°C for the same shear rates; this is really promising in terms of preceramic 3D printing because 200°C is the optimal temperature for PLA to be printed. Data collected cannot be considered precise because M-I tester allows just indirect approximate measurements; therefore, further investigation with capillary or dynamic rheometers are suggested.

Also pyrolysis process has been appropriately designed. Choice of a really low heating rate consents not to project a complicated heating program to let material cross-link; printed structures convert into ceramics maintaining their shape and with no detectable shrinkage. Combination of right mixture and appropriate heat treatment can therefore lead to a near net-shape process, one of the main challenges of new manufacturing techniques.

Problems can still be experienced at the end of this operational sequence: SEM images show cracks formation in pyrolyzed samples. Such structural damages are already appeared in previous studies, and they have been ascribed to micrometric $CaCO_3$ powder. Hypothesis is that powder accumulates in some regions during mixing and when it decomposes to CO_2 it leads to local pressure increase and thus to crack formation.
Cracks have not been found in ceramics made by nanometric $CaCO_3$ powders; further tries replacing micrometric $CaCO_3$ powder with nanometric one are thus suggested.

Success in material synthesis can also be registered from bioactivity tests; even if just preliminary SBF tests have been performed, they already show that there is hydroxyapatite formation soon after 1 and 3 days of immersion under controlled condition.
HA formation mechanism on wollastonite is confirmed and no need of any dopant (like HA itself) in its structure has been needed to activate the process; biological response could not be as good as with bioglass, but material synthesis is much easier.

Most of the obstacles have been encountered in printing process itself: it has not been possible to print porous structures and it has also been really difficult to print even decent dense samples.

This is mainly due to instrumental limits; printer setup does not allow deep personalization. Extrusion system remains a big deal: to install a piston pushing system, a more resistant structure is needed. Challenge is on realizing an extrusion system which does not increase head inertia too much but consents a real control on material flow.

Even if extrusion will be implemented, porous structure will still be almost impossible to be printed; this is because of gravity action on partially molten deposited wires.
A solution can be the use of a bi-material 3D printer: it does not cost much more than the present one but it allows the use of a sacrificial material as support. After the whole structure is printed, support can be eliminated through a selective solvent or a thermal treatment.
Another practicable idea is to realize scaffolds by impregnation of PLA or ABS negative dies produced by 3D printing: no device modifications would be needed and all advantages brought by the use of a low cost rapid prototyping technique would remain.

After the realization of more repeatable and complex samples, it would be interesting to go on with pH, protein and cell tests; also mechanical tests have to be performed to see if scaffolds resistance is higher than bioglass ones (which are quite weak).

Wollastonite scaffolds can still be a good alternative to bioglass and some steps toward an affordable and advantageous forming process have been performed.

BIBLIOGRAPHY

1. Colombo P, Mera G, Riedel R, Sorarù G. Polymer-derived ceramics: 40 years of research and innovation in advanced ceramics. *Journal of the American Ceramic Society*. 2010;93(7):1805-1837.

2. Miele P, Bernard S, Cornu D, Toury B. Recent developments in Polymer-Derived ceramic fibers (PDCFs): Preparation, properties and applications – A review. *Soft Materials*. 2007;4(2-4):249-286.

3. Pace M. *Sviluppo di bioceramici cellulari da polimeri caricati con micro e nano fillers.* [Laurea Magistrale in Ingegneria dei Materiali]. Università degli Studi di Padova; 2011-12.

4. Greil P. *Innovative prozesstechniken fuer moderne keramische materialien.* Department Werkstoffwissenschaften Universitaet Erlangen-Nuernberg; 2010.

5. Still rapid, but much more than prototyping. *Foundry Management &Technology*. 2012;140(3):16-18.

6. Kouhi E, Masood S, Morsi Y. Design and fabrication of reconstructive mandibular models using fused deposition modeling. *Assembly Automation*. 2008;28(3):246-254.

7. Melchels F, Wiggenhauser P, Warne D, et al. CAD/CAM-assisted breast reconstruction. *Biofabrication*. 2011;3.

8. Sekou S, Liu Y, Li D, Lu B, He S, Li G. Fabrication of customised maxillo-facial prosthesis using computer-aided design and rapid prototyping techniques. *Rapid Prototyping Journal*. 2006;12(4):206-213.

9. Tian X, Li D, JÃ¼rgen G. Heinrich. Net-shaping of ceramic components by using rapid prototyping technologies. In: ; 2011.

10. Zocca A. *3D ceramic scaffolds by laser sintering (LSD).* [Laurea Magistrale in Ingegneria dei Materiali]. Università degli Studi di Padova; 2011-12.

11. Zocca A, Gomes C, Bernardo E, Müller R, Günster J, Colombo P. LAS glass–ceramic scaffolds by three-dimensional printing. *Journal of the European Ceramic Society*. 2013;33:1525-1533.

12. Seitz H, Rieder W, Irsen S, Leukers B, Tille C. Three-dimensional printing of porous ceramic scaffolds for bone tissue engineering. *Wiley InterScience*. 2005:782-788.

13. Ratner B, Hoffman A, Schoen F, Lemons J. *Biomaterials science: An introduction to materials in medicine.* ; 2004.

14. Jones J, Hench LL. Regeneration of trabecular bone using porous ceramics. *Current Opinion in Solid State and Materials Science*. 2003;7:301-307.

15. Hench LL. Genetic design of bioactive glass. *Journal of the European Ceramic Society*. 2009;29:1257-1265.

16. Wilson J, Low SB. Bioactive ceramics for periodontal treatment: Comparative studies in the patus monkey. *Journal of Applied Biomaterials*. 1992;3(2):123-129.

17. Shumkova VV, Pogrebenkov VM, Karlov AV, Kozik VV, Vereshchagin VI. Hydroxyapatite-wollastonite bioceramics. *Glass and Ceramics*. 2000;57(9-10):350-353.

18. Kokubo T, Kushitani H, Sakka S, Kitsugi T, Yamamuro T. Solutions able to reproduce in vivo surface-structure changes in bioactive glass-ceramic A-W3. *J Biomed Mater Res*. 1990;24(6):721-734.

19. Liu X, Ding C, Chu PK. Mechanism of apatite formation on wollastonite coatings in simulated body fluids. *Biomaterials*. 2004;25:1755-1761.

20. Lakes R. Materials with structural hierarchy. *Nature*. 1993;361(511):515.

21. Nakamura T, Yamashita K, Neo M. Morphological and dimensional characteristics of bone mineral crystals. *Key Engineering Materials*. 2006;309-311:3-6.

22. Rho J, Kuhn-Spearing L, Zioupos P. Mechanical properties and the hierarchical structure of bone. *Med Eng Phys*. 1998;20(2):92-102.

23. Somaglia di Stoppazzola C. *Estrusione di polimeri preceramici per la realizzazione di scaffold ossei.* [Laurea Specialistica in Ingegneria Meccanica]. Università degli Studi di Padova; 2009-10.

24. Shenoy A, Chattopadhyay S, Nadkarni V. From melt flow index to rheogram. *Rheologica Acta*. 1983;22:90-101.

25. KU Leuven. X-ray diffraction – bruker D8 discover. http://fys.kuleuven.be/iks/nvsf/experimental-facilities/x-ray-diffraction-2013-bruker-d8-discover. Updated 2010. Accessed 09/23, 2013.

26. Balan C, Riedel R. Rheological investigations of a polymeric precursor for ceramic materials: Experiments and theoretical modeling. *Journal of Optoelectronics and Advanced Materials*. 2006;8(2):561-567.

27. Balan C, Riedel R. Sol – gel modelling associated with the rheology of polymeric precursors of ceramic materials. *Applied Rheology*. 2003;13(5):251-258.

28. Ceron-Nicolat B, Wolff F, Dakkouri-Baldauf A, Fey T, Münstedt H, Greil P. Graded cellular ceramics from continuous foam extrusion. *Advanced Engineering Materials*. 2012;14(12):1097-1103.

29. Takahashi T, Colombo P. SiOC ceramic foams through melt foaming of a methylsilicone preceramic polymer. *Journal of Porous Materials*. 2003;10:113-121.

30. Takahashi T, Kaschta J, MÃ¼nstedt H. Melt rheology and structure of silicone resins. *Rheologica Acta*. 2001;40(5):490-498.

31. Wang C, Wang J, Park C. Cross-linking behavior of a polysiloxane in preceramic foam processing. *Journal of Material Science*. 2004;39:4913-4915.

32. Wolff F, Kugler C, Münstedt H. Time- and temperature-dependent crosslinking behaviour of a silicone resin. *Rheological Acta*. 2012;51:71-80.

33. Wolff F, Ceron Nicolat B, Fey T, Greil P, Münstedt H. Extrusion foaming of a preceramic silicone resin with a variety of profiles and morphologies. *Advanced Engineering Materials*. 2012;14(12):1110-1115.

34. Endlein E, Peleikis K-. Natural waxes – properties, compositions and applications. *SOFW-Journal*. 2011;4(137):1-8.

35. Conrad J. *The rheology, degradation, processing, and characterization of renewable resource polymers.* [Doctor of Philosophy - Chemical Engineering]. Clemson University; 2009.

36. Tanihara M, Miyazaki T, Ogata S, Ohtsuki C. Design and development of functional biocompatible hybrid materials for medical applications. In: Nalwa H, ed. *Handbook of organic-inorganic hybrid materials and nanocomposites, vol. 2.* Vol 2. American Scientific Publishers; 2003:265-293.

37. Fiocco L. *Bioceramici porosi da polimeri preceramici e fillers.* [Laurea Magistrale in Ingegneria dei Materiali]. Università degli Studi di Padova; 2011-12.